

THE μ TAU ASSOCIATION: A 60 MYR-OLD COEVAL GROUP AT 150 pc FROM THE SUN

JONATHAN GAGNÉ,^{1,2} TREVOR J. DAVID,^{3,4} ERIC E. MAMAJEK,^{4,5} ANDREW W. MANN,⁶ JACQUELINE K. FAHERTY,⁷ AND ANTOINE BÉDARD⁸

¹ Planétarium Rio Tinto Alcan, Espace pour la Vie, 4801 av. Pierre-de Coubertin, Montréal, Québec, Canada

² Institute for Research on Exoplanets, Université de Montréal, Département de Physique, C.P. 6128 Succ. Centre-ville, Montréal, QC H3C 3J7, Canada

³ Center for Computational Astrophysics, Flatiron Institute, New York, NY 10010, USA

⁴ Jet Propulsion Laboratory, California Institute of Technology, 4800 Oak Grove Drive, Pasadena, CA 91109, USA

⁵ Department of Physics & Astronomy, University of Rochester, Rochester, NY 14627, USA

⁶ Department of Physics and Astronomy, University of North Carolina at Chapel Hill, Chapel Hill, NC 27599-3255, USA

⁷ Department of Astrophysics, American Museum of Natural History, Central Park West at 79th St., New York, NY 10024, USA

⁸ Département de Physique, Université de Montréal, C.P. 6128 Succ. Centre-ville, Montréal, QC H3C 3J7, Canada

Submitted to ApJ

ABSTRACT

We present an analysis of the newly identified μ Tau Association (MUTA) of young stars at $\simeq 150$ pc from the Sun that is part of the large Cas-Tau structure, coeval and co-moving with the α Persei cluster. This association is also located in the vicinity of the Taurus-Auriga star-forming region and the Pleiades association, although it is unrelated to them. We identify more than 500 candidate members of MUTA using *Gaia* DR2 data and the BANYAN Σ tool (Gagné et al. 2018) and we determine an age of 62 ± 7 Myr for its population based on an empirical comparison of its color-magnitude diagram sequence with those of other nearby young associations. The MUTA association is related to the Theia 160 group of Kounkel & Covey (2019) and corresponds to the e Tau group of Liu et al. (2020). It is also part of the Cas-Tau group of Blaauw (1956). As part of this analysis, we introduce an iterative method based on spectral templates to perform an accurate correction of interstellar extinction of *Gaia* DR2 photometry, needed because of its wide photometric bandpasses. We show that the members of MUTA display an expected increased rate of stellar activity and faster rotation rates compared with older stars, and that literature measurements of the lithium equivalent width of nine G0 to K3-type members are consistent with our age determination. We show that the present-day mass function of MUTA is consistent with other known nearby young associations. We identify WD 0340+103 as a hot, massive white dwarf remnant of a B2 member that left its planetary nebula phase only 270,000 years ago, posing an independent age constraint of 60^{+8}_{-6} Myr for MUTA, consistent with our isochrone age. This relatively large collection of co-moving young stars near the Sun indicates that more work is required to unveil the full kinematic structure of the complex of young stars surrounding α Persei and Cas-Tau.

Keywords: methods: data analysis — stars: kinematics and dynamics — proper motions

1. INTRODUCTION

Young stellar associations in the Solar neighborhood ($\lesssim 200$ pc) are valuable laboratories to study stellar evolution and refine our age-dating methods because they contain groups of stars with many different masses that

formed coevally from the same molecular cloud (e.g., Zuckerman & Song 2004; Torres et al. 2008). Their proximity is valuable because their members appear brighter, but it also causes them to be spread over larger areas of the sky, which makes their initial identification less straightforward. Obtaining credible lists of members with low contamination by unrelated field stars is challenging and typically requires measuring the six-

dimensional position and space velocity of each member. As these stars formed from a single molecular cloud, they share the same velocities typically within $\simeq 2\text{--}4 \text{ km s}^{-1}$, allowing us to distinguish them from most field stars.

Until recently, trigonometric distance measurements were only available for a limited set of bright stars (e.g., Perryman et al. 1997), and radial velocity measurements of stars in the Solar neighborhood were even more limited to small-scale samples (e.g., see Gontcharov 2006; White et al. 2007). This led to the identification of co-moving and coeval massive stars that represented only the tip of the iceberg of each young association of stars in our neighborhood (Zuckerman & Song 2004; Torres et al. 2008). Efforts have been made to identify the lower-mass population based on various methods that can assign membership probabilities with missing parts of the 6-dimensional space and velocity, including the convergent point method (Mamajek 2005; Torres et al. 2006) and various other flavors of selection cuts in space-velocity and/or photometry (Zuckerman & Song 2004; Kraus et al. 2014; Riedel et al. 2017; Shkolnik et al. 2017) as well as methods based on Bayesian statistics (Malo et al. 2013; Gagné et al. 2014, 2018).

The second data release of the *Gaia* mission (*Gaia* DR2 hereafter; Gaia Collaboration et al. 2018a; Lindegren et al. 2018)¹ changed this landscape completely in April of 2018 by providing trigonometric distance measurements for $\simeq 1.3$ billion stars with an unprecedented precision, as well as radial velocities for more than 7.2 million bright stars. This allowed us to complete the 6-dimensional kinematics for a number of stars on a completely new scale, which led to a plethora of scientific discoveries that quickly unveiled the spatial and kinematic structure of the Solar neighborhood as well as the Milky Way in general. Some of these discoveries include many new associations of stars (Oh et al. 2017; Faherty et al. 2018; Gagné et al. 2018a; Kounkel & Covey 2019; Meingast et al. 2019), a large number of new M-type members of known associations (Gagné et al. 2018c; Gagné & Faherty 2018; Luhman 2018; Reino et al. 2018; Zuckerman 2019; Tang et al. 2019), as well as the discovery of tidal disruption tails around three older, nearby clusters: the Hyades (Röser et al. 2019), Praesepe (Röser & Schilbach 2019) and Coma Ber (Tang et al. 2019).

¹ See also Luri et al. (2018), Mignard et al. (2018), Babusiaux et al. (2018), Sartoretti et al. (2018), Soubiran et al. (2018), Cropper et al. (2018), Evans et al. (2018b), Hambly et al. (2018), and Riello et al. (2018) for relevant calibration.

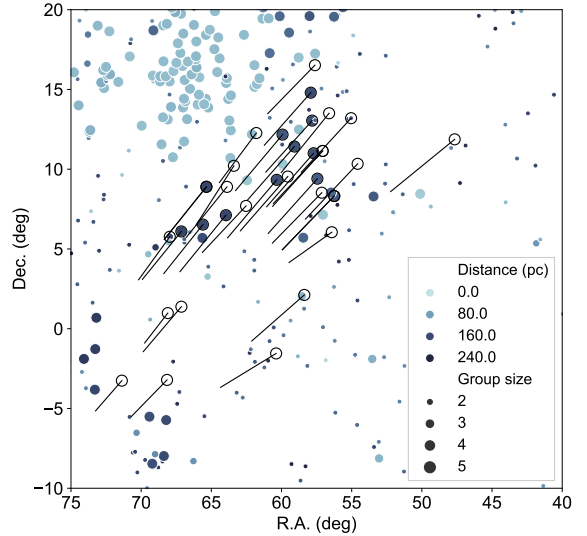


Figure 1. Sky position and proper motions of MUTA members (empty circles with proper motion arrows), compared with nearby co-moving systems recovered by Oh et al. (2017; filled blue circles). The larger circles belong to Oh et al. (2017) co-moving systems with more members (the maximum symbol size indicates 5 or more members), and the darker-shaded circles correspond to objects further away from the Sun. The tip of the Taurus star-forming region can be seen as large, dark blue circles at R.A. $\simeq 55\text{--}60^\circ$, Dec. $\simeq 20^\circ$, and part of the foreground Hyades cluster can be seen as large, pale blue circles at R.A. $\simeq 65\text{--}75^\circ$, Dec. $\simeq 10\text{--}20^\circ$. See Section 2 for more details.

This paper presents the discovery and characterization the MUTA association, based on an initial list of massive co-moving and coeval members that had been discovered in historical surveys but never before published. The advent of *Gaia* DR2 allowed us to complete this list and characterize MUTA such that it will become yet another important laboratory for the investigation of stellar evolution and the grounds for discovery of age-calibrated brown dwarfs and exoplanets. In Section 2, we present the initial list of MUTA members, which we use to build a spatial-kinematic model (Section 3) to search for additional members with the BANYAN Σ Bayesian identification tool (Gagné et al. 2018) in Section 4. In Section 5, we present an iterative method to correct interstellar extinction in *Gaia* DR2 color-magnitude diagrams, required because the photometric bandpasses are wider than usual. We discuss the properties of MUTA as a whole and its individual members in Section 6, including their present-day mass function and stellar activity indicators, and a comparison with the Galactic kinematic structures recently un-

veiled by Kounkel & Covey (2019). We summarize and conclude this work in Section 7.

2. INITIAL SAMPLE OF MEMBERS

The existence of a distinct group of co-moving young stars in the vicinity of the Taurus-Auriga (Kenyon et al. 2008) star-forming region first appeared in a spatial distribution of Cas-Tau OB-type stars assembled by Blaauw (1956). Cas-Tau was identified by Blaauw (1956) as an extended group of co-moving stars with an expansion age of $\simeq 50$ Myr that seems to be on the way to being dissolved. They noted that Cas-Tau may share a common origin with an extended stream of stars around the α Persei cluster (e.g., see Heckmann & Lübeck 1958; Lodieu et al. 2019) identified by Rasmussen (1921). An over-density in the Cas-Tau stars seemed to be located at Galactic coordinates $(\ell, b) = (190^\circ, -10^\circ)$, and was recovered as part of the de Zeeuw et al. (1999) census of nearby OB associations (see their Fig. 19). This over-density overlaps with subgroup 5 of Cas-Tau defined by Blaauw (1956), with five B-type stars in common (29 Tau, 30 Tau, 35 Eri, μ Tau, μ Eri) and one additional star (40 Tau) not in common that seems to be an unrelated background star. Combining this list of 12 early-type stars assembled by de Zeeuw et al. (1999) to other co-moving B, A and F-type stars in the range ℓ from 170° to 205° and b from -40° to -27° as well as nearby ROSAT entries (Boller et al. 2016) in the same region yielded a total set of 35 stars that appeared to be young and co-moving within 15 mas yr^{-1} of the average proper motions of the de Zeeuw et al. (1999) list ($\mu_\alpha \cos \delta = 21.0 \text{ mas yr}^{-1}$, $\mu_\delta = -20.5 \text{ mas yr}^{-1}$). Four of these 37 stars are clear outliers either in XYZ (HD 23110, TYC 657–794–2, and HD 28796) or UVW (HIP 18778) and were excluded from our initial list. The resulting 33 stars are listed in Table 1 with their properties. We tentatively named this group μ Tau Association (MUTA) after one of its brightest members. We assigned initial members with MUTA identification numbers (from 1 to 30) in order of decreasing V -band brightness. We assigned the same MUTA ID to binaries with separations below $15''$.

In a more recent analysis of the *Gaia* Data Release 1 (DR1), Oh et al. (2017) recovered about a third of the stars in Table 1 as three broken up groups of co-moving

systems, which they named Groups 43 (6 matches), 52 (3 matches) and 60 (4 matches). The overlap between our initial list of MUTA members and the Oh et al. (2017) sample are shown in Figure 1, where part of the Taurus star-forming region can be seen at a similar distance from the Sun (see e.g. Wichmann et al. 2000), and the Hvades cluster (Perryman et al. 1998) also appears in

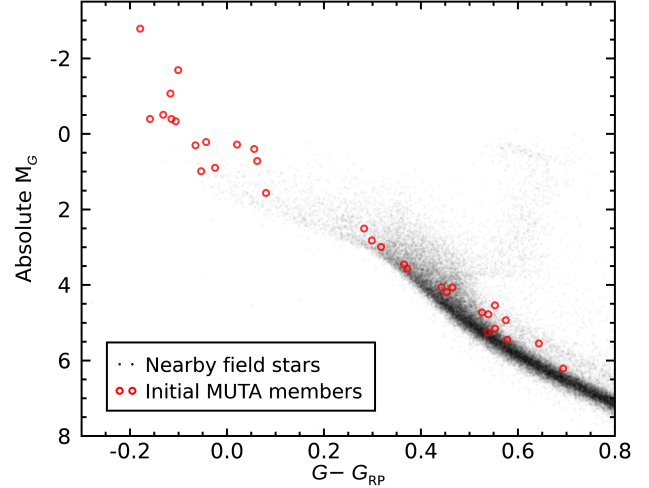


Figure 2. *Gaia* DR2 Color-magnitude diagram of our initial list of MUTA members (red circles), compared with field stars within 100 pc of the Sun (black dots). This list of MUTA members contains several OBA-type stars ($G - G_{RP} < 0.2$) indicative of its young age, as well as later-type stars ($G - G_{RP} > 0.2$) that constitute a narrow sequence. The *Gaia* DR2 photometry was not corrected for interstellar extinction. 2MASS J04212444+0853488 is outside the range of this figure at $G - G_{RP} = 1.12$. See Section 2 for more details.

the foreground. The method that Oh et al. (2017) used to identify systems of co-moving stars works directly in proper motion and parallax space, which tends to recover spatially large moving groups only as broken parts, explaining why the spatially extended MUTA was broken up in three groups, similarly to other nearby young moving groups (Faherty et al. 2018).

We cross-matched our initial list of MUTA members with *Gaia* DR2 data to build a color-magnitude sequence shown in Figure 2 to demonstrate they constitute massive OBA-type stars ($G - G_{RP} < 0.2$) and a well-defined sequence of later-type stars ($G - G_{RP} > 0.2$), providing further evidence that they are coeval and young.

Table 1. Initial members of MUTA.

MUTA		Spectral	R.A.	Decl.	Distance ^a	<i>Gaia</i> DR2	
ID	Name	Type	(hh:mm:ss.sss)	(dd:mm:ss.ss)	(pc)	<i>G</i> mag	Ref. ^b
1	μ Eri	B3+A3	04:45:30.167	-03:15:16.97	160 \pm 5	3.931 \pm 0.004	16
2	μ Tau	B3IV	04:15:32.079	+08:53:32.14	149 \pm 7	4.183 \pm 0.003	5
3 A	30 Tau	B3V	03:48:16.292	+11:08:35.52	129 \pm 3	5.040 \pm 0.002	5
3 B	TYC 661-1404-1	F5+F5	03:48:16.835	+11:08:40.16	138 \pm 1	9.2693 \pm 0.0002	2
4	35 Eri	B5V	04:01:32.077	-01:32:59.02	133 \pm 3	5.230 \pm 0.002	5
5	29 Tau	B3+A7	03:45:40.466	+06:02:59.78	187 \pm 9	5.295 \pm 0.001	4
6	HD 28375	B5V	04:28:32.142	+01:22:50.65	146 \pm 4	5.491 \pm 0.001	14
7	HD 28843	B9III	04:32:37.573	-03:12:34.60	169 \pm 3	5.740 \pm 0.002	15
8	HD 19698	B8V	03:10:38.828	+11:52:21.07	134 \pm 2	5.9439 \pm 0.0008	1
9	HR 1307	B8V	04:13:34.588	+10:12:44.52	144 \pm 3	6.1900 \pm 0.0006	13
10	V766 Tau	B9	03:51:15.896	+13:02:45.52	161 \pm 2	6.247 \pm 0.001	9
11	HD 28715	B9	04:31:50.463	+05:45:51.74	187 \pm 4	6.6396 \pm 0.0004	3
12	HD 24456	B9.5V	03:53:30.257	+02:07:08.57	138.7 \pm 0.9	6.6983 \pm 0.0004	10
13	HD 23990	B9.5V	03:49:46.521	+09:24:26.60	147 \pm 1	6.7410 \pm 0.0004	6
14	HD 23538	A0	03:46:26.278	+13:30:32.46	168 \pm 2	6.8479 \pm 0.0003	3
15	HD 25978	B9V	04:07:11.204	+12:16:05.10	166 \pm 2	7.6661 \pm 0.0003	12
16	HD 26323	A2V	04:10:06.873	+07:41:52.12	161 \pm 2	8.5401 \pm 0.0005	10
17	HD 27687	A3	04:22:24.213	+06:31:45.14	165 \pm 1	8.9125 \pm 0.0004	3
18	HD 28356	A3	04:28:32.733	+06:05:52.07	157 \pm 2	8.9675 \pm 0.0004	3
19 A	HD 23376	G5	03:44:58.957	+08:19:10.09	145 \pm 1	9.2549 \pm 0.0003	3
19 B	TYC 658-1007-2	...	03:44:59.048	+08:19:13.81	142 \pm 1	10.493 \pm 0.002	–
20	HIP 17133	A0	03:40:09.988	+13:11:55.07	150 \pm 1	9.949 \pm 0.001	3
21	HD 286374	F5	03:56:19.224	+11:25:10.84	152 \pm 2	9.9776 \pm 0.0005	11
22	PPM 119410	F8	03:50:50.558	+11:00:05.12	151 \pm 1	10.0929 \pm 0.0006	8
23	[LH98] 108	G5IV	03:50:28.436	+16:31:14.80	146 \pm 1	10.364 \pm 0.001	7
24	RX J0348.5+0832	G7	03:48:31.461	+08:31:36.43	152 \pm 2	10.841 \pm 0.002	2
25	TYC 80-202-1	...	04:15:51.119	+07:07:03.76	167 \pm 1	10.8894 \pm 0.0006	–
26	TYC 662-217-1	...	03:59:42.158	+12:10:08.14	148 \pm 1	11.111 \pm 0.002	–
27	RX J0338.3+1020	G9	03:38:18.266	+10:20:16.32	146 \pm 1	10.976 \pm 0.001	2
28	TYC 664-136-1	...	03:51:39.673	+14:47:47.84	160 \pm 1	11.566 \pm 0.002	–
29	RX J0358.2+0932	K3	03:58:12.749	+09:32:21.97	146.8 \pm 0.9	12.045 \pm 0.001	2
30 A	TYC 668-737-1	...	04:21:24.386	+08:53:54.34	151 \pm 1	11.356 \pm 0.002	–
30 B	2MASS J04212444+0853488	...	04:21:24.473	+08:53:48.52	151 \pm 1	14.7603 \pm 0.0007	–

^a *Gaia* DR2 distances assuming a 0.029 mas zero point (Lindegren et al. 2018).^b References for spectral types.

NOTE—See section 2 for more details.

References—(1) Cowley et al. 1969; (2) Magazzù et al. 1997; (3) Cannon & Pickering 1993; (4) Beavers & Cook 1980; (5) Lesh 1968; (6) Abt 2008; (7) White et al. 2007; (8) Wright et al. 2003; (9) Cowley 1968; (10) Grenier et al. 1999; (11) Nesterov et al. 1995; (12) Bidelman et al. 1988; (13) Cowley 1972; (14) Molnar 1972; (15) Jaschek & Jaschek 1980; (16) van Leeuwen 2007.

Table 2. Core members of MUTA used in the construction of a kinematic model.

MUTA		$\mu_\alpha \cos \delta$	μ_δ	Parallax	RV	RV
ID	Name	(mas yr $^{-1}$)	(mas yr $^{-1}$)	(mas)	(km s $^{-1}$)	Ref.
1	μ Eri	13.51 ± 0.75	-13.66 ± 0.64	6.3 ± 0.2	23 ± 4	1
2	μ Tau	20.88 ± 0.62	-22.79 ± 0.52	6.7 ± 0.3	16.3 ± 0.6	1
3 A	30 Tau	25.27 ± 0.28	-23.69 ± 0.23	7.7 ± 0.2	16.2 ± 0.1	1
4	35 Eri	28.45 ± 0.30	-15.28 ± 0.25	7.5 ± 0.2	15.7 ± 0.8	1
5	29 Tau	21.88 ± 0.29	-13.65 ± 0.26	5.3 ± 0.2	17 ± 2	3
6	HD 28375	19.53 ± 0.33	-20.27 ± 0.18	6.8 ± 0.2	18 ± 4	1
7	HD 28843	18.28 ± 0.19	-16.50 ± 0.13	5.9 ± 0.1	18 ± 7	6
8	HD 19698	32.84 ± 0.16	-23.58 ± 0.17	7.4 ± 0.1	1 ± 4	1
9	HR 1307	19.37 ± 0.39	-26.69 ± 0.23	6.9 ± 0.1	10 ± 7	6
10	V766 Tau	23.77 ± 0.11	-23.228 ± 0.079	6.19 ± 0.06	16 ± 2	5
12	HD 24456	26.93 ± 0.10	-20.785 ± 0.074	7.18 ± 0.05	18 ± 3	1
15	HD 25978	18.91 ± 0.16	-22.323 ± 0.076	5.99 ± 0.07	22 ± 7	6
16	HD 26323	22.38 ± 0.12	-20.975 ± 0.071	6.18 ± 0.06	14 ± 3	1
18	HD 28356	20.00 ± 0.15	-21.659 ± 0.072	6.36 ± 0.07	20.6 ± 0.6	2
19 A	HD 23376	26.61 ± 0.11	-24.306 ± 0.066	6.89 ± 0.06	16.5 ± 0.5	2
20	HIP 17133	25.53 ± 0.10	-24.403 ± 0.073	6.63 ± 0.05	14 ± 6	2
21	HD 286374	24.05 ± 0.11	-24.124 ± 0.067	6.54 ± 0.07	14 ± 2	2
22	PPM 119410	24.14 ± 0.10	-24.167 ± 0.068	6.58 ± 0.05	15.0 ± 0.6	2
23	[LH98] 108	24.24 ± 0.14	-21.892 ± 0.072	6.80 ± 0.05	8.0 ± 0.7	4
24	RX J0348.5+0832	25.33 ± 0.11	-22.738 ± 0.070	6.56 ± 0.08	10 ± 10	2
25	TYC 80–202–1	23.547 ± 0.086	-25.480 ± 0.054	5.96 ± 0.05	20.7 ± 0.6	2
26	TYC 662–217–1	24.07 ± 0.11	-25.242 ± 0.063	6.71 ± 0.05	15.3 ± 0.6	2
27	RX J0338.3+1020	26.75 ± 0.10	-24.923 ± 0.070	6.82 ± 0.06	15 ± 1	2
29	RX J0358.2+0932	24.321 ± 0.071	-24.493 ± 0.051	6.78 ± 0.04	16 ± 2	2
30 A	TYC 668–737–1	21.501 ± 0.085	-23.632 ± 0.056	6.57 ± 0.05	20 ± 7	2

NOTE—All proper motion and parallax measurements are from *Gaia* DR2, except for the parallax of μ Eri, which is from Hipparcos (van Leeuwen 2007). See section 3 for more details.

References—(1) Gontcharov 2006; (2) Gaia Collaboration et al. 2018a; (3) Evans 1967; (4) White et al. 2007; (5) Wilson 1953; (6) Kharchenko et al. 2007.

The earliest-type member in our initial list is 29 Tau (MUTA 5), a B3 V-type star (Beavers & Cook 1980), which corresponds to a mass of $\simeq 5.4 M_\odot$ (Pecaut & Mamajek 2013). Hohle et al. (2010) and Gullikson et al. (2016) estimated the mass of 29 Tau based on evolutionary tracks and found respective values of $6.0 \pm 0.7 M_\odot$ and $5.4 \pm 0.6 M_\odot$, consistent with the expected mass for a B3 star. Following the evolutionary tracks of Choi et al. (2016), such a star has a main-sequence life of only $\simeq 80$ Myr, indicating that the MUTA association is likely younger than the Pleiades.

We note that both μ Tau (MUTA 2) and τ^1 Ari are known eclipsing binaries (Avvakumova et al. 2013). While the first is part of our initial list of members, τ^1 Ari was identified in an earlier parsing of de Zeeuw et al. (1999) but was not included because of its discrepant UVW motion (it is separated from the other stars by $\simeq 6.3$ km s $^{-1}$). A further analysis of their respective light curves might be useful for constraining models of stellar structure at young ages.

3. A KINEMATIC MODEL OF MUTA MEMBERS

The BANYAN Σ tool (Gagné et al. 2018) makes it possible to identify additional stars with similar Galactic positions XYZ and space velocities UVW compared to our initial list of MUTA members, if we provide it a 6-dimensional multivariate Gaussian model for MUTA in $XYZUVW$ space. One of the main benefits of BANYAN Σ is its ability to recover stars with only partial kinematics, often a consequence of missing radial velocity or parallax measurements. The BANYAN Σ tool currently includes kinematic models for 29 nearby young associations, which consist of the 27 associations described in Gagné et al. (2018), as well as the recently discovered Volans-Carina (Gagné et al. 2018a) and the Argus associations (Makarov & Urban 2000), whose census of members was recently revised by Zuckerman (2019).

We compiled literature radial velocity measurements for the stars listed in Table 1 to identify a set of 25 core members with complete kinematics (see Table 2). This list excludes any gravitationally bound companion to avoid artificially giving each system more weight in the kinematic construction of the MUTA model (consistent with the model construction method of Gagné et al. 2018). HD 28715, HD 23990, HD 23538, and HD 27687 (MUTA 11, 13, 14, and 17, respectively) currently do not have radial velocity measurements and were not included in Table 2 although they are likely part of MUTA based on their position in a color-magnitude diagram (see Figure 2) and their common proper motion and parallax compared to the other members.

The methodology described in Gagné et al. (2018; see their Section 5) was used to build a $XYZUVW$ multivariate Gaussian model of the stars listed in Table 2. In summary, a 6-dimensional average vector and covariance matrix in $XYZUVW$ space were built by calculating the average, variances and covariances of the 25 core members with full kinematics listed in Table 2. When calculating the averages, variances and covariances, the individual measurements were weighted proportionally to the squared inverse of their individual error bars to minimize the impact of low quality measurements. The covariance matrix is then regularized to ensure its determinant is finite and positive with a singular value decomposition step. The resulting model is shown in Figure 3.

The multivariate Gaussian model in $XYZUVW$ space that was found to best represent MUTA has the following central position \bar{x}_0 and covariance matrix $\bar{\Sigma}$:

$$\bar{x}_0 = [-130.7 \ 0.2 \ -79.7 \ -14.15 \ -24.20 \ -6.21],$$

$$\bar{\Sigma} = \begin{bmatrix} 478 & 286 & 196 & 16 & 11.9 & 15 \\ 286 & 432 & 136 & 6.7 & 7.6 & 6.0 \\ 196 & 136 & 155 & 5.2 & 4.7 & -3.9 \\ 16 & 6.7 & 5.2 & 9.1 & 0.46 & 5.5 \\ 12 & 7.6 & 4.7 & 0.46 & 2.8 & 0.76 \\ 15 & 6.0 & -3.9 & 5.5 & 0.76 & 5.9 \end{bmatrix}.$$

both in units of pc and km s^{-1} .

The average sky position of MUTA members is 04:01:29.54, +07:59:33.3 (60.3731° , 7.9926°) with a standard deviation of 5° in both directions. The average galactic coordinates (ℓ, b) are $(182.4658^\circ, -31.8645^\circ)$ with a standard deviation of $(9^\circ, 3^\circ)$. The total velocity S_{tot} of the members averages 28.3 km s^{-1} with a standard deviation of 2.3 km s^{-1} . The UVW values we find correspond to a convergent point of $103.380^\circ, -29.325^\circ$ in right ascension and declination (06:53:31, −29:19:30).

4. A SEARCH FOR ADDITIONAL MEMBERS

The kinematic model described in Section 3 was combined with the BANYAN Σ tool to identify candidate members of MUTA in *Gaia* DR2 data. We pre-selected only *Gaia* DR2 entries with right ascensions in the range $10\text{--}150^\circ$, declinations in the range -20 to $+40^\circ$ and trigonometric distances within 300 pc of the Sun. These limits are significantly wider than the ranges of sky positions (47° to 72° and -3.5° to 16.5° , respectively) and distances (all in the range 130–220 pc) of the initial list of members. The sky positions, proper motions and parallaxes from *Gaia* DR2 were used to determine a membership probability, as well as the *Gaia* DR2 radial velocities when available. We selected only the stars with Bayesian membership probabilities above 90% and a maximum likelihood separation of less than 5 km s^{-1} from the core of our MUTA kinematic model in UVW space as new candidate members. The latter criterion avoids selecting stars that would fit all BANYAN Σ models poorly, including its model of the local Galactic neighborhood.

These selection criteria resulted in a set of 503 additional candidate members which are listed in Table 3. Their common proper motion is illustrated in Figure 4 and their positions in a *Gaia* DR2 $G - G_{\text{RP}}$ color versus absolute G magnitude are shown in Figure 5. Their sky positions are located in the range $37\text{--}74^\circ$ and -4° to $+29^\circ$ in right ascension and declination, and their trigonometric distances are in the range 100–220 pc, indicating that our initial filtering of *Gaia* DR2 entries was likely appropriate to encompass the full distribution of MUTA members.

4.1. A Search for Co-Moving Systems

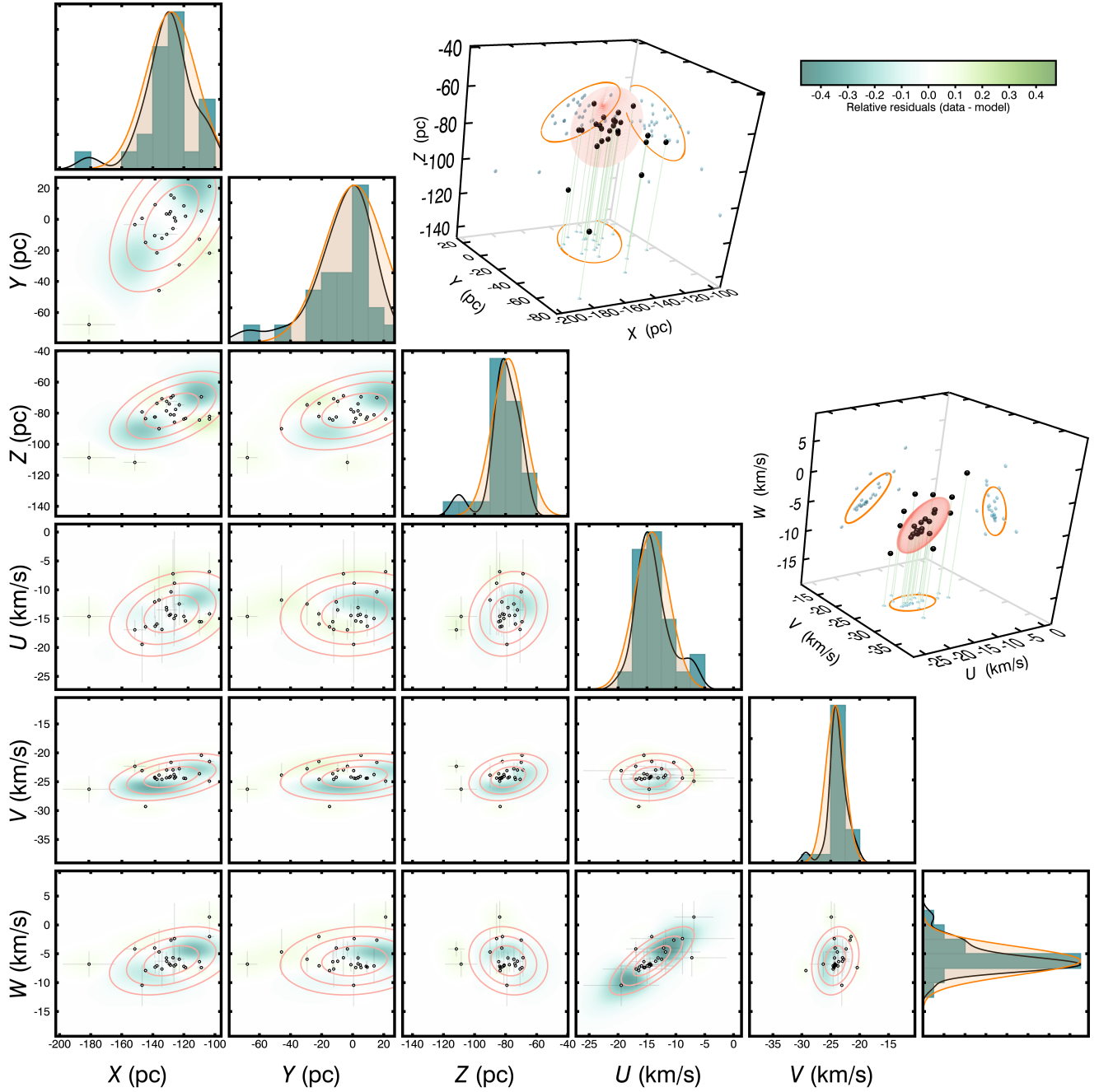


Figure 3. Multivariate Gaussian model of MUTA built for BANYAN Σ . Orange lines show the 1, 2 and 3σ projected contours of the modeled members distribution, and black points represent individual members. Blue and green shadings represent regions of over (green) and under (blue) density of actual members compared to the model, and therefore correspond to departures from a multivariate Gaussian distribution. One-dimensional distributions are displayed as green bars, and are compared with a kernel density estimate distribution of the members (black line) and the projected model (orange lines). A single 1σ contour (orange surfaces) and individual members (black spheres) with their projections on the three axis planes are shown for the 3D model projections (upper right). See Section 3 for more details.

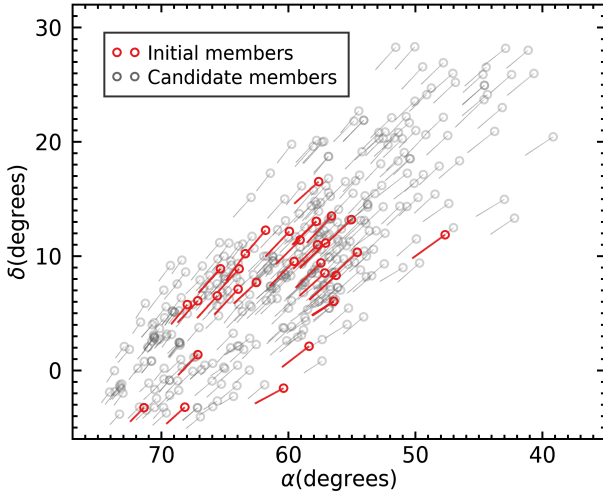


Figure 4. Sky positions and proper motion vectors for initial members of MUTA (red circles and lines) and additional candidate members recovered in this work (gray circles and lines). See Section 4 for more details.

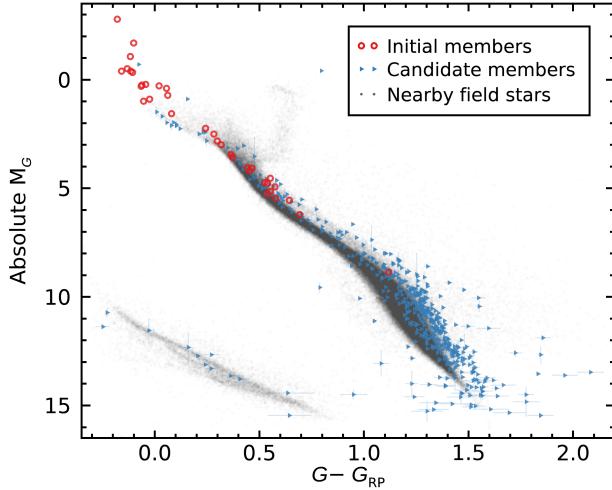


Figure 5. *Gaia* DR2 color-magnitude diagram of initial MUTA members (red circles) and candidate members (blue rightward triangles) recovered by BANYAN Σ based on their *Gaia* DR2 sky positions, proper motions, parallaxes and radial velocities when available. See Section 4 for more details.

We complemented our search for MUTA members with a subsequent search for stars co-moving with any one of the 540 members and candidate members. All *Gaia* DR2 entries within $180''$ of each MUTA candidate were inspected to find objects co-moving within 10 mas yr^{-1} and for which the proper motion difference is smaller than 5% of the measurement. For most *Gaia* DR2 entries, a parallax measurement is also available: in these cases, we also required the trigonometric distance of the two objects to be within 5 pc of each

other², and we set a maximum parallax difference at 5% of the parallax measurement.

This search identified 26 co-moving systems (52 components total) for which both components were already in the list of candidates, and 2 stars (2MASS J03424511+0754507 and 2MASS J02581815+2456552) not already included in our list, each seemingly co-moving with a pair of stars in our list of candidates but failing to meet our membership selection criteria (i.e., their Bayesian membership probabilities are 49% and 0% respectively). In addition to those, we identified 15 systems (21 system components) for which only one component was in our list of candidates because the other component failed to pass our membership selection criteria. All objects were added to our list of low-likelihood candidates for completion, and all co-moving systems are listed in Table 4.

² Throughout this work, we used a parallax zero-point of -0.029 mas (Lindegren et al. 2018) to convert parallaxes to trigonometric distances. We determined trigonometric distances $\varpi = 1/(\pi + 0.029)$ where π is the parallax with a standard error propagation, which is accurate enough for the current purposes given the nearby distances of the stars under consideration.

Table 3. List of new candidate members of MUTA identified in *Gaia* DR2 with BANYAN Σ .

MUTA	Object	R.A.	Decl.	$\mu_\alpha \cos \delta$	μ_δ	Parallax	RV	<i>Gaia</i> DR2
ID	Name	(hh:mm:ss.sss)	(dd:mm:ss.ss)	(mas yr $^{-1}$)	(mas yr $^{-1}$)	(mas)	(km s $^{-1}$)	<i>G</i> mag
31	2MASS J02363660+2026331	02:36:36.648	+20:26:32.84	40.3 \pm 1.4	-26.7 \pm 1.1	8.82 \pm 0.69	...	15.289
32	2MASS J02424085+2558585	02:42:40.905	+25:58:58.08	38.60 \pm 0.16	-31.61 \pm 0.14	8.80 \pm 0.11	...	16.090
33	HD 17008	02:44:30.027	+28:00:53.61	31.19 \pm 0.11	-25.95 \pm 0.10	7.372 \pm 0.066	4 \pm 2	7.909
34	2MASS J02484851+1319378	02:48:48.553	+13:19:37.66	34.627 \pm 0.062	-23.355 \pm 0.054	7.731 \pm 0.035	...	14.077
35	TYC 1785-155-1	02:49:43.813	+25:53:11.25	30.146 \pm 0.087	-26.174 \pm 0.077	7.036 \pm 0.044	7.2 \pm 0.3	11.679
36	2MASS J02513636+2811000	02:51:36.407	+28:10:59.60	32.002 \pm 0.073	-25.265 \pm 0.067	7.866 \pm 0.036	...	13.629
37	2MASS J02515956+1458162	02:51:59.618	+14:58:15.78	41.0 \pm 1.3	-24.72 \pm 0.99	8.68 \pm 0.78	...	19.815
38	2MASS J02523886+2300093	02:52:38.911	+23:00:08.53	35.50 \pm 0.63	-30.31 \pm 0.43	8.30 \pm 0.32	...	18.548
39	GSC 01230-00749	02:55:04.011	+20:55:18.64	39.250 \pm 0.075	-30.957 \pm 0.067	7.892 \pm 0.043	...	11.948
40	2MASS J02571995+2408232	02:57:19.993	+24:08:22.54	36.577 \pm 0.069	-30.638 \pm 0.060	7.144 \pm 0.038	4 \pm 1	12.207
41	TYC 1790-927-1	02:57:43.023	+26:32:03.61	31.150 \pm 0.082	-27.362 \pm 0.075	7.419 \pm 0.043	8 \pm 2	11.326
42 B	Gaia DR2 113410746049727744	02:58:16.476	+24:56:42.65	31.83 \pm 0.38	-28.33 \pm 0.24	6.67 \pm 0.23	...	16.776
42 A	2MASS J02581643+2456424	02:58:16.484	+24:56:41.76	31.65 \pm 0.33	-27.54 \pm 0.26	7.84 \pm 0.21	...	15.193
43	2MASS J02582387+2341382	02:58:23.907	+23:41:37.47	41.63 \pm 0.24	-39.99 \pm 0.20	9.21 \pm 0.20	...	15.832
44	TYC 1786-525-1	02:58:43.640	+25:53:38.92	28.771 \pm 0.096	-25.991 \pm 0.073	6.893 \pm 0.054	...	10.611
45	2MASS J03060696+1820259	03:06:06.995	+18:20:25.43	29.66 \pm 0.81	-25.25 \pm 0.65	7.07 \pm 0.62	...	19.550
46	2MASS J03072480+2512266	03:07:24.844	+25:12:25.96	31.627 \pm 0.096	-30.038 \pm 0.090	7.447 \pm 0.045	...	14.311
47	2MASS J03080089+1229304	03:08:00.939	+12:29:29.89	30.16 \pm 0.25	-24.14 \pm 0.24	7.22 \pm 0.13	...	15.820
48	HAT 258-02140	03:08:12.369	+25:59:26.76	32.075 \pm 0.080	-27.934 \pm 0.066	7.536 \pm 0.048	9 \pm 1	12.372
49	2MASS J03092962+1436212	03:09:29.670	+14:36:21.03	37.35 \pm 0.10	-26.040 \pm 0.076	7.217 \pm 0.064	...	13.889
50	2MASS J03094950+2033183	03:09:49.537	+20:33:17.96	30.47 \pm 0.88	-28.09 \pm 0.62	6.85 \pm 0.39	...	18.117
51	2MASS J03111256+2655141	03:11:12.603	+26:55:13.54	32.06 \pm 0.19	-31.20 \pm 0.12	7.58 \pm 0.11	...	15.099
52	2MASS J03111286+2208510	03:11:12.890	+22:08:50.60	26.66 \pm 0.16	-25.57 \pm 0.12	6.760 \pm 0.087	...	15.496
53	HAT 306-07804	03:12:31.219	+17:52:45.99	28.46 \pm 0.16	-26.85 \pm 0.12	7.130 \pm 0.074	...	15.091
54	WISEA J031350.31+152530.2	03:13:50.319	+15:25:29.96	29.8 \pm 3.5	-27.4 \pm 2.9	8.3 \pm 1.8	...	20.723
55	2MASS J03145892+2442227	03:14:58.962	+24:42:22.03	27.43 \pm 0.49	-26.83 \pm 0.39	6.88 \pm 0.27	...	18.409
56	HAT 259-01962	03:16:28.094	+24:07:40.18	25.01 \pm 0.12	-24.149 \pm 0.087	5.842 \pm 0.061	9 \pm 1	11.905
57	WISEA J031644.41+203733.1	03:16:44.427	+20:37:32.91	31.7 \pm 3.5	-33.7 \pm 2.7	7.4 \pm 1.8	...	20.812
58	2MASS J03173044+1708397	03:17:30.472	+17:08:39.41	27.00 \pm 0.19	-24.36 \pm 0.16	6.582 \pm 0.094	...	16.287
59	2MASS J03174414+2633589	03:17:44.180	+26:33:58.50	30.21 \pm 0.74	-32.37 \pm 0.67	7.57 \pm 0.48	...	17.935
60	2MASS J03184219+0924050	03:18:42.227	+09:24:04.57	31.36 \pm 0.18	-27.61 \pm 0.14	7.637 \pm 0.086	...	16.087
61	2MASS J03191104+1508330	03:19:11.110	+15:08:32.00	27.23 \pm 0.34	-26.54 \pm 0.29	6.65 \pm 0.22	...	18.175

Table 3 *continued*

Table 3 (*continued*)

MUTA	Object	R.A.	Decl.	$\mu_\alpha \cos \delta$	μ_δ	Parallax	RV	<i>Gaia</i> DR2
ID	Name	(hh:mm:ss.sss)	(dd:mm:ss.ss)	(mas yr $^{-1}$)	(mas yr $^{-1}$)	(mas)	(km s $^{-1}$)	<i>G</i> mag
62	2MASS J03194193+1130168	03:19:41.968	+11:30:16.39	27.99 ± 0.18	-24.75 ± 0.15	6.923 ± 0.099	...	16.531
63	2MASS J03195293+2059291	03:19:52.955	+20:59:28.69	24.23 ± 0.19	-24.75 ± 0.18	6.268 ± 0.098	...	15.967
64	2MASS J03201019+2333336	03:20:10.218	+23:33:33.44	28.444 ± 0.076	-27.092 ± 0.057	6.748 ± 0.044	...	13.859
65	HD 20635	03:20:12.410	+28:19:22.21	28.542 ± 0.089	-32.403 ± 0.071	7.137 ± 0.048	...	8.856
66	2MASS J03202513+1622136	03:20:25.170	+16:22:13.22	29.16 ± 0.93	-22.57 ± 0.72	6.00 ± 0.55	...	19.099
67	HAT 307-08212	03:21:38.153	+18:31:27.69	24.12 ± 0.20	-23.23 ± 0.16	5.89 ± 0.10	...	15.190
68	HAT 307-05183	03:21:47.767	+18:31:36.03	35.621 ± 0.091	-31.760 ± 0.078	9.148 ± 0.042	...	13.895
69	2MASS J03215583+2140162	03:21:55.877	+21:40:15.73	33.29 ± 0.38	-28.42 ± 0.27	7.24 ± 0.20	...	14.569
70	2MASS J03223315+1715182	03:22:33.202	+17:15:17.93	41.09 ± 0.29	-31.80 ± 0.23	9.60 ± 0.15	...	16.049
71	2MASS J03223957+1420316	03:22:39.615	+14:20:31.22	29.23 ± 0.19	-27.38 ± 0.15	7.48 ± 0.11	...	16.419
72	HAT 259-12052	03:22:54.201	+22:12:41.40	25.6 ± 1.0	-27.38 ± 0.89	6.86 ± 0.51	...	15.856
73	2MASS J03233089+1903574	03:23:30.933	+19:03:56.97	25.82 ± 0.24	-25.58 ± 0.15	6.83 ± 0.11	...	16.285
74	2MASS J03235482+0859547	03:23:54.865	+08:59:54.52	33.22 ± 0.18	-19.84 ± 0.15	7.94 ± 0.10	...	16.129
75	2MASS J03240542+2016260	03:24:05.456	+20:16:25.53	27.65 ± 0.31	-27.02 ± 0.26	6.18 ± 0.17	...	17.238
76	2MASS J03245387+1422189	03:24:53.906	+14:22:18.48	26.57 ± 0.68	-25.87 ± 0.56	6.88 ± 0.41	...	18.930
77	2MASS J03252139+2048507	03:25:21.425	+20:48:50.36	23.3 ± 1.8	-24.0 ± 1.4	6.5 ± 1.2	...	20.471
78	2MASS J03252961+1819289	03:25:29.653	+18:19:29.07	26.1 ± 1.5	-22.9 ± 1.1	5.76 ± 0.82	...	18.850
79	2MASS J03261339+2816284	03:26:13.431	+28:16:27.98	29.11 ± 0.22	-32.31 ± 0.16	8.01 ± 0.13	...	15.526
80	2MASS J03263469+2021019	03:26:34.742	+20:21:01.57	29.35 ± 0.55	-26.59 ± 0.39	6.28 ± 0.32	...	18.653
81	TYC 1245-1095-1	03:27:29.236	+22:06:51.08	30.69 ± 0.11	-29.241 ± 0.075	7.712 ± 0.069	...	10.523
82	2MASS J03283913+1945195	03:28:39.166	+19:45:19.10	24.92 ± 0.90	-27.46 ± 0.68	6.57 ± 0.46	...	19.382
83	HAT 259-04655	03:29:33.974	+20:51:37.51	26.57 ± 0.17	-24.69 ± 0.13	6.899 ± 0.097	...	13.614
84	2MASS J03293496+1200269	03:29:34.998	+12:00:26.54	28.1 ± 1.2	-27.44 ± 0.89	8.36 ± 0.78	...	19.577
85	2MASS J03294963+0919493	03:29:49.665	+09:19:48.97	29.76 ± 0.19	-25.83 ± 0.14	7.38 ± 0.12	...	15.420
86	2MASS J03300964+1419314	03:30:09.685	+14:19:30.98	26.19 ± 0.19	-24.74 ± 0.14	6.70 ± 0.11	...	16.324
87	HAT 259-09674	03:30:10.617	+20:19:25.25	25.064 ± 0.088	-25.274 ± 0.069	6.328 ± 0.052	...	14.673
88	2MASS J03303685+1610599	03:30:36.887	+16:10:59.58	26.04 ± 0.18	-21.29 ± 0.13	5.697 ± 0.086	...	15.934
89	2MASS J03305533+1804535	03:30:55.357	+18:04:52.97	22.88 ± 0.46	-24.40 ± 0.36	6.37 ± 0.28	...	18.539
90	2MASS J03312734+2015412	03:31:27.389	+20:15:40.71	35.08 ± 0.20	-30.26 ± 0.12	8.988 ± 0.088	...	15.685
91	HAT 259-13539	03:31:31.957	+20:49:10.44	23.90 ± 0.20	-24.17 ± 0.14	5.866 ± 0.096	...	15.419
92	2MASS J03322249+1213231	03:32:22.541	+12:13:22.52	32.5 ± 1.3	-22.87 ± 0.92	6.62 ± 0.68	...	19.743
93	2MASS J03324777+1528240	03:32:47.809	+15:28:23.64	24.91 ± 0.21	-24.57 ± 0.20	6.61 ± 0.11	...	16.278
94	V1267 Tau	03:33:11.649	+10:35:55.67	26.370 ± 0.088	-25.552 ± 0.057	7.277 ± 0.042	15 ± 1	11.861
95	HD 22073	03:33:46.512	+08:17:25.71	27.040 ± 0.095	-23.569 ± 0.091	6.788 ± 0.052	...	8.647

Table 3 *continued*

Table 3 (*continued*)

MUTA	Object	R.A.	Decl.	$\mu_\alpha \cos \delta$	μ_δ	Parallax	RV	<i>Gaia</i> DR2
ID	Name	(hh:mm:ss.sss)	(dd:mm:ss.ss)	(mas yr $^{-1}$)	(mas yr $^{-1}$)	(mas)	(km s $^{-1}$)	<i>G</i> mag
96	2MASS J03350134+1418016	03:35:01.376	+14:18:01.14	28.77 ± 0.14	-20.69 ± 0.12	6.765 ± 0.075	...	13.865
97 B	2MASS J03350317+1431358	03:35:03.209	+14:31:35.33	26.87 ± 0.39	-25.57 ± 0.30	6.84 ± 0.24	...	18.097
97 A	2MASS J03350340+1431490	03:35:03.438	+14:31:48.54	26.99 ± 0.14	-25.93 ± 0.11	7.342 ± 0.081	...	15.369
98	2MASS J03352364+1000080	03:35:23.679	+10:00:07.69	24.58 ± 0.12	-22.256 ± 0.092	6.246 ± 0.070	...	15.040
99	2MASS J03352860+0811571	03:35:28.641	+08:11:56.80	27.44 ± 0.22	-23.75 ± 0.19	6.98 ± 0.12	...	16.491
100	2MASS J03353487+1253011	03:35:34.911	+12:53:00.73	24.773 ± 0.059	-24.208 ± 0.041	6.079 ± 0.031	...	13.788
101	2MASS J03355092+1516555	03:35:50.949	+15:16:55.15	24.01 ± 0.58	-25.83 ± 0.44	6.61 ± 0.29	...	18.294
102	2MASS J03360543+1026514	03:36:05.464	+10:26:51.20	23.36 ± 0.23	-21.64 ± 0.15	5.961 ± 0.097	...	16.632
103	2MASS J03360640+1307422	03:36:06.439	+13:07:41.76	27.85 ± 0.23	-25.85 ± 0.17	6.90 ± 0.13	...	17.180
104 B	2MASS J03361732+2153271	03:36:17.360	+21:53:26.42	29.95 ± 0.71	-31.17 ± 0.52	7.98 ± 0.31	...	18.454
104 A	2MASS J03361762+2153391	03:36:17.665	+21:53:38.50	29.492 ± 0.088	-30.262 ± 0.068	7.526 ± 0.047	10.7 ± 0.7	10.910
105	2MASS J03361892+0441323	03:36:18.952	+04:41:32.11	29.45 ± 0.11	-24.805 ± 0.087	7.496 ± 0.061	...	15.493
106	2MASS J03364987+1908056	03:36:49.894	+19:08:05.23	24.20 ± 0.20	-24.87 ± 0.16	6.60 ± 0.12	...	16.524
107	2MASS J03371337+1307315	03:37:13.411	+13:07:30.93	25.21 ± 0.19	-24.95 ± 0.13	6.379 ± 0.089	...	14.923
108	2MASS J03371793+0847343	03:37:17.966	+08:47:34.12	27.68 ± 0.19	-24.86 ± 0.15	6.98 ± 0.11	...	16.223
109	2MASS J03373508+1705162	03:37:35.111	+17:05:15.93	23.681 ± 0.071	-23.716 ± 0.050	6.298 ± 0.035	13 ± 8	13.062
110	2MASS J03375097+2242056	03:37:51.014	+22:42:05.05	26.09 ± 0.17	-31.44 ± 0.11	6.702 ± 0.090	...	16.095
111	2MASS J03384902+1021482	03:38:49.051	+10:21:48.07	25.72 ± 0.18	-23.97 ± 0.12	6.75 ± 0.11	...	15.552
112	2MASS J03385230+1635406	03:38:52.328	+16:35:40.21	22.94 ± 0.17	-25.65 ± 0.13	6.296 ± 0.096	...	15.867
113	2MASS J03391042+0927570	03:39:10.451	+09:27:56.71	24.434 ± 0.086	-24.441 ± 0.057	6.914 ± 0.043	17 ± 2	12.403
114	HAT 259–10551	03:39:21.160	+21:49:08.74	29.50 ± 0.10	-29.756 ± 0.066	7.361 ± 0.049	...	14.824
115	TYC 1235–156–1	03:39:39.516	+15:29:54.47	25.96 ± 0.19	-26.86 ± 0.14	6.41 ± 0.11	16 ± 1	11.230
116	2MASS J03403696+1117333	03:40:36.991	+11:17:32.97	27.113 ± 0.072	-25.476 ± 0.043	6.979 ± 0.035	...	13.780
117 B	2MASS J03405723+1308577	03:40:57.261	+13:08:57.23	27.03 ± 0.71	-24.78 ± 0.50	7.19 ± 0.33	...	18.437
117 A	TYC 663–362–1	03:40:57.781	+13:09:03.06	24.66 ± 0.25	-25.44 ± 0.21	6.749 ± 0.098	13 ± 1	10.493
118	2MASS J03410548+0527140	03:41:05.509	+05:27:13.69	26.93 ± 0.14	-23.63 ± 0.11	7.035 ± 0.065	...	15.051
119	2MASS J03410792+0917050	03:41:07.955	+09:17:04.85	24.99 ± 0.17	-23.19 ± 0.10	6.662 ± 0.077	...	14.698
120	2MASS J03413165+0401345	03:41:31.685	+04:01:34.21	31.68 ± 0.11	-19.807 ± 0.072	8.167 ± 0.045	...	14.011
121	TYC 660–135–1	03:41:45.000	+10:54:27.46	26.399 ± 0.073	-25.756 ± 0.047	7.108 ± 0.037	14.5 ± 0.9	11.362
122	2MASS J03420359+1631392	03:42:03.617	+16:31:38.80	24.365 ± 0.063	-24.625 ± 0.044	6.616 ± 0.032	...	13.901
123	2MASS J03423560+0945463	03:42:35.636	+09:45:45.89	25.71 ± 0.90	-23.90 ± 0.62	6.24 ± 0.53	...	19.257
124	2MASS J03425497+1114570	03:42:54.990	+11:14:57.28	23.1 ± 2.8	-18.9 ± 1.8	4.9 ± 1.5	...	20.158
125	WD 0340+103	03:43:14.370	+10:29:38.14	31.51 ± 0.18	-22.55 ± 0.12	6.83 ± 0.11	...	16.539
126	2MASS J03431821+1222515	03:43:18.246	+12:22:51.12	23.0 ± 1.3	-21.38 ± 0.76	5.78 ± 0.67	...	19.647

Table 3 *continued*

Table 3 (*continued*)

MUTA	Object	R.A.	Decl.	$\mu_\alpha \cos \delta$	μ_δ	Parallax	RV	<i>Gaia</i> DR2
ID	Name	(hh:mm:ss.sss)	(dd:mm:ss.ss)	(mas yr $^{-1}$)	(mas yr $^{-1}$)	(mas)	(km s $^{-1}$)	<i>G</i> mag
127	2MASS J03433413+0701547	03:43:34.158	+07:01:54.39	21.40 \pm 0.24	-14.78 \pm 0.17	5.46 \pm 0.13	...	17.079
128	2MASS J03441167+1405312	03:44:11.716	+14:05:30.58	27.61 \pm 0.54	-23.26 \pm 0.38	6.58 \pm 0.28	...	18.563
129	2MASS J03441728+1118090	03:44:17.312	+11:18:08.70	26.25 \pm 0.34	-24.83 \pm 0.23	7.31 \pm 0.17	...	17.243
130 A	2MASS J03442859+0716100	03:44:28.602	+07:16:10.10	25.80 \pm 0.18	-22.56 \pm 0.15	6.61 \pm 0.11	...	16.327
130 B	Gaia DR2 3277686910210391424	03:44:28.657	+07:16:08.46	24.39 \pm 0.21	-23.66 \pm 0.17	6.71 \pm 0.12	...	16.596
131	2MASS J03443022+1130035	03:44:30.254	+11:30:03.21	25.26 \pm 0.11	-24.176 \pm 0.086	6.640 \pm 0.060	...	13.875
132	2MASS J03443526+1257315	03:44:35.300	+12:57:31.25	24.61 \pm 0.19	-24.01 \pm 0.13	6.43 \pm 0.11	...	16.583
133	2MASS J03444292+0944150	03:44:42.955	+09:44:14.73	22.64 \pm 0.12	-24.009 \pm 0.070	6.626 \pm 0.058	...	14.663
134	2MASS J03444719+1034332	03:44:47.224	+10:34:32.89	23.6 \pm 1.2	-22.95 \pm 0.81	5.66 \pm 0.77	...	20.045
135	2MASS J03450918+0612030	03:45:09.226	+06:12:02.81	21.83 \pm 0.20	-14.18 \pm 0.17	5.64 \pm 0.14	...	16.903
136	2MASS J03451333+0836589	03:45:13.365	+08:36:58.56	26.36 \pm 0.35	-23.83 \pm 0.23	6.43 \pm 0.17	...	17.080
140	TYC 658-828-1	03:45:52.146	+08:32:26.87	27.78 \pm 0.10	-24.644 \pm 0.058	7.552 \pm 0.050	15.6 \pm 0.6	11.471
141	2MASS J03460026+0628092	03:46:00.288	+06:28:09.02	22.01 \pm 0.46	-14.51 \pm 0.34	5.77 \pm 0.26	...	18.477
142	2MASS J03460029+0836331	03:46:00.335	+08:36:32.86	27.79 \pm 0.22	-24.83 \pm 0.14	7.33 \pm 0.13	...	16.316
143	2MASS J03460544+0553074	03:46:05.468	+05:53:07.16	21.41 \pm 0.20	-13.93 \pm 0.15	5.565 \pm 0.094	...	16.429
144 A	2MASS J03463553+1317056	03:46:35.533	+13:17:06.31	22.17 \pm 0.26	-24.02 \pm 0.17	6.33 \pm 0.14	...	17.335
144 B	Gaia DR2 37943944413361792	03:46:35.594	+13:17:04.31	23.04 \pm 0.30	-24.20 \pm 0.20	6.51 \pm 0.16	...	17.365
145	2MASS J03464763+1514201	03:46:47.664	+15:14:19.68	24.12 \pm 0.45	-25.06 \pm 0.29	6.73 \pm 0.25	...	18.282
146	2MASS J03465210+0704410	03:46:52.139	+07:04:40.66	27.05 \pm 0.16	-22.84 \pm 0.11	6.608 \pm 0.085	...	14.155
147	2MASS J03465422+0720390	03:46:54.253	+07:20:38.64	25.17 \pm 0.39	-22.94 \pm 0.32	6.99 \pm 0.21	...	17.957
148	2MASS J03465779+0956432	03:46:57.820	+09:56:42.80	27.26 \pm 0.40	-27.02 \pm 0.26	7.25 \pm 0.24	...	17.712
149	2MASS J03471144+0526234	03:47:11.466	+05:26:23.15	22.84 \pm 0.12	-19.71 \pm 0.10	6.095 \pm 0.067	...	14.611
150	BD+04 589	03:47:13.551	+05:26:23.49	22.654 \pm 0.098	-17.159 \pm 0.084	5.861 \pm 0.052	18 \pm 2	9.310
151	2MASS J03471736+1155459	03:47:17.401	+11:55:45.34	25.4 \pm 1.1	-25.66 \pm 0.79	6.39 \pm 0.76	...	19.801
152	2MASS J03472334+1533235	03:47:23.378	+15:33:23.17	21.73 \pm 0.19	-24.90 \pm 0.12	6.313 \pm 0.093	...	16.537
153 B	Gaia DR2 44752086050666368	03:47:23.645	+18:43:18.70	21.33 \pm 0.60	-26.33 \pm 0.57	6.36 \pm 0.34	...	17.855
153 A	TYC 1252-301-1	03:47:23.901	+18:43:17.68	21.128 \pm 0.079	-23.175 \pm 0.057	5.926 \pm 0.041	16.3 \pm 0.9	11.689
154	2MASS J03472375+1313154	03:47:23.802	+13:13:14.89	21.8 \pm 2.2	-18.5 \pm 1.5	4.86 \pm 0.99	...	20.281
155	2MASS J03472378+1648282	03:47:23.810	+16:48:27.82	24.81 \pm 0.31	-24.60 \pm 0.18	6.46 \pm 0.14	...	16.900
156	2MASS J03472404+0953136	03:47:24.078	+09:53:13.26	24.04 \pm 0.64	-24.66 \pm 0.44	6.41 \pm 0.38	...	18.901
157	BD+07 543	03:47:31.345	+07:57:26.39	25.369 \pm 0.081	-24.690 \pm 0.061	6.404 \pm 0.044	14.6 \pm 0.4	10.266
158	TYC 661-560-1	03:47:53.694	+11:48:57.98	21.230 \pm 0.076	-25.115 \pm 0.048	6.459 \pm 0.041	16 \pm 1	10.072
159	TYC 71-542-1	03:47:56.865	+06:16:06.67	21.191 \pm 0.082	-13.396 \pm 0.055	5.400 \pm 0.041	17 \pm 1	11.164
160	2MASS J03481036+1608419	03:48:10.391	+16:08:41.59	23.27 \pm 0.30	-25.24 \pm 0.23	6.23 \pm 0.16	...	17.616

Table 3 *continued*

Table 3 (*continued*)

MUTA	Object	R.A.	Decl.	$\mu_\alpha \cos \delta$	μ_δ	Parallax	RV	<i>Gaia</i> DR2
ID	Name	(hh:mm:ss.sss)	(dd:mm:ss.ss)	(mas yr $^{-1}$)	(mas yr $^{-1}$)	(mas)	(km s $^{-1}$)	<i>G</i> mag
161	2MASS J03484419+1213118	03:48:44.233	+12:13:11.48	23.753 ± 0.048	-23.215 ± 0.031	6.259 ± 0.027	12 ± 4	13.336
162	2MASS J03485029+2002281	03:48:50.333	+20:02:27.56	29.39 ± 0.11	-31.963 ± 0.054	7.776 ± 0.052	9 ± 2	12.807
163	2MASS J03485472+0727538	03:48:54.752	+07:27:53.54	24.85 ± 0.21	-22.35 ± 0.16	6.63 ± 0.11	...	16.744
164	2MASS J03492243+0242209	03:49:22.457	+02:42:20.68	23.208 ± 0.056	-13.737 ± 0.036	5.957 ± 0.026	17 ± 8	13.386
165	2MASS J03492441+0049520	03:49:24.445	+00:49:51.87	26.02 ± 0.10	-17.149 ± 0.092	6.261 ± 0.057	...	14.293
166	2MASS J03492817+1958226	03:49:28.213	+19:58:22.15	27.73 ± 0.82	-30.04 ± 0.45	6.95 ± 0.40	...	17.267
167	2MASS J03493857+0640562	03:49:38.593	+06:40:55.89	22.2 ± 1.0	-19.72 ± 0.76	5.83 ± 0.59	...	19.592
168	2MASS J03494198+1035258	03:49:42.006	+10:35:25.51	24.61 ± 0.12	-24.003 ± 0.084	6.642 ± 0.064	...	15.108
169	2MASS J03495031+1440552	03:49:50.345	+14:40:54.73	22.02 ± 0.19	-24.16 ± 0.13	6.43 ± 0.10	...	16.373
170	2MASS J03500539+1204146	03:50:05.425	+12:04:14.18	24.22 ± 0.34	-23.55 ± 0.27	6.50 ± 0.17	...	17.785
171	2MASS J03501719+1129445	03:50:17.220	+11:29:44.31	24.34 ± 0.23	-24.52 ± 0.15	6.63 ± 0.11	...	16.115
172	2MASS J03502412+0602279	03:50:24.145	+06:02:27.52	20.24 ± 0.36	-15.26 ± 0.28	5.61 ± 0.19	...	17.900
173	2MASS J03502880+1356125	03:50:28.831	+13:56:12.16	23.94 ± 0.12	-24.043 ± 0.071	6.662 ± 0.060	...	14.507
174	2MASS J03503310+0855492	03:50:33.122	+08:55:48.93	24.04 ± 0.29	-22.83 ± 0.17	6.46 ± 0.13	...	17.080
175	2MASS J03504400+1148329	03:50:44.033	+11:48:32.54	22.54 ± 0.15	-22.48 ± 0.11	6.015 ± 0.086	...	16.036
176	2MASS J03505375+1042075	03:50:53.778	+10:42:07.07	26.01 ± 0.25	-24.61 ± 0.20	7.07 ± 0.12	...	16.627
177 B	Gaia DR2 3277369048270999936	03:50:56.968	+07:30:53.92	27.9 ± 2.2	-21.7 ± 1.4	6.3 ± 1.3	...	20.438
177 A	2MASS J03505694+0730565	03:50:56.976	+07:30:56.18	30.41 ± 0.23	-22.22 ± 0.16	8.29 ± 0.12	...	16.916
178	2MASS J03510483+0910174	03:51:04.862	+09:10:17.03	24.31 ± 0.53	-22.33 ± 0.35	6.49 ± 0.28	...	18.489
179	2MASS J03510528+1431333	03:51:05.296	+14:31:33.07	20.64 ± 0.24	-23.59 ± 0.17	6.43 ± 0.11	...	16.510
180	2MASS J03510854+0829205	03:51:08.572	+08:29:20.31	25.93 ± 0.21	-24.43 ± 0.15	7.24 ± 0.11	...	16.382
181	2MASS J03510859+2007324	03:51:08.635	+20:07:32.13	29.7 ± 1.8	-31.8 ± 1.0	8.94 ± 0.77	...	18.781
183	2MASS J03514618+0553543	03:51:46.218	+05:53:54.13	23.11 ± 0.22	-16.70 ± 0.16	5.85 ± 0.11	...	16.807
184	2MASS J03514810+0850170	03:51:48.120	+08:50:16.66	25.43 ± 0.59	-24.89 ± 0.44	6.85 ± 0.32	...	18.627
185	2MASS J03520563+1545160	03:52:05.659	+15:45:15.71	28.41 ± 0.17	-32.69 ± 0.11	7.553 ± 0.099	...	15.497
186	2MASS J03521195+1936160	03:52:11.985	+19:36:15.78	26.19 ± 0.90	-29.17 ± 0.51	6.27 ± 0.49	...	19.095
187	2MASS J03523091+1225547	03:52:30.941	+12:25:54.15	25.5 ± 1.3	-26.2 ± 1.0	7.20 ± 0.59	...	19.914
188 B	Gaia DR2 3301507795268229248	03:52:40.165	+08:30:30.19	21.32 ± 0.38	-21.97 ± 0.25	5.51 ± 0.19	...	17.668
188 A	2MASS J03524018+0830333	03:52:40.220	+08:30:33.13	21.96 ± 0.17	-22.24 ± 0.11	5.458 ± 0.084	...	16.006
189	2MASS J03524910+1423538	03:52:49.132	+14:23:53.30	24.9 ± 2.1	-23.8 ± 1.2	6.07 ± 0.91	...	20.410
190	WD 0350+098	03:53:15.739	+09:56:33.41	25.93 ± 0.24	-25.28 ± 0.15	7.14 ± 0.12	...	17.098
191	2MASS J03535812+0520312	03:53:58.148	+05:20:30.94	24.52 ± 0.24	-17.12 ± 0.17	6.46 ± 0.13	...	16.996
192	2MASS J03543000+0419403	03:54:30.036	+04:19:40.10	23.53 ± 0.20	-15.22 ± 0.14	6.026 ± 0.092	...	16.268
193	2MASS J03543784+0742234	03:54:37.870	+07:42:23.14	24.60 ± 0.47	-22.98 ± 0.28	7.04 ± 0.24	...	18.159

Table 3 *continued*

Table 3 (*continued*)

MUTA	Object	R.A.	Decl.	$\mu_\alpha \cos \delta$	μ_δ	Parallax	RV	<i>Gaia</i> DR2
ID	Name	(hh:mm:ss.sss)	(dd:mm:ss.ss)	(mas yr $^{-1}$)	(mas yr $^{-1}$)	(mas)	(km s $^{-1}$)	<i>G</i> mag
194	2MASS J03544964+0437268	03:54:49.676	+04:37:26.45	25.85 ± 0.10	-22.798 ± 0.080	7.027 ± 0.065	...	14.724
195	2MASS J03545074+1232061	03:54:50.776	+12:32:05.61	29.27 ± 0.13	-24.677 ± 0.097	7.919 ± 0.068	16 ± 3	12.524
196	2MASS J03550706+0741539	03:55:07.096	+07:41:53.55	25.97 ± 0.92	-23.20 ± 0.60	8.06 ± 0.63	...	19.272
197	2MASS J03551351+0648484	03:55:13.543	+06:48:48.01	30.19 ± 0.83	-27.80 ± 0.58	7.70 ± 0.47	...	19.036
198	2MASS J03551355+0332501	03:55:13.587	+03:32:49.83	25.48 ± 0.37	-19.35 ± 0.30	5.59 ± 0.20	...	18.214
199	2MASS J03552065+0955146	03:55:20.677	+09:55:14.28	23.75 ± 0.17	-23.32 ± 0.13	6.568 ± 0.090	...	16.318
200	2MASS J03554367+0729535	03:55:43.715	+07:29:53.14	25.73 ± 0.53	-23.81 ± 0.32	6.90 ± 0.26	...	18.250
201	2MASS J03554401+0918030	03:55:44.053	+09:18:02.63	25.20 ± 0.22	-24.60 ± 0.13	6.657 ± 0.099	...	16.500
202	HD 285262	03:55:50.274	+16:08:33.53	22.113 ± 0.095	-27.206 ± 0.062	6.997 ± 0.050	16.3 ± 0.4	9.657
203	2MASS J03555345+0305143	03:55:53.461	+03:05:14.22	20.345 ± 0.061	-12.542 ± 0.047	5.376 ± 0.035	19 ± 1	11.717
204	HD 286380	03:56:20.741	+10:47:47.24	24.658 ± 0.077	-25.252 ± 0.050	6.743 ± 0.045	14.7 ± 0.8	10.293
205	TYC 665-460-1	03:56:31.738	+13:42:38.55	30.67 ± 0.21	-32.01 ± 0.14	8.21 ± 0.11	18.2 ± 0.7	11.718
206	2MASS J03564937+1010254	03:56:49.397	+10:10:25.01	23.90 ± 0.49	-24.14 ± 0.31	6.64 ± 0.26	...	17.467
207	2MASS J03570495+0255022	03:57:04.974	+02:55:01.98	26.00 ± 0.55	-21.34 ± 0.43	6.63 ± 0.30	...	18.701
208	2MASS J03573875+1142322	03:57:38.786	+11:42:31.85	23.298 ± 0.085	-23.208 ± 0.058	6.433 ± 0.040	...	14.377
209	2MASS J03585885+1947174	03:58:58.880	+19:47:16.92	20.94 ± 0.14	-27.129 ± 0.075	5.795 ± 0.080	...	15.233
210	2MASS J03585948+0605315	03:58:59.503	+06:05:31.21	24.36 ± 0.52	-22.55 ± 0.27	6.64 ± 0.22	...	17.435
211	2MASS J03590008+0350125	03:59:00.112	+03:50:12.26	23.78 ± 0.26	-21.91 ± 0.20	6.39 ± 0.15	...	17.500
212	2MASS J03591525+0817203	03:59:15.275	+08:17:19.83	25.603 ± 0.087	-25.603 ± 0.052	6.645 ± 0.049	...	13.249
213	2MASS J03595819+0527061	03:59:58.221	+05:27:05.66	24.33 ± 0.39	-23.23 ± 0.31	6.74 ± 0.20	...	17.954
214	2MASS J04000097+1136402	04:00:01.009	+11:36:40.01	24.19 ± 0.17	-25.30 ± 0.11	6.779 ± 0.087	...	16.114
215	2MASS J04000304+0839111	04:00:03.068	+08:39:10.67	23.29 ± 0.21	-22.67 ± 0.14	6.28 ± 0.11	...	16.703
216	2MASS J04003178+0235333	04:00:31.808	+02:35:33.07	23.92 ± 0.14	-20.77 ± 0.11	6.520 ± 0.080	...	15.539
217	2MASS J04003789+0921594	04:00:37.913	+09:21:59.15	22.72 ± 0.15	-22.632 ± 0.089	6.341 ± 0.079	...	15.592
218	2MASS J04004014+0806279	04:00:40.176	+08:06:27.61	24.01 ± 0.53	-24.11 ± 0.29	6.60 ± 0.28	...	18.413
219	2MASS J04005555+1306243	04:00:55.592	+13:06:24.00	18.52 ± 0.18	-21.32 ± 0.10	4.984 ± 0.098	...	16.165
220	2MASS J04005940+0826212	04:00:59.429	+08:26:20.90	21.35 ± 0.77	-19.34 ± 0.51	4.89 ± 0.38	...	18.532
221	2MASS J04011013+0824204	04:01:10.160	+08:24:20.04	23.11 ± 0.23	-22.33 ± 0.15	6.53 ± 0.11	...	16.796
222	2MASS J04011073+1459513	04:01:10.773	+14:59:51.01	24.81 ± 0.48	-27.77 ± 0.28	6.23 ± 0.25	...	18.212
223	2MASS J04012320+0342315	04:01:23.221	+03:42:31.11	24.90 ± 0.15	-22.77 ± 0.12	7.078 ± 0.092	...	15.515
224	2MASS J04014357+0345102	04:01:43.594	+03:45:09.93	21.02 ± 0.25	-19.90 ± 0.21	6.11 ± 0.14	...	17.282
225 B	2MASS J04021257+0817410	04:02:12.593	+08:17:40.67	22.00 ± 0.36	-23.46 ± 0.25	6.19 ± 0.19	...	17.316
225 A	2MASS J04021281+0817400	04:02:12.839	+08:17:39.75	23.38 ± 0.24	-22.68 ± 0.17	6.62 ± 0.13	...	16.635
226	2MASS J04024742+0946340	04:02:47.438	+09:46:33.61	20.112 ± 0.061	-25.812 ± 0.043	6.781 ± 0.030	...	13.898

Table 3 *continued*

Table 3 (*continued*)

MUTA	Object	R.A.	Decl.	$\mu_\alpha \cos \delta$	μ_δ	Parallax	RV	<i>Gaia</i> DR2
ID	Name	(hh:mm:ss.sss)	(dd:mm:ss.ss)	(mas yr $^{-1}$)	(mas yr $^{-1}$)	(mas)	(km s $^{-1}$)	<i>G</i> mag
227	2MASS J04032655+1218397	04:03:26.599	+12:18:39.32	24.30 \pm 0.53	-25.91 \pm 0.32	6.61 \pm 0.33	...	18.748
228	2MASS J04033422+0617517	04:03:34.258	+06:17:51.37	23.74 \pm 0.29	-22.36 \pm 0.19	6.99 \pm 0.17	...	17.197
229	2MASS J04035178+0709082	04:03:51.798	+07:09:07.97	20.11 \pm 0.40	-22.27 \pm 0.22	6.08 \pm 0.21	...	17.710
230	2MASS J04041708+0924123	04:04:17.095	+09:24:11.81	25.4 \pm 2.6	-24.2 \pm 1.6	8.2 \pm 2.1	...	20.892
231 A	2MASS J04044937+0935076	04:04:49.382	+09:35:07.13	22.40 \pm 0.18	-24.31 \pm 0.11	6.599 \pm 0.096	...	15.410
231 B	Gaia DR2 3301900595795159040	04:04:49.493	+09:35:07.71	24.12 \pm 0.28	-23.21 \pm 0.17	6.90 \pm 0.15	...	16.845
232	2MASS J04045070+0956109	04:04:50.733	+09:56:10.59	22.90 \pm 0.21	-23.90 \pm 0.13	6.61 \pm 0.11	...	16.198
233	2MASS J04050036+1000386	04:05:00.348	+10:00:38.31	21.6 \pm 3.5	-24.1 \pm 2.1	6.3 \pm 1.6	...	20.494
234	2MASS J04051287+0710190	04:05:12.893	+07:10:18.85	22.50 \pm 0.28	-21.91 \pm 0.18	6.31 \pm 0.14	...	17.087
235	2MASS J04052254+0615339	04:05:22.561	+06:15:33.36	23.33 \pm 0.40	-22.65 \pm 0.25	6.52 \pm 0.22	...	17.489
236 B	Gaia DR2 3297969498128206208	04:05:40.167	+07:22:12.08	19.0 \pm 1.9	-17.24 \pm 0.93	4.69 \pm 0.84	...	20.068
236 A	2MASS J04054018+0722109	04:05:40.210	+07:22:10.83	20.45 \pm 0.35	-18.09 \pm 0.20	4.74 \pm 0.17	...	17.633
237	2MASS J04054131+1715471	04:05:41.327	+17:15:46.81	20.05 \pm 0.14	-25.796 \pm 0.078	6.602 \pm 0.066	...	15.456
238	2MASS J04061902+0845408	04:06:19.044	+08:45:40.59	18.1 \pm 4.1	-16.0 \pm 2.2	4.7 \pm 1.5	...	20.583
239	2MASS J04064005+0856259	04:06:40.090	+08:56:25.62	23.44 \pm 0.33	-24.54 \pm 0.24	7.18 \pm 0.18	...	17.955
240	2MASS J04064920+1000435	04:06:49.247	+10:00:43.19	18.65 \pm 0.72	-19.75 \pm 0.44	5.35 \pm 0.37	...	19.063
241	2MASS J04070083+0607080	04:07:00.864	+06:07:07.56	27.86 \pm 0.17	-26.03 \pm 0.10	8.357 \pm 0.093	...	15.701
242	2MASS J04072953-0115000	04:07:29.559	-01:15:00.13	24.02 \pm 0.15	-20.20 \pm 0.10	6.927 \pm 0.081	...	15.713
243	2MASS J04074422+0959349	04:07:44.244	+09:59:34.57	22.41 \pm 0.42	-22.01 \pm 0.24	6.29 \pm 0.20	...	17.906
244	TYC 666-80-1	04:09:47.527	+07:48:03.29	21.62 \pm 0.11	-22.284 \pm 0.065	6.309 \pm 0.051	19 \pm 3	10.367
245	2MASS J04100909+0216157	04:10:09.119	+02:16:15.24	20.08 \pm 0.30	-20.56 \pm 0.20	6.62 \pm 0.17	...	18.136
246	2MASS J04104612+1040529	04:10:46.132	+10:40:52.68	18.06 \pm 0.63	-16.99 \pm 0.51	5.82 \pm 0.41	...	18.900
247	2MASS J04110212+0822096	04:11:02.165	+08:22:09.33	17.4 \pm 1.5	-15.5 \pm 1.3	5.86 \pm 0.86	...	20.313
248	2MASS J04112808+1143403	04:11:28.115	+11:43:40.10	16.60 \pm 0.47	-21.43 \pm 0.34	5.30 \pm 0.24	...	16.337
249	2MASS J04114261+0534427	04:11:42.638	+05:34:42.48	20.50 \pm 0.95	-22.89 \pm 0.50	6.25 \pm 0.46	...	19.039
250	2MASS J04114611+1508252	04:11:46.135	+15:08:24.90	25.57 \pm 0.47	-28.48 \pm 0.33	7.24 \pm 0.26	...	15.689
251	2MASS J04121099+0248564	04:12:11.023	+02:48:56.36	17.30 \pm 0.27	-12.33 \pm 0.17	5.24 \pm 0.15	...	17.809
252	2MASS J04121147+0638125	04:12:11.490	+06:38:12.26	21.5 \pm 1.3	-21.5 \pm 1.1	7.00 \pm 0.67	...	19.670
253	2MASS J04121402+0543526	04:12:14.058	+05:43:52.28	21.97 \pm 0.95	-23.13 \pm 0.54	7.03 \pm 0.44	...	19.065
254	TYC 74-1393-1	04:12:18.449	+00:01:31.28	19.633 \pm 0.077	-17.562 \pm 0.052	5.747 \pm 0.047	20 \pm 1	11.151
255	2MASS J04140593+0150284	04:14:05.959	+01:50:28.17	19.41 \pm 0.18	-17.88 \pm 0.10	5.659 \pm 0.090	...	15.828
256	2MASS J04142242+1103304	04:14:22.433	+11:03:29.92	15.84 \pm 0.32	-21.36 \pm 0.19	5.69 \pm 0.14	...	15.203
257	2MASS J04143043+0509324	04:14:30.466	+05:09:31.97	22.4 \pm 3.0	-23.4 \pm 1.9	7.0 \pm 1.1	...	20.586
258	2MASS J04151163+0745505	04:15:11.657	+07:45:50.08	20.50 \pm 0.32	-21.18 \pm 0.23	6.09 \pm 0.18	...	17.161

Table 3 *continued*

Table 3 (*continued*)

MUTA	Object	R.A.	Decl.	$\mu_\alpha \cos \delta$	μ_δ	Parallax	RV	<i>Gaia</i> DR2
ID	Name	(hh:mm:ss.sss)	(dd:mm:ss.ss)	(mas yr $^{-1}$)	(mas yr $^{-1}$)	(mas)	(km s $^{-1}$)	<i>G</i> mag
259	2MASS J04153196+0208232	04:15:31.984	+02:08:23.22	18.921 \pm 0.080	-12.276 \pm 0.051	5.488 \pm 0.043	...	14.735
260	2MASS J04153792+0545414	04:15:37.957	+05:45:41.10	21.22 \pm 0.21	-26.68 \pm 0.12	7.619 \pm 0.093	...	16.185
261	2MASS J04154515+1053367	04:15:45.165	+10:53:36.50	14.8 \pm 1.7	-19.3 \pm 1.0	5.29 \pm 0.66	...	18.902
262	2MASS J04154665+0921245	04:15:46.680	+09:21:24.17	19.99 \pm 0.21	-21.41 \pm 0.14	6.088 \pm 0.092	...	15.906
263	HD 26991	04:16:01.464	+00:27:13.71	23.95 \pm 0.12	-21.121 \pm 0.064	6.741 \pm 0.074	...	7.334
264	2MASS J04160164+0208148	04:16:01.666	+02:08:14.71	19.54 \pm 0.41	-12.93 \pm 0.29	5.69 \pm 0.23	...	18.332
265 B	Gaia DR2 3254162137382331136	04:16:13.147	-01:19:54.96	22.95 \pm 0.15	-18.42 \pm 0.14	6.865 \pm 0.091	...	16.068
266	2MASS J04161776+0807409	04:16:17.792	+08:07:40.48	19.42 \pm 0.18	-21.473 \pm 0.095	6.333 \pm 0.070	...	14.648
267	UCAC2 30946195	04:17:18.672	-02:16:02.15	19.267 \pm 0.047	-11.584 \pm 0.022	5.638 \pm 0.036	21 \pm 1	11.491
268	2MASS J04172026+0831017	04:17:20.280	+08:31:01.47	15.105 \pm 0.052	-17.322 \pm 0.035	4.566 \pm 0.030	...	13.908
269	TYC 77-1284-1	04:17:24.077	+03:14:44.87	23.42 \pm 0.13	-23.623 \pm 0.070	7.043 \pm 0.055	19.3 \pm 0.7	10.509
270	2MASS J04180199+0912488	04:18:02.016	+09:12:48.54	17.97 \pm 0.29	-17.83 \pm 0.15	5.77 \pm 0.13	...	15.983
271	2MASS J04181095+0934586	04:18:10.980	+09:34:58.24	15.97 \pm 0.27	-21.58 \pm 0.21	5.83 \pm 0.16	...	17.228
272	2MASS J04181171+0159007	04:18:11.727	+01:59:00.56	19.02 \pm 0.14	-20.42 \pm 0.10	6.524 \pm 0.080	...	16.180
273	2MASS J04183610+0614399	04:18:36.121	+06:14:39.52	22.56 \pm 0.13	-21.392 \pm 0.083	6.257 \pm 0.068	...	13.615
274	2MASS J04184388+1108254	04:18:43.885	+11:08:25.18	14.75 \pm 0.28	-20.72 \pm 0.21	5.10 \pm 0.15	...	15.866
275	2MASS J04191246+0659166	04:19:12.488	+06:59:16.41	19.50 \pm 0.20	-20.49 \pm 0.14	6.12 \pm 0.11	...	16.876
276	2MASS J04195888+0813546	04:19:58.900	+08:13:54.44	14.11 \pm 0.22	-17.86 \pm 0.15	4.88 \pm 0.13	...	16.740
277 A	2MASS J04200165+0759584	04:20:01.666	+07:59:57.72	22.83 \pm 0.68	-23.94 \pm 0.47	6.31 \pm 0.34	...	15.336
277 B	Gaia DR2 3298956138016754048	04:20:01.719	+07:59:58.51	19.87 \pm 0.90	-21.65 \pm 0.42	6.69 \pm 0.14	...	16.289
278 B	Gaia DR2 3254797311502540032	04:20:02.874	+00:10:08.62	17.18 \pm 0.70	-15.91 \pm 0.46	4.56 \pm 0.47	...	19.318
279	2MASS J04201617+0959534	04:20:16.202	+09:59:53.06	17.34 \pm 0.38	-20.97 \pm 0.19	6.14 \pm 0.17	...	17.379
280 A	CRTS J042024.3+001725	04:20:24.319	+00:17:25.43	18.484 \pm 0.037	-12.270 \pm 0.024	5.610 \pm 0.025	...	13.280
281	2MASS J04205517+0649544	04:20:55.204	+06:49:53.97	21.4 \pm 1.3	-18.95 \pm 0.98	5.93 \pm 0.74	...	15.510
282	2MASS J04210781-0111328	04:21:07.848	-01:11:33.15	20.918 \pm 0.081	-18.823 \pm 0.047	7.005 \pm 0.052	...	14.264
283	2MASS J04212496+0613103	04:21:24.983	+06:13:10.05	18.12 \pm 0.26	-20.60 \pm 0.18	6.15 \pm 0.15	...	16.537
284	2MASS J04213975+1111071	04:21:39.778	+11:11:06.72	19.70 \pm 0.93	-23.05 \pm 0.42	5.49 \pm 0.38	...	18.801
285	2MASS J04215979+0447054	04:21:59.842	+04:47:05.75	18.5 \pm 3.0	-18.4 \pm 1.6	5.1 \pm 1.4	...	20.507
286	2MASS J04220837+0847244	04:22:08.399	+08:47:24.15	20.59 \pm 0.28	-20.44 \pm 0.18	5.81 \pm 0.16	...	17.842
287	2MASS J04221374+0945434	04:22:13.765	+09:45:43.00	20.15 \pm 0.91	-23.21 \pm 0.43	6.36 \pm 0.36	...	18.255
288	BD-03 753	04:22:23.528	-02:40:04.13	19.704 \pm 0.069	-12.138 \pm 0.040	5.995 \pm 0.046	20 \pm 2	9.741
289	2MASS J04222577+0734399	04:22:25.798	+07:34:39.52	19.14 \pm 0.23	-21.84 \pm 0.18	6.14 \pm 0.17	...	17.076
290	BD+05 638	04:22:33.022	+05:41:38.82	20.63 \pm 0.11	-21.387 \pm 0.068	6.284 \pm 0.056	...	9.033
291	2MASS J04234971-0309472	04:23:49.737	-03:09:47.47	19.350 \pm 0.065	-12.401 \pm 0.038	5.268 \pm 0.030	...	13.303

Table 3 *continued*

Table 3 (*continued*)

MUTA	Object	R.A.	Decl.	$\mu_\alpha \cos \delta$	μ_δ	Parallax	RV	<i>Gaia</i> DR2
ID	Name	(hh:mm:ss.sss)	(dd:mm:ss.ss)	(mas yr $^{-1}$)	(mas yr $^{-1}$)	(mas)	(km s $^{-1}$)	<i>G</i> mag
292	2MASS J04235045+0037286	04:23:50.454	+00:37:28.52	17.5 ± 1.1	-16.88 ± 0.50	6.19 ± 0.54	...	18.361
293	2MASS J04240254-0055122	04:24:02.572	-00:55:12.59	25.0 ± 1.1	-21.20 ± 0.61	7.49 ± 0.67	...	19.772
294	2MASS J04244312+0819072	04:24:43.162	+08:19:07.03	20.10 ± 0.11	-22.507 ± 0.072	6.235 ± 0.061	...	15.048
295	2MASS J04245775+0725550	04:24:57.780	+07:25:54.80	14.169 ± 0.083	-19.709 ± 0.055	4.813 ± 0.046	15 ± 2	12.059
296	2MASS J04251032+0632542	04:25:10.358	+06:32:53.95	17.82 ± 0.27	-21.24 ± 0.14	6.09 ± 0.11	...	15.807
297	2MASS J04262075+0027363	04:26:20.785	+00:27:36.01	21.00 ± 0.11	-20.439 ± 0.074	6.51 ± 0.15	18 ± 8	11.352
298	2MASS J04263992+0710085	04:26:39.939	+07:10:08.17	18.620 ± 0.076	-20.252 ± 0.052	5.896 ± 0.044	...	14.349
299	2MASS J04270667+0908332	04:27:06.684	+09:08:32.74	16.10 ± 0.10	-20.512 ± 0.078	5.693 ± 0.049	21.5 ± 0.4	11.726
300	2MASS J04271508+0634143	04:27:15.116	+06:34:14.34	14.87 ± 0.20	-19.72 ± 0.13	5.60 ± 0.10	...	16.367
301	2MASS J04272511+0004224	04:27:25.145	+00:04:22.60	16.28 ± 0.16	-13.467 ± 0.086	4.651 ± 0.090	...	13.191
302	2MASS J04274452-0403155	04:27:44.547	-04:03:15.90	20.42 ± 0.20	-16.83 ± 0.13	6.57 ± 0.13	...	16.999
303	2MASS J04275113+0755147	04:27:51.156	+07:55:14.29	20.18 ± 0.23	-19.99 ± 0.18	6.48 ± 0.14	...	17.084
304	2MASS J04281033+0345325	04:28:10.354	+03:45:32.06	16.31 ± 0.16	-19.422 ± 0.084	6.08 ± 0.11	...	16.336
305 A	BD-03 789	04:28:37.716	-03:15:44.58	21.005 ± 0.058	-18.285 ± 0.043	6.718 ± 0.042	22 ± 2	9.988
305 B	2MASS J04283839-0315371	04:28:38.423	-03:15:37.42	21.409 ± 0.061	-17.884 ± 0.045	6.781 ± 0.045	...	14.304
306	2MASS J04290785+0111529	04:29:07.865	+01:11:52.42	18.367 ± 0.088	-14.933 ± 0.044	5.314 ± 0.045	...	14.623
307	2MASS J04294933+0108565	04:29:49.346	+01:08:56.18	18.58 ± 0.22	-18.88 ± 0.12	6.55 ± 0.11	...	16.631
308	2MASS J04300516+0545074	04:30:05.173	+05:45:07.11	14.76 ± 0.79	-19.92 ± 0.36	5.57 ± 0.39	...	18.810
309	2MASS J04300781-0004307	04:30:07.834	-00:04:31.19	21.059 ± 0.066	-20.013 ± 0.043	7.268 ± 0.044	22 ± 2	12.606
310	2MASS J04315156+0458221	04:31:51.590	+04:58:21.80	16.03 ± 0.19	-19.32 ± 0.11	5.80 ± 0.12	...	16.708
311	2MASS J04322380+0836544	04:32:23.819	+08:36:54.17	16.526 ± 0.085	-20.843 ± 0.044	5.981 ± 0.046	...	15.013
312	2MASS J04333159+0017365	04:33:31.610	+00:17:36.29	20.27 ± 0.13	-18.141 ± 0.077	6.205 ± 0.070	...	15.762
313	2MASS J04333390+0939039	04:33:33.919	+09:39:03.60	14.41 ± 0.61	-19.58 ± 0.33	5.57 ± 0.31	...	19.055
314	2MASS J04334594+0621571	04:33:45.976	+06:21:56.83	15.18 ± 0.29	-19.76 ± 0.15	5.89 ± 0.15	...	17.598
315	2MASS J04335466+0058219	04:33:54.685	+00:58:21.56	20.091 ± 0.082	-18.976 ± 0.046	5.387 ± 0.043	19 ± 3	13.321
316	2MASS J04340478+0221361	04:34:04.800	+02:21:35.96	15.34 ± 0.46	-18.61 ± 0.25	5.67 ± 0.27	...	18.168
317	2MASS J04341114+0212190	04:34:11.143	+02:12:18.67	14.93 ± 0.30	-18.26 ± 0.17	5.50 ± 0.17	...	17.255
318 B	Gaia DR2 3279527149078835712	04:34:19.467	+02:26:25.91	15.62 ± 0.75	-21.63 ± 0.44	6.24 ± 0.33	20.6 ± 0.5	15.960
318 A	2MASS J04341953+0226260	04:34:19.560	+02:26:25.89	16.32 ± 0.42	-20.02 ± 0.29	5.77 ± 0.22	19 ± 3	12.150
319	2MASS J04342738+0227328	04:34:27.421	+02:27:32.60	16.404 ± 0.076	-15.738 ± 0.040	5.214 ± 0.037	...	14.651
320	2MASS J04342758+0513284	04:34:27.592	+05:13:28.18	15.0 ± 1.2	-18.45 ± 0.70	6.40 ± 0.66	...	20.103
321	2MASS J04343476-0144108	04:34:34.776	-01:44:11.12	17.42 ± 0.17	-15.88 ± 0.13	5.76 ± 0.11	...	15.958
322	WISEA J043452.91-005432.9	04:34:52.905	-00:54:32.97	16.6 ± 3.0	-17.2 ± 1.8	6.0 ± 1.7	...	20.665
323	2MASS J04350272+0733430	04:35:02.756	+07:33:42.74	18.54 ± 0.46	-21.91 ± 0.21	5.87 ± 0.23	...	18.271

Table 3 *continued*

Table 3 (*continued*)

MUTA	Object	R.A.	Decl.	$\mu_\alpha \cos \delta$	μ_δ	Parallax	RV	<i>Gaia</i> DR2
ID	Name	(hh:mm:ss.sss)	(dd:mm:ss.ss)	(mas yr $^{-1}$)	(mas yr $^{-1}$)	(mas)	(km s $^{-1}$)	<i>G</i> mag
324 A	HD 29182	04:35:53.776	+05:06:15.36	13.562 ± 0.084	-18.825 ± 0.051	5.497 ± 0.051	...	8.692
325 B	Gaia DR2 3282460371222713728	04:36:33.274	+05:11:31.41	14.77 ± 0.14	-19.544 ± 0.089	5.710 ± 0.088	...	16.270
325 A	2MASS J04363330+0511304	04:36:33.328	+05:11:29.84	15.123 ± 0.081	-19.524 ± 0.050	5.632 ± 0.049	...	14.831
326	2MASS J04364894+0309231	04:36:48.955	+03:09:22.90	13.93 ± 0.49	-18.71 ± 0.29	5.93 ± 0.29	...	18.510
327	2MASS J04370987+0910564	04:37:09.894	+09:10:56.04	16.89 ± 0.51	-22.58 ± 0.28	6.28 ± 0.31	...	18.517
328	2MASS J04372578-0210117	04:37:25.800	-02:10:12.12	18.11 ± 0.14	-16.732 ± 0.097	6.011 ± 0.083	...	16.275
329 A	2MASS J04372971-0051241	04:37:29.730	-00:51:24.47	15.026 ± 0.042	-16.665 ± 0.027	6.050 ± 0.025	21 ± 2	13.223
329 B	Gaia DR2 3229491776511286016	04:37:29.780	-00:51:25.66	14.70 ± 0.36	-17.42 ± 0.19	5.75 ± 0.14	...	16.507
330	2MASS J04381823+0310336	04:38:18.245	+03:10:33.35	16.40 ± 0.18	-18.79 ± 0.10	6.159 ± 0.077	...	15.963
331 B	Gaia DR2 3201810884087980800	04:38:27.437	-03:42:46.23	19.59 ± 0.85	-17.76 ± 0.49	6.77 ± 0.40	...	18.416
332	2MASS J04382994+0258279	04:38:29.963	+02:58:27.54	17.17 ± 0.12	-17.131 ± 0.072	6.028 ± 0.063	...	14.967
333	2MASS J04383297+0534306	04:38:32.989	+05:34:30.14	15.04 ± 0.50	-18.67 ± 0.26	5.80 ± 0.27	...	18.382
334	2MASS J04390108+0436555	04:39:01.103	+04:36:55.25	14.68 ± 0.40	-17.91 ± 0.24	5.35 ± 0.21	...	17.795
335	2MASS J04390925+0011215	04:39:09.277	+00:11:21.38	14.17 ± 0.50	-17.35 ± 0.28	5.86 ± 0.24	...	18.487
336	2MASS J04391308-0045039	04:39:13.102	-00:45:04.39	15.34 ± 0.14	-16.827 ± 0.085	6.104 ± 0.067	...	15.326
337	BD+06 731	04:39:15.500	+07:01:43.92	22.605 ± 0.066	-29.118 ± 0.038	7.131 ± 0.036	15.2 ± 0.3	9.261
338 A	TYC 4739-1225-1	04:39:20.251	-03:14:21.79	14.784 ± 0.080	-16.007 ± 0.056	6.089 ± 0.036	24.4 ± 0.3	10.962
339	2MASS J04403353+0245052	04:40:33.544	+02:45:04.87	16.0 ± 1.3	-17.87 ± 0.75	5.76 ± 0.69	...	19.753
340	2MASS J04403721+0340342	04:40:37.219	+03:40:33.91	12.96 ± 0.56	-17.99 ± 0.39	5.90 ± 0.31	...	18.793
341	2MASS J04411983+0238201	04:41:19.851	+02:38:19.86	14.12 ± 0.11	-17.833 ± 0.060	5.783 ± 0.049	...	14.996
342	2MASS J04413233-0226442	04:41:32.362	-02:26:44.48	16.64 ± 0.28	-15.53 ± 0.21	5.27 ± 0.15	...	17.805
343	HD 29850	04:42:08.711	-01:39:54.10	15.93 ± 0.11	-14.733 ± 0.080	5.274 ± 0.065	...	8.874
344	2MASS J04421064-0313504	04:42:10.660	-03:13:50.71	16.98 ± 0.14	-15.84 ± 0.11	5.933 ± 0.088	...	16.565
345	HD 29839	04:42:13.732	+02:59:23.74	13.52 ± 0.30	-17.93 ± 0.23	5.40 ± 0.17	...	7.218
346 B	2MASS J04421451+0250336	04:42:14.531	+02:50:33.42	14.70 ± 0.23	-16.73 ± 0.18	5.81 ± 0.15	...	17.743
346 A	2MASS J04421498+0250387	04:42:14.998	+02:50:38.54	14.310 ± 0.082	-17.815 ± 0.056	5.816 ± 0.045	...	14.830
347	2MASS J04421761+0410207	04:42:17.635	+04:10:20.28	18.08 ± 0.26	-20.71 ± 0.19	6.36 ± 0.16	...	17.235
348	2MASS J04421931+0255038	04:42:19.321	+02:55:03.57	14.02 ± 0.14	-18.25 ± 0.10	5.697 ± 0.082	...	16.619
349	2MASS J04423067+0305301	04:42:30.685	+03:05:29.79	14.19 ± 0.19	-18.43 ± 0.14	5.78 ± 0.12	...	17.224
350	TYC 91-702-1	04:42:54.742	+04:00:11.23	15.299 ± 0.060	-17.910 ± 0.046	5.703 ± 0.039	23 ± 2	10.839
351	TYC 83-1232-1	04:43:04.063	+00:49:47.45	14.188 ± 0.095	-17.190 ± 0.058	5.814 ± 0.048	25 ± 5	11.189
352	2MASS J04430440+0234219	04:43:04.418	+02:34:21.69	13.79 ± 0.14	-18.01 ± 0.10	5.709 ± 0.085	...	16.110
353	2MASS J04431309+0048174	04:43:13.116	+00:48:17.19	13.76 ± 0.14	-16.967 ± 0.083	5.793 ± 0.075	...	14.479
354	2MASS J04435852-0106309	04:43:58.538	-01:06:31.17	13.13 ± 0.19	-12.28 ± 0.14	4.53 ± 0.10	...	16.474

Table 3 *continued*

Table 3 (*continued*)

MUTA	Object	R.A.	Decl.	$\mu_\alpha \cos \delta$	μ_δ	Parallax	RV	<i>Gaia</i> DR2
ID	Name	(hh:mm:ss.sss)	(dd:mm:ss.ss)	(mas yr $^{-1}$)	(mas yr $^{-1}$)	(mas)	(km s $^{-1}$)	<i>G</i> mag
355	2MASS J04441632+0202201	04:44:16.349	+02:02:19.80	14.83 ± 0.15	-17.11 ± 0.11	5.651 ± 0.082	...	16.092
356	2MASS J04444613-0327546	04:44:46.150	-03:27:54.91	14.800 ± 0.033	-14.434 ± 0.032	5.759 ± 0.023	20 ± 4	13.114
357	HD 30124	04:45:03.984	+05:52:17.71	13.672 ± 0.098	-21.479 ± 0.068	6.269 ± 0.055	...	8.421
358	2MASS J04452559+0047028	04:45:25.612	+00:47:02.68	13.99 ± 0.10	-17.164 ± 0.069	5.944 ± 0.056	...	14.895
359	2MASS J04463404+0413418	04:46:34.055	+04:13:41.71	11.401 ± 0.061	-16.421 ± 0.036	4.989 ± 0.030	...	14.095
360	2MASS J04465626-0311357	04:46:56.284	-03:11:36.12	16.42 ± 0.28	-16.45 ± 0.21	6.30 ± 0.14	...	17.308
361	2MASS J04472676+0011355	04:47:26.782	+00:11:35.27	12.77 ± 0.29	-16.26 ± 0.19	5.75 ± 0.15	...	17.629
362	V1831 Ori	04:50:04.711	+01:50:42.31	16.470 ± 0.066	-18.982 ± 0.050	5.729 ± 0.038	23 ± 4	11.522
363	2MASS J04514147+0205555	04:51:41.493	+02:05:55.24	12.52 ± 0.13	-16.323 ± 0.084	5.172 ± 0.066	...	15.520
364	BD-02 1047	04:52:07.364	-01:58:57.43	12.91 ± 0.12	-17.606 ± 0.088	5.600 ± 0.070	24.5 ± 0.8	9.860
365	2MASS J04523044-0110409	04:52:30.465	-01:10:41.31	12.65 ± 0.34	-15.40 ± 0.23	5.43 ± 0.17	...	15.408
366	2MASS J04524130-0135000	04:52:41.324	-01:35:00.29	12.78 ± 0.15	-15.53 ± 0.10	5.676 ± 0.080	...	16.022
367	2MASS J04530475-0127086	04:53:04.767	-01:27:08.86	13.825 ± 0.093	-18.215 ± 0.066	5.626 ± 0.066	...	14.235
368	HD 31125	04:53:04.828	-01:16:33.04	12.67 ± 0.11	-15.782 ± 0.072	5.644 ± 0.051	...	7.918
369	TYC 4745-475-1	04:53:12.066	-03:49:10.26	13.631 ± 0.053	-14.909 ± 0.044	5.993 ± 0.031	26.2 ± 0.6	11.383
370	2MASS J04543831-0151186	04:54:38.330	-01:51:18.88	14.00 ± 0.32	-18.39 ± 0.23	5.39 ± 0.18	24 ± 9	12.986
371 B	Gaia DR2 3228318975563766784	04:54:46.875	-00:01:10.21	11.191 ± 0.065	-16.437 ± 0.050	5.322 ± 0.039	...	14.858
372 A	TYC 4741-307-1	04:56:18.287	-01:53:33.04	11.95 ± 0.12	-15.188 ± 0.075	5.612 ± 0.060	25 ± 2	10.775
376	TYC 665-150-1	03:57:21.412	+12:58:16.37	28.05 ± 0.31	-24.71 ± 0.22	6.54 ± 0.15	6.8 ± 0.8	10.833
...	2MASS J02300007+2815305	02:30:00.126	+28:15:30.00	39.51 ± 0.42	-33.01 ± 0.36	8.65 ± 0.23	...	18.285
...	2MASS J02355804+1946474	02:35:58.096	+19:46:47.02	45.33 ± 0.16	-27.92 ± 0.12	8.728 ± 0.082	...	15.679
...	2MASS J02365857+1822006	02:36:58.621	+18:22:00.16	36.13 ± 0.16	-24.96 ± 0.13	7.850 ± 0.079	...	16.235
...	Gaia DR2 127856640916806528	02:38:41.656	+28:08:56.54	47.33 ± 0.39	-37.26 ± 0.32	10.43 ± 0.19	...	18.202
...	2MASS J02514834+1542531	02:51:48.392	+15:42:52.31	39.89 ± 0.59	-31.46 ± 0.47	9.32 ± 0.37	...	18.896
...	2MASS J02564263+2122182	02:56:42.677	+21:22:17.63	35.65 ± 0.23	-27.88 ± 0.15	7.665 ± 0.096	...	15.925
...	2MASS J02571402+1329246	02:57:14.061	+13:29:24.21	37.61 ± 0.17	-25.58 ± 0.15	8.836 ± 0.081	...	16.207
...	2MASS J02591008+2830202	02:59:10.136	+28:30:19.82	31.48 ± 0.11	-30.731 ± 0.089	7.984 ± 0.056	...	15.027
...	2MASS J02592884+1417534	02:59:28.891	+14:17:52.96	37.61 ± 0.18	-28.83 ± 0.16	8.073 ± 0.079	...	16.197
...	2MASS J03001278+1151455	03:00:12.823	+11:51:45.10	35.20 ± 0.35	-26.03 ± 0.29	7.74 ± 0.20	...	17.869
...	2MASS J03022099+2253470	03:02:21.016	+22:53:46.60	28.02 ± 0.41	-21.71 ± 0.32	6.74 ± 0.20	...	18.013
...	WISEA J030230.82+240842.1	03:02:30.837	+24:08:41.81	37.9 ± 2.9	-29.9 ± 2.8	8.8 ± 1.9	...	20.528
...	2MASS J03032741+1404418	03:03:27.453	+14:04:41.40	30.61 ± 0.15	-23.75 ± 0.13	6.746 ± 0.073	...	16.078
...	2MASS J03070447+2934216	03:07:04.519	+29:34:20.77	36.17 ± 0.32	-38.26 ± 0.21	9.30 ± 0.16	...	16.917
...	2MASS J03081211+1521139	03:08:12.158	+15:21:13.34	44.21 ± 0.15	-35.72 ± 0.12	10.203 ± 0.088	...	15.788

Table 3 *continued*

Table 3 (*continued*)

MUTA	Object	R.A.	Decl.	$\mu_\alpha \cos \delta$	μ_δ	Parallax	RV	<i>Gaia</i> DR2
ID	Name	(hh:mm:ss.sss)	(dd:mm:ss.ss)	(mas yr $^{-1}$)	(mas yr $^{-1}$)	(mas)	(km s $^{-1}$)	<i>G</i> mag
...	2MASS J03085284+1052232	03:08:52.883	+10:52:22.78	39.09 ± 0.13	-23.94 ± 0.12	8.482 ± 0.067	...	15.423
...	2MASS J03091404+2018084	03:09:14.086	+20:18:07.96	37.61 ± 0.13	-32.34 ± 0.11	7.808 ± 0.087	...	15.424
...	Gaia DR2 59117372971786880	03:17:00.436	+18:27:21.96	32.94 ± 0.25	-24.73 ± 0.18	6.78 ± 0.12	...	17.380
...	2MASS J03175490+0420281	03:17:54.941	+04:20:27.63	39.31 ± 0.27	-25.85 ± 0.25	8.75 ± 0.16	...	17.871
...	2MASS J03192523+1845233	03:19:25.273	+18:45:22.78	35.29 ± 0.23	-29.76 ± 0.20	7.30 ± 0.13	...	17.349
...	Gaia DR2 59375998722290304	03:19:26.873	+19:44:53.78	28.72 ± 0.92	-23.00 ± 0.75	6.35 ± 0.56	...	19.613
...	2MASS J03204354+2356091	03:20:43.590	+23:56:08.36	32.58 ± 0.17	-38.85 ± 0.14	8.952 ± 0.089	...	16.447
...	τ^1 Ari	03:21:13.653	+21:08:49.13	26.57 ± 0.55	-21.33 ± 0.44	6.37 ± 0.27	14.7 ± 0.9	5.265
...	2MASS J03212919+1604380	03:21:29.223	+16:04:37.59	28.18 ± 0.30	-28.33 ± 0.25	7.36 ± 0.17	...	17.589
...	2MASS J03213476+1654136	03:21:34.794	+16:54:13.30	25.48 ± 0.49	-21.94 ± 0.35	6.01 ± 0.34	...	18.366
...	2MASS J03215751+1601394	03:21:57.552	+16:01:39.10	32.28 ± 0.13	-22.92 ± 0.11	7.047 ± 0.084	...	15.977
...	2MASS J03230385+1709370	03:23:03.904	+17:09:36.49	39.51 ± 0.20	-31.98 ± 0.16	8.903 ± 0.092	...	15.894
...	2MASS J03244896+1020589	03:24:49.008	+10:20:58.39	41.09 ± 0.28	-28.07 ± 0.23	9.34 ± 0.17	...	17.448
...	2MASS J03245419+1555078	03:24:54.240	+15:55:07.18	38.11 ± 0.50	-35.49 ± 0.39	8.23 ± 0.30	...	18.275
...	2MASS J03250457+0728193	03:25:04.592	+07:28:18.82	31.22 ± 0.26	-21.79 ± 0.20	6.83 ± 0.16	...	17.360
...	Gaia DR2 9977797439144320	03:25:04.736	+07:28:20.43	31.93 ± 0.38	-21.57 ± 0.31	6.76 ± 0.25	...	18.012
...	2MASS J03261888+2153335	03:26:18.933	+21:53:32.98	40.49 ± 0.21	-40.59 ± 0.16	9.29 ± 0.12	...	16.861
...	2MASS J03270898+0933595	03:27:09.019	+09:33:59.24	26.94 ± 0.53	-20.75 ± 0.46	6.89 ± 0.34	...	18.677
...	2MASS J03274866+0547180	03:27:48.706	+05:47:17.65	36.58 ± 0.28	-28.25 ± 0.20	8.47 ± 0.15	...	17.397
...	2MASS J03282792+1524230	03:28:27.961	+15:24:22.57	32.01 ± 0.20	-23.45 ± 0.15	7.95 ± 0.10	...	16.798
...	2MASS J03284348+0843451	03:28:43.521	+08:43:44.79	37.2 ± 2.6	-27.1 ± 2.3	7.4 ± 1.3	...	20.658
...	2MASS J03292961+1051560	03:29:29.653	+10:51:55.53	32.09 ± 0.14	-29.802 ± 0.097	8.497 ± 0.065	...	15.263
...	2MASS J03304846+1034093	03:30:48.497	+10:34:08.92	25.076 ± 0.076	-16.325 ± 0.056	6.153 ± 0.042	...	14.607
...	2MASS J03310140+1200052	03:31:01.444	+12:00:04.75	31.93 ± 0.23	-28.33 ± 0.15	8.39 ± 0.12	...	16.609
...	2MASS J03313540+0645326	03:31:35.446	+06:45:32.52	34.01 ± 0.14	-19.70 ± 0.11	7.826 ± 0.075	...	16.243
...	2MASS J03322564+1857138	03:32:25.671	+18:57:13.38	22.67 ± 0.48	-24.68 ± 0.31	6.01 ± 0.25	...	17.956
...	2MASS J03323893+1512173	03:32:38.982	+15:12:16.99	26.34 ± 0.83	-21.69 ± 0.58	5.84 ± 0.45	...	19.335
...	2MASS J03334166+1924263	03:33:41.669	+19:24:26.22	23.5 ± 1.4	-23.0 ± 1.0	6.97 ± 0.81	...	20.217
...	Gaia DR2 40541334474313728	03:34:33.106	+12:12:29.76	28.23 ± 0.88	-29.63 ± 0.62	7.50 ± 0.54	...	19.087
...	2MASS J03350086+1539436	03:35:00.896	+15:39:43.16	22.06 ± 0.20	-23.23 ± 0.16	6.36 ± 0.12	...	16.458
...	WISEA J033651.60+154553.3	03:36:51.600	+15:45:53.00	25.4 ± 3.7	-28.7 ± 3.1	7.6 ± 3.3	...	20.777
...	2MASS J03373345+0616472	03:37:33.487	+06:16:46.69	32.75 ± 0.14	-28.71 ± 0.10	8.128 ± 0.092	...	15.625
...	WISEA J033742.99+191646.7	03:37:42.991	+19:16:46.69	25.3 ± 4.0	-27.7 ± 2.8	6.9 ± 1.7	...	20.716
...	2MASS J03375620+0841417	03:37:56.241	+08:41:41.50	27.66 ± 0.13	-21.108 ± 0.095	6.172 ± 0.067	...	15.761

Table 3 *continued*

Table 3 (*continued*)

MUTA	Object	R.A.	Decl.	$\mu_\alpha \cos \delta$	μ_δ	Parallax	RV	<i>Gaia</i> DR2
ID	Name	(hh:mm:ss.sss)	(dd:mm:ss.ss)	(mas yr $^{-1}$)	(mas yr $^{-1}$)	(mas)	(km s $^{-1}$)	<i>G</i> mag
...	2MASS J03380150+1638387	03:38:01.544	+16:38:38.07	36.35 ± 0.20	-33.91 ± 0.16	8.00 ± 0.11	...	16.476
...	2MASS J03402733+0811017	03:40:27.369	+08:11:01.28	33.39 ± 0.68	-27.63 ± 0.46	8.01 ± 0.30	...	18.544
...	2MASS J03412704+0811542	03:41:27.091	+08:11:53.99	29.66 ± 0.34	-21.64 ± 0.26	6.20 ± 0.18	...	18.093
...	2MASS J03422624+1416494	03:42:26.282	+14:16:48.95	32.318 ± 0.074	-28.272 ± 0.056	6.956 ± 0.036	...	14.273
...	TYC 71-674-1	03:43:48.922	+06:22:09.72	21.940 ± 0.078	-14.034 ± 0.054	5.526 ± 0.041	16.7 ± 0.6	11.764
...	2MASS J03453877+2113077	03:45:38.814	+21:13:07.23	27.06 ± 0.32	-27.67 ± 0.23	6.57 ± 0.17	...	17.873
...	WISEA J034623.66+130512.5	03:46:23.699	+13:05:13.10	22.6 ± 3.2	-18.2 ± 1.9	6.2 ± 1.8	...	20.643
...	2MASS J03463262+1825551	03:46:32.653	+18:25:54.77	23.37 ± 0.29	-26.78 ± 0.20	5.87 ± 0.13	...	17.291
...	2MASS J03473025+0203437	03:47:30.270	+02:03:43.20	24.55 ± 0.24	-18.65 ± 0.24	5.99 ± 0.14	...	17.765
...	2MASS J03475182+1043255	03:47:51.852	+10:43:25.14	27.64 ± 0.27	-25.46 ± 0.17	6.27 ± 0.11	...	17.095
...	2MASS J03480732+1342170	03:48:07.349	+13:42:16.44	27.390 ± 0.097	-32.642 ± 0.061	7.223 ± 0.049	...	14.689
...	2MASS J03483524+0931435	03:48:35.249	+09:31:43.42	20.2 ± 1.8	-15.6 ± 1.2	5.69 ± 0.87	...	19.038
...	Gaia DR2 39495385383245568	03:48:36.265	+13:47:27.18	26.70 ± 0.83	-32.33 ± 0.56	7.15 ± 0.47	...	19.501
...	2MASS J03485224+0620302	03:48:52.278	+06:20:29.88	23.64 ± 0.28	-20.33 ± 0.22	6.39 ± 0.14	...	16.797
...	2MASS J03502829+1753586	03:50:28.333	+17:53:58.17	29.43 ± 0.27	-28.97 ± 0.16	7.01 ± 0.11	...	16.941
...	2MASS J03505011+1205084	03:50:50.135	+12:05:08.14	22.18 ± 0.20	-16.88 ± 0.13	6.20 ± 0.11	...	17.045
...	2MASS J03522921+1037209	03:52:29.239	+10:37:20.63	29.47 ± 0.77	-27.50 ± 0.53	6.46 ± 0.40	...	19.289
...	2MASS J03523586+0709204	03:52:35.898	+07:09:20.05	21.23 ± 0.13	-22.856 ± 0.088	6.301 ± 0.071	...	15.097
...	2MASS J03531715+1823316	03:53:17.251	+18:23:30.59	29.4 ± 2.8	-35.5 ± 1.4	7.5 ± 1.2	...	20.569
...	2MASS J03531923+1321065	03:53:19.280	+13:21:06.14	28.19 ± 0.58	-28.70 ± 0.35	7.57 ± 0.26	...	18.676
...	2MASS J03541484+1618297	03:54:14.874	+16:18:29.32	20.5 ± 1.9	-22.6 ± 1.4	5.9 ± 1.2	...	20.408
...	2MASS J03544106+0912233	03:54:41.079	+09:12:23.12	23.0 ± 1.7	-19.7 ± 1.0	6.17 ± 0.92	...	18.979
...	WISEA J035552.96+051855.6	03:55:52.992	+05:18:56.29	22.3 ± 4.4	-17.5 ± 3.1	6.0 ± 1.9	...	20.961
...	2MASS J03565177+0511102	03:56:51.810	+05:11:10.05	24.5 ± 1.0	-18.70 ± 0.84	5.32 ± 0.46	...	19.460
...	WISEA J035656.05+112815.8	03:56:56.042	+11:28:15.36	20.4 ± 3.3	-17.8 ± 2.1	6.4 ± 1.6	...	20.562
...	2MASS J03573966+1441432	03:57:39.695	+14:41:42.55	23.86 ± 0.77	-30.25 ± 0.47	7.83 ± 0.41	...	19.217
...	2MASS J03574260+0551215	03:57:42.630	+05:51:21.16	28.11 ± 0.17	-25.25 ± 0.13	7.905 ± 0.095	...	16.049
...	2MASS J03580299+1726283	03:58:03.024	+17:26:27.95	18.20 ± 0.16	-23.694 ± 0.093	6.178 ± 0.080	...	16.133
...	2MASS J03581131+0611071	03:58:11.336	+06:11:07.00	20.90 ± 0.58	-15.14 ± 0.41	6.26 ± 0.31	...	18.454
...	2MASS J03585422+1318017	03:58:54.255	+13:18:01.14	28.47 ± 0.37	-28.37 ± 0.22	6.63 ± 0.19	...	17.977
...	2MASS J04001889+1117530	04:00:18.930	+11:17:52.66	28.781 ± 0.059	-32.344 ± 0.037	7.524 ± 0.030	...	13.739
...	2MASS J04004600+1543113	04:00:46.046	+15:43:10.84	27.60 ± 0.22	-27.12 ± 0.12	8.17 ± 0.11	...	16.738
...	2MASS J04011928+0132374	04:01:19.312	+01:32:37.10	26.69 ± 0.44	-21.85 ± 0.34	6.36 ± 0.22	...	18.292
...	2MASS J04013237+0002523	04:01:32.411	+00:02:51.85	25.31 ± 0.33	-16.13 ± 0.28	6.31 ± 0.18	...	18.162

Table 3 *continued*

Table 3 (*continued*)

MUTA	Object	R.A.	Decl.	$\mu_\alpha \cos \delta$	μ_δ	Parallax	RV	<i>Gaia</i> DR2
ID	Name	(hh:mm:ss.sss)	(dd:mm:ss.ss)	(mas yr $^{-1}$)	(mas yr $^{-1}$)	(mas)	(km s $^{-1}$)	<i>G</i> mag
...	2MASS J04021909+1117014	04:02:19.090	+11:17:01.23	17.2 ± 1.6	-16.78 ± 0.86	5.21 ± 0.79	...	18.698
...	2MASS J04023974+0356420	04:02:39.778	+03:56:41.76	25.9 ± 1.3	-17.37 ± 0.88	6.62 ± 0.75	...	19.951
...	2MASS J04034941+0951155	04:03:49.434	+09:51:14.90	25.74 ± 0.31	-24.54 ± 0.19	5.93 ± 0.16	...	17.903
...	2MASS J04040646+1132063	04:04:06.475	+11:32:05.86	16.2 ± 1.3	-19.93 ± 0.68	5.33 ± 0.61	...	19.636
...	2MASS J04043739+0730434	04:04:37.407	+07:30:42.90	26.34 ± 0.85	-24.45 ± 0.42	6.58 ± 0.43	...	18.936
...	2MASS J04044493+0611385	04:04:44.961	+06:11:38.14	19.8 ± 1.5	-21.32 ± 0.86	5.02 ± 0.85	...	20.092
...	2MASS J04044544+1052456	04:04:45.463	+10:52:45.52	19.40 ± 0.31	-20.13 ± 0.21	4.82 ± 0.18	...	17.747
...	Gaia DR2 3260444330208719104	04:05:07.086	+03:53:23.29	21.56 ± 0.58	-13.82 ± 0.43	6.03 ± 0.29	...	18.802
...	2MASS J04053132+0742252	04:05:31.344	+07:42:24.88	21.98 ± 0.30	-23.20 ± 0.17	5.67 ± 0.15	...	17.506
...	2MASS J04060831+0540134	04:06:08.318	+05:40:13.35	20.26 ± 0.20	-15.47 ± 0.17	4.91 ± 0.11	...	16.840
...	2MASS J04074808+0757523	04:07:48.105	+07:57:52.14	15.93 ± 0.50	-18.59 ± 0.32	5.37 ± 0.25	...	18.604
...	2MASS J04080091+1031113	04:08:00.930	+10:31:11.12	16.9 ± 2.8	-21.2 ± 1.5	6.0 ± 1.5	...	20.540
...	2MASS J04080870+0909272	04:08:08.721	+09:09:26.86	15.36 ± 0.56	-16.97 ± 0.32	5.05 ± 0.29	...	18.712
...	2MASS J04083351+0457383	04:08:33.534	+04:57:37.83	25.67 ± 0.53	-26.72 ± 0.34	6.49 ± 0.28	...	18.685
...	Gaia DR2 3305092233237657984	04:08:34.341	+12:22:22.55	16.9 ± 4.4	-21.4 ± 2.5	5.4 ± 1.7	...	20.756
...	2MASS J04092969+1615365	04:09:29.713	+16:15:36.06	20.85 ± 0.20	-30.59 ± 0.17	6.70 ± 0.13	...	16.540
...	2MASS J04104079+1029064	04:10:40.805	+10:29:05.83	22.0 ± 1.9	-28.9 ± 1.1	7.91 ± 0.90	...	19.498
...	2MASS J04112019-0103368	04:11:20.182	-01:03:37.12	20.11 ± 0.87	-16.22 ± 0.67	5.66 ± 0.56	...	17.335
...	2MASS J04114302+1201505	04:11:43.049	+12:01:50.53	20.16 ± 0.54	-23.97 ± 0.52	7.16 ± 0.33	...	18.826
...	2MASS J04114604+1131038	04:11:46.059	+11:31:03.41	19.58 ± 0.79	-23.08 ± 0.43	6.46 ± 0.26	...	18.413
...	Gaia DR2 3284355203419497088	04:11:52.187	+04:26:32.33	25.63 ± 0.38	-28.63 ± 0.18	7.10 ± 0.22	...	18.059
...	2MASS J04121061+0742039	04:12:10.657	+07:42:03.47	16.8 ± 3.6	-14.3 ± 2.0	5.2 ± 1.5	...	20.471
...	2MASS J04122904+0942220	04:12:29.061	+09:42:21.64	17.47 ± 0.29	-20.86 ± 0.25	6.21 ± 0.15	...	17.708
...	2MASS J04124666+0614198	04:12:46.682	+06:14:19.72	17.93 ± 0.75	-13.72 ± 0.45	5.08 ± 0.30	...	18.456
...	2MASS J04131221+0836469	04:13:12.240	+08:36:46.65	19.5 ± 2.2	-16.8 ± 1.3	5.92 ± 0.85	...	19.861
...	2MASS J04144878+1348588	04:14:48.806	+13:48:58.59	18.50 ± 0.47	-21.49 ± 0.34	5.47 ± 0.24	...	18.052
...	2MASS J04153145-0125053	04:15:31.476	-01:25:05.46	21.53 ± 0.45	-13.33 ± 0.46	5.38 ± 0.25	...	18.644
...	2MASS J04160719+0411019	04:16:07.210	+04:11:01.68	17.25 ± 0.32	-13.79 ± 0.19	5.44 ± 0.14	...	17.148
...	2MASS J04162916+0722379	04:16:29.187	+07:22:37.84	17.97 ± 0.16	-20.01 ± 0.12	5.675 ± 0.091	...	16.108
...	2MASS J04164032+0030538	04:16:40.348	+00:30:53.49	24.35 ± 0.34	-22.76 ± 0.23	6.35 ± 0.23	...	17.956
...	WISEA J041646.88+040134.1	04:16:46.901	+04:01:33.88	22.8 ± 2.7	-19.5 ± 1.4	7.2 ± 1.2	...	20.238
...	Gaia DR2 3253988341527871488	04:18:21.383	-01:20:55.20	17.93 ± 0.46	-13.36 ± 0.20	5.08 ± 0.38	...	19.121
...	2MASS J04191862+0707428	04:19:18.640	+07:07:42.59	19.24 ± 0.53	-16.58 ± 0.35	5.77 ± 0.28	...	18.766
...	Gaia DR2 325556657429771008	04:19:31.874	+00:23:34.72	23.6 ± 2.2	-22.9 ± 1.8	8.7 ± 1.7	...	20.755

Table 3 *continued*

Table 3 (*continued*)

MUTA	Object	R.A.	Decl.	$\mu_\alpha \cos \delta$	μ_δ	Parallax	RV	<i>Gaia</i> DR2
ID	Name	(hh:mm:ss.sss)	(dd:mm:ss.ss)	(mas yr $^{-1}$)	(mas yr $^{-1}$)	(mas)	(km s $^{-1}$)	<i>G</i> mag
...	2MASS J04201559-0132340	04:20:15.622	-01:32:34.38	24.31 ± 0.25	-19.22 ± 0.12	6.23 ± 0.17	...	17.779
...	2MASS J04213553+0128517	04:21:35.551	+01:28:51.35	19.51 ± 0.33	-20.36 ± 0.23	6.62 ± 0.18	...	17.804
...	WISEA J042242.08+025448.7	04:22:42.098	+02:54:48.47	18.8 ± 2.5	-19.2 ± 1.4	5.48 ± 0.98	...	20.330
...	HD 27860	04:24:14.495	+12:09:28.39	14.99 ± 0.11	-23.760 ± 0.068	5.372 ± 0.053	16.6 ± 0.2	5.925
...	2MASS J04254368+0506464	04:25:43.699	+05:06:46.15	14.82 ± 0.67	-14.65 ± 0.40	5.01 ± 0.32	...	18.873
...	2MASS J04265837+0126246	04:26:58.385	+01:26:24.36	19.4 ± 1.0	-16.29 ± 0.53	4.78 ± 0.54	...	16.156
...	2MASS J04270307+0148468	04:27:03.095	+01:48:46.71	18.9 ± 1.7	-14.98 ± 0.77	6.5 ± 1.1	...	19.640
...	2MASS J04272827-0236149	04:27:28.295	-02:36:15.14	17.25 ± 0.40	-13.25 ± 0.27	5.36 ± 0.22	...	18.229
...	2MASS J04283451+0129362	04:28:34.531	+01:29:36.10	17.22 ± 0.45	-15.68 ± 0.24	5.11 ± 0.21	...	18.082
...	WISEA J042913.82-002417.0	04:29:13.841	-00:24:17.21	16.6 ± 2.3	-15.1 ± 1.4	4.6 ± 1.5	...	19.750
...	2MASS J04304508+0756242	04:30:45.103	+07:56:23.69	15.24 ± 0.43	-21.78 ± 0.23	5.63 ± 0.24	...	18.181
...	2MASS J04304930+1019441	04:30:49.319	+10:19:43.77	18.29 ± 0.66	-23.63 ± 0.40	6.52 ± 0.34	...	18.784
...	2MASS J04310354+0036313	04:31:03.558	+00:36:31.10	22.90 ± 0.88	-19.14 ± 0.44	6.46 ± 0.47	...	16.009
...	2MASS J04325031-0253281	04:32:50.340	-02:53:28.45	19.12 ± 0.25	-15.08 ± 0.17	5.71 ± 0.16	...	17.697
...	WISEA J043304.99+053543.9	04:33:04.994	+05:35:43.68	19.3 ± 2.2	-22.0 ± 1.6	5.4 ± 2.2	...	20.832
...	2MASS J04345817-0050299	04:34:58.194	-00:50:30.19	16.061 ± 0.057	-16.806 ± 0.042	5.104 ± 0.038	...	14.079
...	WISEA J043503.94+034239.6	04:35:03.926	+03:42:39.41	18.7 ± 4.3	-18.9 ± 2.1	6.6 ± 2.2	...	20.967
...	Gaia DR2 3204500079076340480	04:35:09.342	-03:32:16.93	17.99 ± 0.62	-14.13 ± 0.46	5.70 ± 0.36	...	19.324
...	2MASS J04351726+0310298	04:35:17.290	+03:10:29.61	14.23 ± 0.27	-15.11 ± 0.18	5.47 ± 0.15	...	17.823
...	2MASS J04353654+0204009	04:35:36.562	+02:04:00.59	15.69 ± 0.51	-13.72 ± 0.28	4.82 ± 0.24	...	18.411
...	2MASS J04404378+0409468	04:40:43.808	+04:09:46.58	13.70 ± 0.17	-16.36 ± 0.12	4.81 ± 0.10	...	16.839
...	2MASS J04415810+0223059	04:41:58.131	+02:23:05.76	12.76 ± 0.21	-16.77 ± 0.13	5.49 ± 0.13	...	17.125
...	2MASS J04424602+0723403	04:42:46.049	+07:23:39.96	15.13 ± 0.52	-22.87 ± 0.29	5.92 ± 0.26	...	17.422
...	WISEA J044514.79+020926.4	04:45:14.811	+02:09:25.97	15.3 ± 1.3	-16.9 ± 1.1	5.66 ± 0.94	...	20.345
...	2MASS J04451739-0046433	04:45:17.416	-00:46:43.56	12.26 ± 0.15	-12.94 ± 0.11	4.980 ± 0.085	...	16.242
...	2MASS J04455269+0118408	04:45:52.712	+01:18:40.47	15.38 ± 0.25	-19.70 ± 0.21	6.06 ± 0.16	...	17.350
...	2MASS J04482662+0236432	04:48:26.639	+02:36:43.03	13.73 ± 0.27	-16.57 ± 0.15	4.99 ± 0.13	...	17.480
...	2MASS J04502730-0318287	04:50:27.329	-03:18:29.05	15.43 ± 0.12	-16.275 ± 0.090	5.749 ± 0.077	...	16.208
...	2MASS J04503202-0050182	04:50:32.037	-00:50:18.54	12.90 ± 0.43	-15.70 ± 0.29	5.06 ± 0.21	...	18.272

NOTE—The MUTA identifiers listed in this table are defined in Section 4.4. Some identifiers listed here contain only one component of a binary system (either A or B) because the other component was recovered in either comover searches of sections 4.1 and 4.4. Only a portion of the table is shown here. The full table is available as online-only additional material. Targets without a MUTA ID number were flagged as problematic (i.e., low-likelihood candidates). See section 4 for more details.

Table 4. Wide multiple systems recovered in MUTA.

MUTA		R.A.	Decl.	$\mu_\alpha \cos \delta$	μ_δ	Parallax	<i>Gaia</i> DR2	Sep.	Pos. Ang.
ID	Name	(hh:mm:ss.sss)	(dd:mm:ss.ss)	(mas yr $^{-1}$)	(mas yr $^{-1}$)	(mas)	<i>G</i> mag	($''$)	($^{\circ}$)
5	29 Tau	03:45:40.466	+06:02:59.78	21.88 \pm 0.29	-13.65 \pm 0.26	5.3 \pm 0.2	5.295 \pm 0.001
137	2MASS J03454104+0602349	03:45:41.066	+06:02:34.59	21.27 \pm 0.21	-14.11 \pm 0.17	5.5 \pm 0.1	16.660 \pm 0.002	26.7278 \pm 0.0001	160.4167 \pm 0.0004
138	2MASS J03454269+0603039	03:45:42.712	+06:03:03.66	21.11 \pm 0.12	-13.801 \pm 0.091	5.55 \pm 0.07	15.389 \pm 0.001	33.7294 \pm 0.0002	83.3927 \pm 0.0002
139	2MASS J03454440+0603283	03:45:44.425	+06:03:28.04	19.950 \pm 0.077	-13.189 \pm 0.053	5.56 \pm 0.05	12.3683 \pm 0.0004	65.4671 \pm 0.0002	64.4250 \pm 0.0001
10	V766 Tau	03:51:15.896	+13:02:45.52	23.77 \pm 0.11	-23.228 \pm 0.079	6.19 \pm 0.06	6.247 \pm 0.001
182	2MASS J03511041+1302467	03:51:10.454	+13:02:46.16	23.10 \pm 0.17	-23.14 \pm 0.12	6.1 \pm 0.1	16.117 \pm 0.001	79.5332 \pm 0.0001	270.4681 \pm 0.0001
19 A	HD 23376	03:44:58.957	+08:19:10.09	26.61 \pm 0.11	-24.306 \pm 0.066	6.89 \pm 0.06	9.2549 \pm 0.0003
19 B	TYC 658-1007-2	03:44:59.048	+08:19:13.81	26.577 \pm 0.099	-24.198 \pm 0.062	6.99 \pm 0.07	10.493 \pm 0.002	3.9534 \pm 0.0001	19.894 \pm 0.001
30 A	TYC 668-737-1	04:21:24.386	+08:53:54.34	21.501 \pm 0.085	-23.632 \pm 0.056	6.57 \pm 0.05	11.356 \pm 0.002
30 B	2MASS J04212444+0853488	04:21:24.473	+08:53:48.52	21.62 \pm 0.10	-23.778 \pm 0.064	6.59 \pm 0.06	14.7603 \pm 0.0007	5.9608 \pm 0.0001	167.5144 \pm 0.0006
42 A	2MASS J02581643+2456424	02:58:16.484	+24:56:41.76	31.65 \pm 0.33	-27.54 \pm 0.26	7.84 \pm 0.21	15.193
42 B	Gaia DR2 113410746049727744	02:58:16.476	+24:56:42.65	31.83 \pm 0.38	-28.33 \pm 0.24	6.67 \pm 0.23	16.776	0.9011 \pm 0.0002	353.00 \pm 0.02
373	2MASS J02581815+2456552	02:58:18.198	+24:56:54.67	24.1 \pm 1.5	-33.7 \pm 1.3	6.9 \pm 1.2	20.136	26.6513 \pm 0.0009	61.016 \pm 0.002
130 A	2MASS J03442859+0716100	03:44:28.602	+07:16:10.10	25.80 \pm 0.18	-22.56 \pm 0.15	6.6 \pm 0.1	16.3270 \pm 0.0007
130 B	Gaia DR2 3277686910210391424	03:44:28.657	+07:16:08.46	24.39 \pm 0.21	-23.66 \pm 0.17	6.7 \pm 0.1	16.596 \pm 0.001	1.8368 \pm 0.0001	153.315 \pm 0.004
144 A	2MASS J03463553+1317056	03:46:35.533	+13:17:06.31	22.17 \pm 0.26	-24.02 \pm 0.17	6.3 \pm 0.1	17.335 \pm 0.002
144 B	Gaia DR2 37943944413361792	03:46:35.594	+13:17:04.31	23.04 \pm 0.30	-24.20 \pm 0.20	6.5 \pm 0.2	17.365 \pm 0.002	2.1835 \pm 0.0001	156.243 \pm 0.005
149	2MASS J03471144+0526234	03:47:11.466	+05:26:23.15	22.84 \pm 0.12	-19.71 \pm 0.10	6.09 \pm 0.07	14.6109 \pm 0.0005	31.1351 \pm 0.0001	269.3679 \pm 0.0001
150	BD+04 589	03:47:13.551	+05:26:23.49	22.654 \pm 0.098	-17.159 \pm 0.084	5.86 \pm 0.05	9.3101 \pm 0.0003
159	TYC 71-542-1	03:47:56.865	+06:16:06.67	21.191 \pm 0.082	-13.396 \pm 0.055	5.40 \pm 0.04	11.164 \pm 0.002
374	2MASS J03475024+0617499	03:47:50.279	+06:17:49.65	20.96 \pm 0.18	-13.27 \pm 0.13	5.42 \pm 0.09	16.910 \pm 0.001	142.3001 \pm 0.0001	316.3645 \pm 0.0001
188 A	2MASS J03524018+0830333	03:52:40.220	+08:30:33.13	21.96 \pm 0.17	-22.24 \pm 0.11	5.46 \pm 0.08	16.0063 \pm 0.0008
188 B	Gaia DR2 3301507795268229248	03:52:40.165	+08:30:30.19	21.32 \pm 0.38	-21.97 \pm 0.25	5.5 \pm 0.2	17.668 \pm 0.001	3.0421 \pm 0.0001	195.371 \pm 0.003
231 A	2MASS J04044937+0935076	04:04:49.382	+09:35:07.13	22.40 \pm 0.18	-24.31 \pm 0.11	6.6 \pm 0.1	15.4101 \pm 0.0007
231 B	Gaia DR2 3301900595795159040	04:04:49.493	+09:35:07.71	24.12 \pm 0.28	-23.21 \pm 0.17	6.9 \pm 0.2	16.845 \pm 0.002	1.7370 \pm 0.0002	70.514 \pm 0.003
236 A	2MASS J04054018+0722109	04:05:40.210	+07:22:10.83	20.45 \pm 0.35	-18.09 \pm 0.20	4.7 \pm 0.2	17.633 \pm 0.001
236 B	Gaia DR2 3297969498128206208	04:05:40.167	+07:22:12.08	19.0 \pm 1.9	-17.24 \pm 0.93	4.7 \pm 0.8	20.068 \pm 0.005	1.3996 \pm 0.0005	333.19 \pm 0.03
265 A	2MASS J04161320-0119554	04:16:13.253	-01:19:55.93	21.61 \pm 0.13	-19.673 \pm 0.098	7.20 \pm 0.08	15.205 \pm 0.001
265 B	Gaia DR2 3254162137382331136	04:16:13.147	-01:19:54.96	22.95 \pm 0.15	-18.42 \pm 0.14	6.86 \pm 0.09	16.068 \pm 0.002	1.8653 \pm 0.0001	301.262 \pm 0.003
267	UCAC2 30946195	04:17:18.672	-02:16:02.15	19.267 \pm 0.047	-11.584 \pm 0.022	5.64 \pm 0.04	11.4912 \pm 0.0009	26.7762 \pm 0.0001	25.0444 \pm 0.0001
375	HD 27162	04:17:17.915	-02:16:26.41	19.235 \pm 0.083	-11.433 \pm 0.039	5.70 \pm 0.06	8.3164 \pm 0.0003
287 A	2MASS J04200281+0010109	04:20:02.840	+00:10:10.78	16.170 \pm 0.070	-15.678 \pm 0.042	4.43 \pm 0.04	15.0711 \pm 0.0004
287 B	Gaia DR2 3254797311502540032	04:20:02.874	+00:10:08.62	17.18 \pm 0.70	-15.91 \pm 0.46	4.6 \pm 0.5	19.318 \pm 0.004	2.2205 \pm 0.0003	166.80 \pm 0.01
280 A	CRTS J042024.3+001725	04:20:24.319	+00:17:25.43	18.484 \pm 0.037	-12.270 \pm 0.024	5.61 \pm 0.03	13.280 \pm 0.002

Table 4 *continued*

GAGNÉ ET AL.

Table 4 (*continued*)

MUTA		R.A.	Decl.	$\mu_\alpha \cos \delta$	μ_δ	Parallax	<i>Gaia</i> DR2	Sep.	Pos. Ang.
ID	Name	(hh:mm:ss.sss)	(dd:mm:ss.ss)	(mas yr $^{-1}$)	(mas yr $^{-1}$)	(mas)	<i>G</i> mag	($''$)	($^{\circ}$)
280 B	Gaia DR2 3254823940299749376	04:20:24.331	+00:17:26.71	19.99 \pm 0.28	-11.05 \pm 0.16	5.6 \pm 0.2	16.220 \pm 0.002	1.2880 \pm 0.0001	7.395 \pm 0.007
305 A	BD-03 789	04:28:37.716	-03:15:44.58	21.005 \pm 0.058	-18.285 \pm 0.043	6.72 \pm 0.04	9.9877 \pm 0.0007
305 B	2MASS J04283839-0315371	04:28:38.423	-03:15:37.42	21.409 \pm 0.061	-17.884 \pm 0.045	6.78 \pm 0.05	14.304 \pm 0.002	12.7788 \pm 0.0001	55.9407 \pm 0.0002
324 A	HD 29182	04:35:53.776	+05:06:15.36	13.562 \pm 0.084	-18.825 \pm 0.051	5.50 \pm 0.05	8.6917 \pm 0.0002
324 B	TYC 90-953-1	04:35:52.439	+05:05:30.40	14.070 \pm 0.062	-18.775 \pm 0.037	5.58 \pm 0.04	11.4861 \pm 0.0009	49.1962 \pm 0.0001	203.9532 \pm 0.0001
325 A	2MASS J04363330+0511304	04:36:33.328	+05:11:29.84	15.123 \pm 0.081	-19.524 \pm 0.050	5.63 \pm 0.05	14.831 \pm 0.001
325 B	Gaia DR2 3282460371222713728	04:36:33.274	+05:11:31.41	14.77 \pm 0.14	-19.544 \pm 0.089	5.71 \pm 0.09	16.270 \pm 0.001	1.7658 \pm 0.0001	333.156 \pm 0.002
338 A	TYC 4739-1225-1	04:39:20.251	-03:14:21.79	14.784 \pm 0.080	-16.007 \pm 0.056	6.09 \pm 0.04	10.9621 \pm 0.0008
338 B	2MASS J04392073-0314301	04:39:20.752	-03:14:30.44	15.80 \pm 0.13	-15.330 \pm 0.095	6.21 \pm 0.06	14.3892 \pm 0.0005	11.4482 \pm 0.0001	139.0309 \pm 0.0003
346 A	2MASS J04421498+0250387	04:42:14.998	+02:50:38.54	14.310 \pm 0.082	-17.815 \pm 0.056	5.82 \pm 0.05	14.8299 \pm 0.0008
346 B	2MASS J04421451+0250336	04:42:14.531	+02:50:33.42	14.70 \pm 0.23	-16.73 \pm 0.18	5.8 \pm 0.1	17.743 \pm 0.001	8.6712 \pm 0.0001	233.8027 \pm 0.0006
351	TYC 83-1232-1	04:43:04.063	+00:49:47.45	14.188 \pm 0.095	-17.190 \pm 0.058	5.81 \pm 0.05	11.189 \pm 0.002
353	2MASS J04431309+0048174	04:43:13.116	+00:48:17.19	13.76 \pm 0.14	-16.967 \pm 0.083	5.79 \pm 0.08	14.479 \pm 0.001	163.0508 \pm 0.0001	123.6116 \pm 0.0001
371 A	2MASS J04544679-0001085	04:54:46.790	-00:01:08.42	10.897 \pm 0.033	-15.313 \pm 0.027	5.40 \pm 0.02	13.325 \pm 0.002
371 B	Gaia DR2 3228318975563766784	04:54:46.875	-00:01:10.21	11.191 \pm 0.065	-16.437 \pm 0.050	5.32 \pm 0.04	14.858 \pm 0.001	2.1970 \pm 0.0001	144.7240 \pm 0.0009
372 A	TYC 4741-307-1	04:56:18.287	-01:53:33.04	11.95 \pm 0.12	-15.188 \pm 0.075	5.61 \pm 0.06	10.775 \pm 0.001
372 B	2MASS J04561830-0153393	04:56:18.315	-01:53:39.53	12.59 \pm 0.16	-14.91 \pm 0.10	5.62 \pm 0.07	15.877 \pm 0.001	6.5078 \pm 0.0001	176.3739 \pm 0.0008
...	2MASS J03250457+0728193	03:25:04.592	+07:28:18.82	31.22 \pm 0.26	-21.79 \pm 0.20	6.8 \pm 0.2	17.360 \pm 0.002
...	Gaia DR2 9977797439144320	03:25:04.736	+07:28:20.43	31.93 \pm 0.38	-21.57 \pm 0.31	6.8 \pm 0.3	18.012 \pm 0.003	2.6658 \pm 0.0002	53.045 \pm 0.004
...	HD 23110	03:42:45.949	+07:54:10.34	33.89 \pm 0.26	-18.72 \pm 0.23	7.8 \pm 0.1	7.7818 \pm 0.0004
...	TYC 657-794-2	03:42:46.021	+07:54:09.49	35.75 \pm 0.65	-9.83 \pm 0.69	7.5 \pm 0.2	10.038 \pm 0.005	1.3660 \pm 0.0002	128.34 \pm 0.01
...	2MASS J03424511+0754507	03:42:45.157	+07:54:50.35	31.74 \pm 0.28	-18.06 \pm 0.20	7.9 \pm 0.1	17.864 \pm 0.002	41.7030 \pm 0.0001	343.5988 \pm 0.0002

NOTE—See section 4.1 for more details.

One notable case of a star with co-moving components is 29 Tau, the most massive member of MUTA. 29 Tau (MUTA 5, Gaia DR2 3276605295710700032) is a B3 + A7 binary star (Beavers & Cook 1980), with three co-moving systems within 70'': 29 Tau B (MUTA 139; 2MASS J03454440+0603283; Gaia DR2 3276604922051089664), which is itself a spectral binary (Mason et al. 2001); 29 Tau C (MUTA 137; 2MASS J03454104+0602349; Gaia DR2 3276604544094119424); and 29 Tau D (MUTA 138; 2MASS J03454269+0603039; Gaia DR2 3276604544093968896). In addition to these six system components, there are two other *Gaia* DR2 entries within $\simeq 42''$ of 29 Tau (Gaia DR2 3276604509734231808 and Gaia DR2 3276605265648475776) located within 300 pc of the Sun with inconsistent proper motions and parallaxes. Both of them have re-normalised unit weight error (RUWE) values of $\simeq 1.1$ which is not clearly indicative of bad parallax solutions, and indicates that they are probably unrelated to 29 Tau. For this reason, we ignored them in this analysis but we would recommend re-visiting this when further *Gaia* data releases are published. Two additional MUTA candidates are within 700–715'' of 29 Tau: MUTA 143 (2MASS J03460544+0553074; Gaia DR2 3276586333432639744) and MUTA 135 (2MASS J03450918+0612030; Gaia DR2 3276798401738487808). Gaia DR2 3276584478006772224 also seems co-moving with 29 Tau at a separation of 977''.5, but was not recovered in our search because its MUTA probability (89.7%) is below our selection threshold.

Cross-matching our list of candidates with the Oh et al. (2017) catalog of co-moving systems yielded a total of 28 matches, to Groups 39, 43, 52, 60, 124, 242, 1099 and 1109. Each of these groups have a total of members between 2 and 7. We verified that each of these groups were included in their entirety in our list of MUTA candidates, and found 4 missing components of Group 39 and one missing component of Group 1109. We added these objects to our list of low-likelihood MUTA candidates despite their BANYAN Σ membership probabilities below 90% (ranging from 0% to 64%) for completion. As demonstrated by Faherty et al. (2018), the algorithm of Oh et al. (2017) tends to break up nearby associations in many sub-groups because of the strong variations and correlations in direct kinematic observables (sky position, proper motion and parallax) caused by their wide distributions on the sky. The full list of matches between our candidates and Oh et al. (2017) groups are shown in Table 5.

4.2. Red Giant Stars

One candidate member of the MUTA association, HD 27860, is located far above the main sequence and within the red giant branch in Figure 5. A literature search revealed that this object has a spectral type K2 III (Woolley et al. 1981), consistent with its position in the color-magnitude diagram. Based on the compilations of stars within 40 pc established by Gray et al. (2003) and Gray et al. (2006), stars with the same spectral type have an average color $B - V = 1.16$ and absolute magnitude $M_V = 1.3$ ³.

Using the three-dimensional extinction map *STructuring by Inversion of the Local InterStellar Medium* (STILISM; Lallemand et al. 2014; Capitanio et al. 2017; Lallemand et al. 2018)⁴, we can expect HD 27860 to be subject to an extinction $E(B - V) = 0.12 \pm 0.02$ based on its sky position and distance, which translates to $A_V = 0.43 \pm 0.08$ (using a total to selective extinction ratio $R = 3.54$ for this photometric band). Correcting its observed properties in the same photometric bands ($B - V = 1.41 \pm 0.01$ and $M_V = 0.05 \pm 0.02$; ESA 1997) for extinction yields an intrinsic color of $B - V = 1.29 \pm 0.02$ and an absolute magnitude $M_V = -0.38 \pm 0.08$, placing it closer in colors to the average value for K3 III giants ($B - V = 1.37$).

Using the bolometric correction of Flower (1996) for this color ($BC_V = -0.73$), we estimate a bolometric magnitude $M_{\text{bol}} = -1.11 \pm 0.08$ and $\log L/L_\odot = 2.36 \pm 0.03$. We estimated its effective temperature at $T_{\text{eff}} \approx 4400$ K by interpolating its extinction-corrected $B - V$ color and comparing them with averages from Gray et al. (2003) and Gray et al. (2006) for spectral types K2 III and K3 III. These physical parameters are consistent with a luminosity class III; the Bertelli et al. (2009) solar-metallicity isochrones predict a mass of $2.44 M_\odot$, a surface gravity $\log g \approx 2.0$ and an age of $\simeq 650$ Myr.

HD 27860 seems significantly too old to be a member of MUTA based on the color-magnitude sequence of this young association (Figure 5). The main-sequence turn-off of a 650 Myr association would be located at spectral types A0 or later⁵ (i.e., at absolute *Gaia* DR2 magnitudes $M_G \approx 1.5$). The fact that MUTA includes several members more massive than A0 strongly suggests that HD 27860 is a chance interloper despite its high 98.6%

³ See also <http://www.pas.rochester.edu/~emamajek/spt/K2III.txt>

⁴ Available at <https://stilism.ospm.fr>

⁵ See http://www.pas.rochester.edu/~emamajek/EEM_dwarf-UBVIJHK_colors_Teff.txt

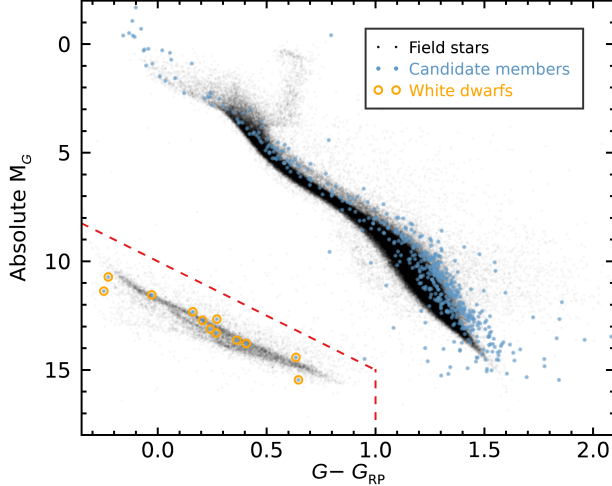


Figure 6. Selection criterion for white dwarfs based on *Gaia* DR2 color-magnitude positions. See Section 4.3 for more details.

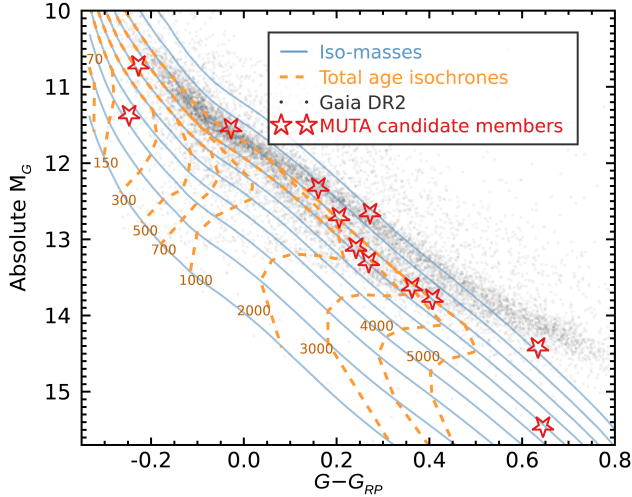


Figure 7. MUTA candidates recovered in *Gaia* DR2 data which color-magnitude positions are consistent with white dwarfs (red star symbols). Nearby white dwarfs in *Gaia* DR2 are indicated with black dots, and total age isochrones from 70 Myr to 5 Gyr are indicated with orange dashed lines. Iso-masses from $0.4 M_{\odot}$ (top) to $1.3 M_{\odot}$ (bottom) by steps of $0.1 M_{\odot}$ are displayed with blue lines. Most white dwarfs recovered here are too old to be coeval with MUTA. No correction for interstellar extinction was applied in this figure. See Section 4.3 for more details.

Bayesian membership probability, and we therefore reject it from our list of candidate members.

4.3. White Dwarfs

A subset of MUTA members are located below the main sequence and within the color-magnitude sequence of white dwarfs in Figure 2. We flagged all candi-

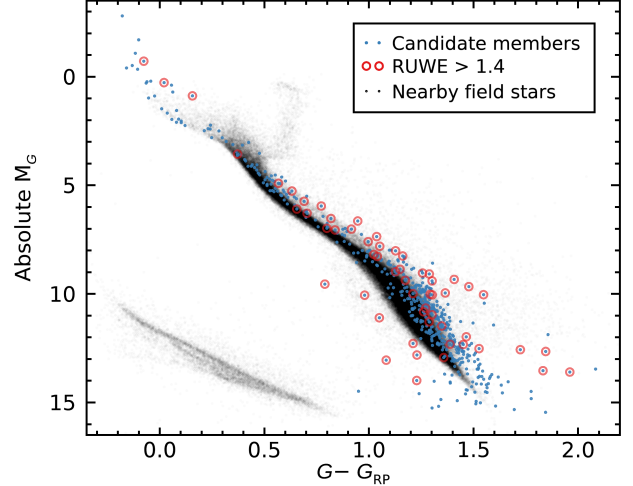


Figure 8. *Gaia* DR2 color-magnitude diagram of MUTA members and candidates (red circles) compared with nearby field stars (black circles). All objects flagged as problematic because of their poor *Gaia* DR2 astrometric solutions ($\text{RUWE} > 1.4$) are marked with red circles. A large fraction of these problematic solutions are located below the sequence of members, likely because of contamination by an unresolved source, or consist of possible multiple systems located above the MUTA sequence. See Section 4.4 for more details.

dates with an absolute G -band magnitude fainter than $(G - G_{RP}) \cdot 5 + 10$ and a color $G - G_{RP} < 1.0$ (shown in Figure 6) as likely white dwarfs, and compared them to total age isochrones obtained by combining MIST stellar main-sequence lifetimes (Choi et al. 2016) and the the Montréal white dwarf cooling tracks (Fontaine et al. 2001)⁶ in Figure 7.

All but two white dwarfs in our sample are clearly much older than 150 Myr, inconsistent with the main-sequence turn-off age of MUTA ($\lesssim 80$ Myr). The two youngest and hottest white dwarfs in this figure are WD 0350+098 (MUTA 190; other designations include 1RXS J035315.5+095700, SDSS J035315.72+095633.7) and WD 0340+103 (MUTA 125; other designations include RBS 466, 1RXS J034314.1+102941, and SDSS J034314.35+102938.4), and are discussed further in Section 6.4.

We can estimate a false-positive rate for our list of MUTA candidate members based on the fact that we uncovered 10 white dwarfs that are clearly too old for this young association. The number density of white

⁶ Available at <http://www.astro.umontreal.ca/~bergeron/CoolingModels/>, see also Holberg & Bergeron (2006); Kowalski & Saumon (2006); Tremblay et al. (2011) and Bergeron et al. (2011).

dwarfs, $4.49 \pm 0.38 \times 10^{-3}$ objects pc $^{-3}$ (Hollands et al. 2018), is small compared with that of main-sequence stars ($98.4 \pm 6.8 \times 10^{-3}$ objects pc $^{-3}$; Kirkpatrick et al. 2012). Assuming that white dwarfs have similar kinematics to main-sequence stars, this means we could expect as many as 220^{+25}_{-22} stars in our sample to be contaminants if we applied no other cuts than BANYAN Σ probabilities based on proper motion and parallax without radial velocity measurements (none of the white dwarf contaminants have radial velocity measurements). An additional 28 *Gaia* DR2 sources would have been uncovered in our survey if we used only these observables and no other criteria, leaving our estimated number of contaminants to 192^{+25}_{-22} in our final list of candidates, or $34^{+5}_{-4}\%$ of our full sample of 503 objects. The majority of contaminants are expected to be M dwarfs.

4.4. Poor Astrometric Solutions

The *Gaia* DR2 team recommends placing low confidence in astrometric solutions with a RUWE larger than 1.4⁷. We therefore flagged all 52 MUTA candidates and members with $\text{RUWE} > 1.4$ (shown in Figure 8) and consider them as low-likelihood candidates; we consider that an observational follow-up of these objects will potentially be useful, but should be less prioritary. It is likely that some of these issues will be resolved in the next *Gaia* DR2 data release.

4.5. Visual Inspection of Finder Charts

We generated finder charts for all MUTA objects with available survey data from DSS, SDSS (Alam et al. 2015), UKIDSS (Lawrence et al. 2007), VHS (McMahon et al. 2013), Pan-STARRS (Chambers et al. 2016), *WISE* (Wright et al. 2010) and 2MASS (Skrutskie et al. 2006) data with the `finder_charts.py` Python package (Gagné et al. 2018)⁸, on which we overlaid *Gaia* DR2 catalog entries with arrows and symbol sizes indicating their individual proper motions and distances. We used these figures to identify and correct any mismatches in our automated cross-matches to 2MASS and *WISE*, which tends to happen when a target has a missing entry in either catalog.

We also verified that binaries and co-moving systems had the correct component attached to each catalog, and noted 12 stars that visually appeared co-moving with one of our targets at a similar distance, but were not recovered with our co-moving search described in Section 4.1. Those usually have *Gaia* DR2 proper motions

or parallaxes that are slight mis-matches to our MUTA candidate or member, and are listed in Table 6. It is possible that some of these systems suffer from a bad parallax solution, either because they are themselves multiple systems (e.g., 30 Tau and TYC 661–1404–1, respectively MUTA 3 A and MUTA 3 B), or contaminated by a background source (althoug they all have $\text{RUWE} \leq 1.4$). We listed these systems that almost seem co-moving in Table 6 for later follow-up, but we excluded them from the current analysis.

A number of MUTA candidates are located well below the main sequence in a *Gaia* DR2 color-magnitude diagram (see Figure 5), but yet not faint enough to be credible white dwarfs (see Section 4.3). A fraction of these objects failed the *Gaia* DR2 $\text{RUWE} \leq 1.4$ selection criterion for good astrometric solutions, indicating that bad parallax solutions are likely part of the explanation. Figure 9 shows a finder chart for one such object (WISEA J033742.99+191646.7)⁹. In this example, the finder chart shows that it is well detected at red-optical wavelengths (e.g., Pan-STARRS) and in *WISE W1*, but too faint to be detected in 2MASS in the near-infrared. This unusual combination indicates a likely contribution from two distinct blackbodies. The presence of an accretion disks could potentially explain this, however those usually result in much redder *Gaia* DR2 $G - G_{\text{RP}}$ colors, which would push the object far to the right of, rather than below, the main sequence. The simplest explanation seems to be that this object is a blend of two sources, maybe located at different distances, but at an angular separation small enough that they are unresolved in all the aforementioned surveys.

We assigned MUTA identifiers (31 to 372) to all candidate members that were not rejected or defined as low-likelihood candidates based either on their poor astrometric solutions, ages that are definitely too old, or problematic position in a color-magnitude diagram. We ordered these identifiers by right ascension. Stars identified in Section 4.1 as co-moving with a well-behaved MUTA candidate or member which did not have a MUTA identified were assigned identifiers 373–375. Those still without identifiers that belong in one of the Oh et al. (2017) groups associated with MUTA were assigned identifiers 376–382, and those visually identified as co-moving with a well-behaved candidate in this section were assigned identifiers 383–386.

⁷ As described at <https://www.cosmos.esa.int/web/gaia/dr2-known-issues>.

⁸ Available at https://github.com/jgagneastro/finder_charts.

⁹ All finder charts are available as online-only supplementary data.

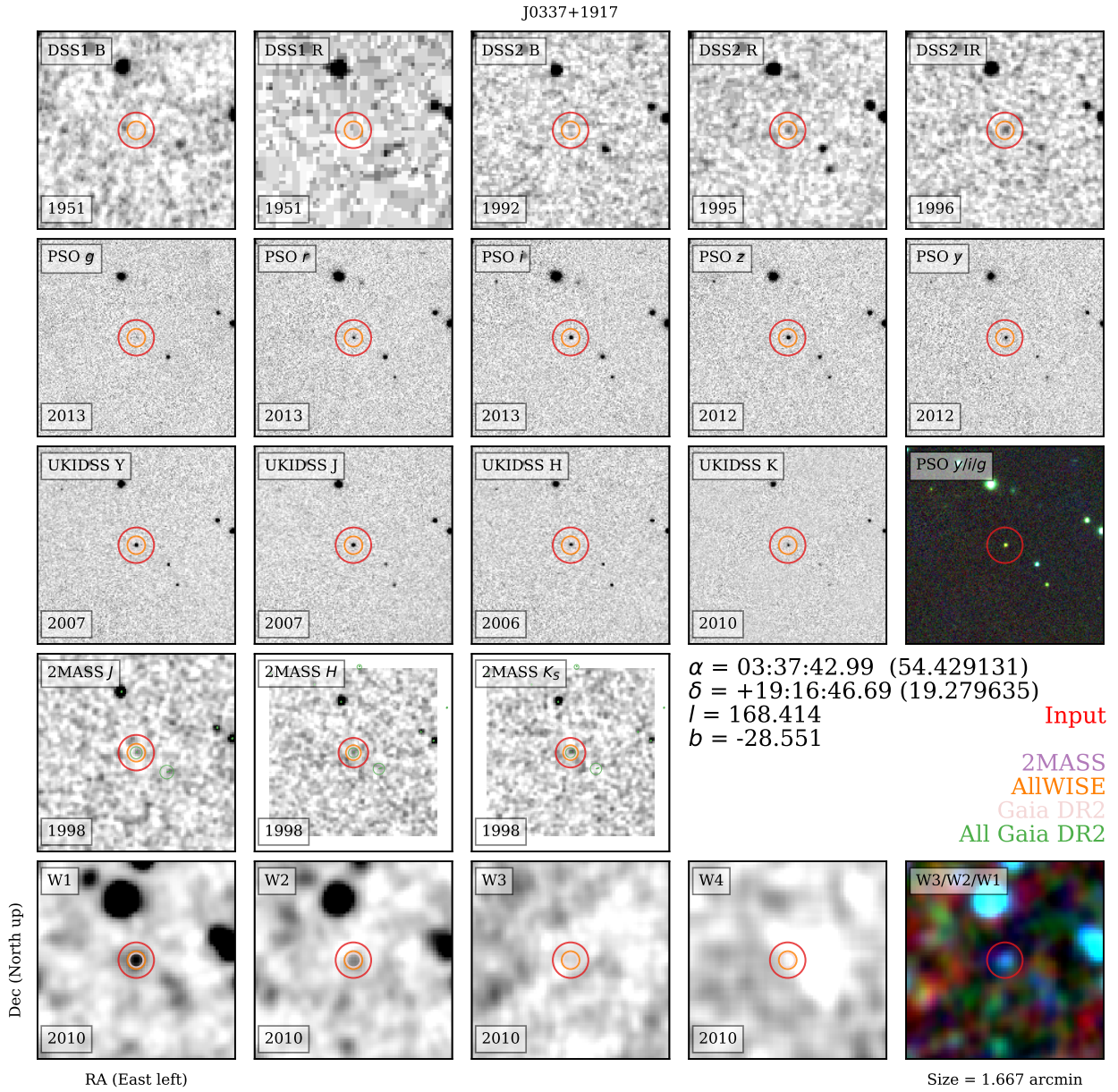


Figure 9. Finder charts for WISEA J033742.99+191646.7, a problematic candidate because its position in a *Gaia* DR2 color-magnitude diagram is well below the main sequence, likely because of contamination from a background source at a very small angular separation. See Section 4.5 for more details.

Table 5. MUTA objects in common with Oh et al. (2017).

MUTA		<i>Gaia</i> DR2	Oh et al. (2017)	Object
ID	Name	ID	Group	Type ^a
368	HD 31125	3226496187146449920	39	Candidates
369	TYC 4745–475–1	3224698799168916864	39	Candidates
372 A	TYC 4741–307–1	3225639289631939456	39	Candidates
379	BD+00 884	3231439080323844864	39	Incomplete
380	HD 32264	3225291882613467520	39	Incomplete
381	HD 32721	3212973572810773120	39	Incomplete
382	HD 33023	3212956839618107648	39	Incomplete
10	V766 Tau	37136834159399808	43	Initial
21	HD 286374	3303308245556503296	43	Initial
22	PPM 119410	36595943156045824	43	Initial
26	TYC 662–217–1	3304906145189468416	43	Initial
28	TYC 664–136–1	39841357885932288	43	Initial
377	HIP 18778	3301831773241303552	43	Initial
13	HD 23990	3302396166303947904	52	Initial
19 A	HD 23376	3278197770802258944	52	Initial
19 B	TYC 658–1007–2	3278197766505583232	52	Initial
95	HD 22073	11397988505713536	52	Candidates
140	TYC 658–828–1	3278300987456845440	52	Candidates
17	HD 27687	3286590824092307200	60	Initial
18	HD 28356	3285720938596464640	60	Initial
25	TYC 80–202–1	3297372944352021120	60	Initial
30 A	TYC 668–737–1	3299167141170181888	60	Initial
290	BD+05 638	3284966433101477376	60	Candidates
33	HD 17008	127148009968227584	124	Candidates
35	TYC 1785–155–1	114510012864474112	124	Candidates
41	TYC 1790–927–1	115353480017970560	124	Candidates
11	HD 28715	3285542336676520448	242	Initial
324 A	HD 29182	3282435563491664896	242	Candidates
324 B	TYC 90–953–1	3282434979377650176	242	Incomplete
20	HIP 17133	3808873789758720	1099	Initial
117 A	TYC 663–362–1	38076641722829440	1099	Candidates
376	TYC 665–150–1	38398936068862464	1109	Candidates
378	HD 286412	3305439511410844800	1109	Incomplete

^a Initial: members of MUTA from our initial list. Candidates: candidates of MUTA recovered in Section 4. Incomplete: Targets missing from our list of MUTA initial members and new candidates.

NOTE—See section 4.1 for more details.

Table 6. Wide multiple candidate systems in MUTA visually identified but not recovered in Section 4.1.

MUTA		R.A.	Decl.	$\mu_\alpha \cos \delta$	μ_δ	Parallax	<i>Gaia</i> DR2	Sep.	Pos. Ang.
ID	Name	(hh:mm:ss.sss)	(dd:mm:ss.ss)	(mas yr $^{-1}$)	(mas yr $^{-1}$)	(mas)	G mag	($''$)	($^{\circ}$)
3 A	30 Tau	03:48:16.292	+11:08:35.52	25.27 \pm 0.28	-23.69 \pm 0.23	7.74 \pm 0.17	5.040
3 B	TYC 661-1404-1	03:48:16.835	+11:08:40.16	25.62 \pm 0.15	-24.97 \pm 0.11	7.223 \pm 0.070	9.269	9.2389 \pm 0.0001	59.8505 \pm 0.0007
5	29 Tau	03:45:40.466	+06:02:59.78	21.88 \pm 0.29	-13.65 \pm 0.26	5.31 \pm 0.25	5.295
383	2MASS J03453759+0603048	03:45:37.587	+06:03:04.31	-1.86 \pm 0.11	-25.471 \pm 0.085	5.427 \pm 0.070	15.481	43.1779 \pm 0.0002	276.0326 \pm 0.0001
97 A	2MASS J03350340+1431490	03:35:03.438	+14:31:48.54	26.99 \pm 0.14	-25.93 \pm 0.11	7.342 \pm 0.081	15.369
97 B	2MASS J03350317+1431358	03:35:03.209	+14:31:35.33	26.87 \pm 0.39	-25.57 \pm 0.30	6.84 \pm 0.24	18.097	13.6275 \pm 0.0002	194.1236 \pm 0.0008
104 A	2MASS J03361762+2153391	03:36:17.665	+21:53:38.50	29.492 \pm 0.088	-30.262 \pm 0.068	7.526 \pm 0.047	10.910
104 B	2MASS J03361732+2153271	03:36:17.360	+21:53:26.42	29.95 \pm 0.71	-31.17 \pm 0.52	7.98 \pm 0.31	18.454	12.8056 \pm 0.0002	199.354 \pm 0.002
117 A	TYC 663-362-1	03:40:57.781	+13:09:03.06	24.66 \pm 0.25	-25.44 \pm 0.21	6.749 \pm 0.098	10.493
117 B	2MASS J03405723+1308577	03:40:57.261	+13:08:57.23	27.03 \pm 0.71	-24.78 \pm 0.50	7.19 \pm 0.33	18.437	9.5851 \pm 0.0003	232.539 \pm 0.002
153 A	TYC 1252-301-1	03:47:23.901	+18:43:17.68	21.128 \pm 0.079	-23.175 \pm 0.057	5.926 \pm 0.041	11.689
153 B	Gaia DR2 44752086050666368	03:47:23.645	+18:43:18.70	21.33 \pm 0.60	-26.33 \pm 0.57	6.36 \pm 0.34	17.855	3.7781 \pm 0.0003	285.639 \pm 0.004
177 A	2MASS J03505694+0730565	03:50:56.976	+07:30:56.18	30.41 \pm 0.23	-22.22 \pm 0.16	8.29 \pm 0.12	16.916
177 B	Gaia DR2 3277369048270999936	03:50:56.968	+07:30:53.92	27.9 \pm 2.2	-21.7 \pm 1.4	6.3 \pm 1.3	20.438	2.2609 \pm 0.0005	183.03 \pm 0.03
225 A	2MASS J04021281+0817400	04:02:12.839	+08:17:39.75	23.38 \pm 0.24	-22.68 \pm 0.17	6.62 \pm 0.13	16.635
225 B	2MASS J04021257+0817410	04:02:12.593	+08:17:40.67	22.00 \pm 0.36	-23.46 \pm 0.25	6.19 \pm 0.19	17.316	3.7653 \pm 0.0002	284.200 \pm 0.002
271	2MASS J04181095+0934586	04:18:10.980	+09:34:58.24	15.97 \pm 0.27	-21.58 \pm 0.21	5.83 \pm 0.16	17.228	26.4111 \pm 0.0001	326.8006 \pm 0.0003
384	2MASS J04181193+0934365	04:18:11.958	+09:34:36.14	19.11 \pm 0.19	-21.51 \pm 0.14	4.74 \pm 0.11	16.800
277 A	2MASS J04200165+0759584	04:20:01.666	+07:59:57.72	22.83 \pm 0.68	-23.94 \pm 0.47	6.31 \pm 0.34	15.336
277 B	Gaia DR2 3298956138016754048	04:20:01.719	+07:59:58.51	19.87 \pm 0.90	-21.65 \pm 0.42	6.69 \pm 0.14	16.289	1.1173 \pm 0.0003	44.75 \pm 0.02
279	2MASS J04201617+0959534	04:20:16.202	+09:59:53.06	17.34 \pm 0.38	-20.97 \pm 0.19	6.14 \pm 0.17	17.379	7.1832 \pm 0.0001	18.446 \pm 0.001
385	TYC 671-129-1	04:20:16.048	+09:59:46.25	16.91 \pm 0.14	-22.140 \pm 0.066	5.668 \pm 0.061	10.795
318 A	2MASS J04341953+0226260	04:34:19.560	+02:26:25.89	16.32 \pm 0.42	-20.02 \pm 0.29	5.77 \pm 0.22	12.150
318 B	Gaia DR2 3279527149078835712	04:34:19.467	+02:26:25.91	15.62 \pm 0.75	-21.63 \pm 0.44	6.24 \pm 0.33	15.960	1.4009 \pm 0.0003	270.61 \pm 0.01
329 A	2MASS J04372971-0051241	04:37:29.730	-00:51:24.47	15.026 \pm 0.042	-16.665 \pm 0.027	6.050 \pm 0.025	13.223
329 B	Gaia DR2 3229491776511286016	04:37:29.780	-00:51:25.66	14.70 \pm 0.36	-17.42 \pm 0.19	5.75 \pm 0.14	16.507	1.4169 \pm 0.0001	147.563 \pm 0.006
331 A	2MASS J04382750-0342441	04:38:27.523	-03:42:44.47	23.399 \pm 0.072	-20.462 \pm 0.051	6.076 \pm 0.041	14.931
331 B	Gaia DR2 3201810884087980800	04:38:27.437	-03:42:46.23	19.59 \pm 0.85	-17.76 \pm 0.49	6.77 \pm 0.40	18.416	2.1809 \pm 0.0003	216.359 \pm 0.007
368	HD 31125	04:53:04.828	-01:16:33.04	12.67 \pm 0.11	-15.782 \pm 0.072	5.644 \pm 0.051	7.918
386	HD 31124	04:53:04.574	-01:15:52.17	19.54 \pm 0.19	-17.88 \pm 0.12	6.081 \pm 0.098	8.046	41.0425 \pm 0.0001	354.6787 \pm 0.0001
...	2MASS J03343284+1212290	03:34:32.872	+12:12:28.55	27.892 \pm 0.090	-30.240 \pm 0.063	6.740 \pm 0.044	12.302
...	Gaia DR2 40541334474313728	03:34:33.106	+12:12:29.76	28.23 \pm 0.88	-29.63 \pm 0.62	7.50 \pm 0.54	19.087	3.6272 \pm 0.0004	70.436 \pm 0.005

NOTE—See section 4.5 for more details.

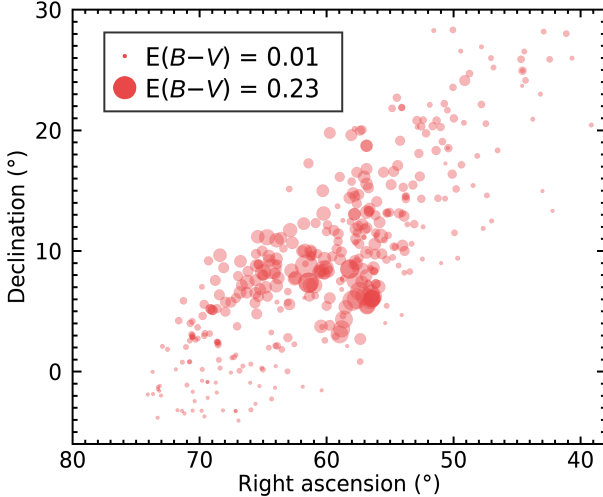


Figure 10. Individual $E(B - V)$ extinctions of MUTA objects based on the STILISM three-dimensional extinction map combined with the sky positions and *Gaia* DR2 distances of MUTA objects. See Section 5 for more details.

5. CORRECTING EXTINCTION IN GAIA DR2 PHOTOMETRY

The MUTA association is distant enough that some of its members appear slightly reddened by interstellar dust. We used STILISM (Lallemand et al. 2014; Capitanio et al. 2017; Lallemand et al. 2018)¹⁰ to determine the individual $E(B - V)$ extinction values for individual MUTA objects based on their sky position and *Gaia* DR2 distance. The resulting individual extinction values are displayed in Figure 10.

We corrected the color-magnitude diagram position of MUTA members and candidates with an iterative method to account for the wide *Gaia* DR2 photometric bandpasses. As shown in Figure 11, even the G_{RP} bandpass spans a significant region over which both the extinction curve of Fitzpatrick (1999) and the spectral energy density of an M-type star vary significantly. As a consequence, the reddening vectors in *Gaia* DR2 color-magnitude sequences will differ significantly across spectral types.

The flux of a star with a spectral energy density S_λ observed through an instrument with a bandpass P_λ is given by:

$$F = \frac{\int_0^\infty S_\lambda P_\lambda d\lambda}{\int_0^\infty P_\lambda d\lambda}. \quad (1)$$

In the presence of interstellar extinction E_λ , the observed flux is:

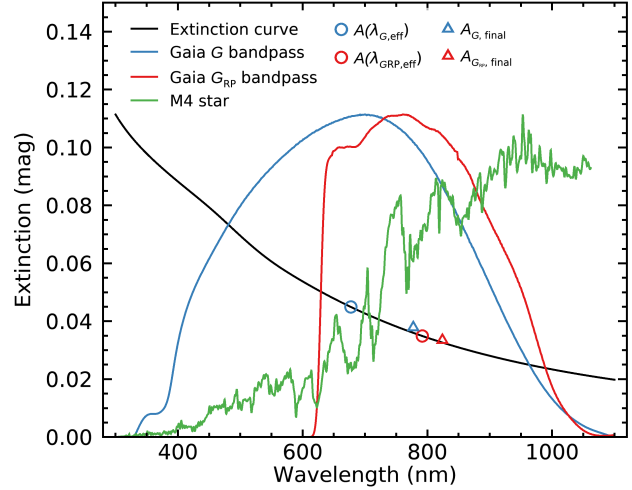


Figure 11. Fitzpatrick (1999) interstellar extinction curve (black line) compared with *Gaia* DR2 G and $G - G_{RP}$ bandpasses (blue and red, respectively) and the spectral flux density of an M4 low-mass star (green). Using only the effective wavelength of *Gaia* DR2 bandpasses to estimate extinction (blue and red circles) leads to an over estimation of de-reddening and a mistaken reddening vector angle compared with a more careful extinction correction that accounts for the stellar flux across the *Gaia* DR2 bandpasses (blue and red triangles). This effect is highly dependent on the spectral type of the star because of the wide *Gaia* DR2 bandpasses. See Section 5 for more detail.

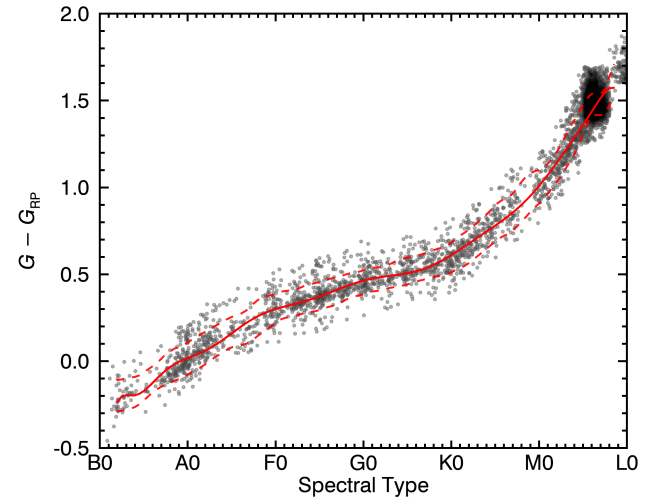


Figure 12. *Gaia* DR2 $G - G_{RP}$ colors as a function of spectral type for known nearby young stars and brown dwarfs (black dots). A polynomial fit is shown as a solid red line with 1σ scatter as a dashed red line. We used this relation to estimate spectral types when no literature data was available. See Section 6.1 for more details. The polynomial coefficients for the red line are available as online-only material.

¹⁰ Available at <https://stilism.obspm.fr>

$$F_{\text{reddened}} = \frac{\int_0^{\infty} E_{\lambda} S_{\lambda} P_{\lambda} d\lambda}{\int_0^{\infty} P_{\lambda} d\lambda}, \quad (2)$$

and therefore the correction factor that remains valid for wide bandpasses is:

$$\frac{F_{\text{reddened}}}{F} = \frac{\int_0^{\infty} E_{\lambda} S_{\lambda} P_{\lambda} d\lambda}{\int_0^{\infty} S_{\lambda} P_{\lambda} d\lambda}. \quad (3)$$

In effect, this correction is a weighted average of the extinction curve, where the weight is given by the product of the stellar spectral energy density with the instrumental bandpass. In general, the spectral energy densities of MUTA members and candidates have not been measured, and their spectral types are unknown. We therefore used an iterative method where the photometric spectral type of each star is first estimated from its $G - G_{\text{RP}}$ color. The $G - G_{\text{RP}}$ versus spectral type relation for stars with spectral types B0 to L0 is shown in Figure 12. These data were drawn from the list of nearby young association members of Gagné et al. (2018) and the List of Ultracool Dwarfs¹¹ that includes data from previous lists of brown dwarfs (Dupuy & Liu 2012; Mace 2014; Gagné et al. 2015; Liu et al. 2016; Faherty et al. 2016). A polynomial relation was fitted to the data and is also displayed in the figure; the coefficients to this polynomial sequence are available as online-only material. We preferred using a *Gaia* DR2 color to spectral type relation rather than a *Gaia* DR2 absolute magnitude to spectral type relation, because unresolved multiples would bias the latter more significantly.

We used the Pickles Atlas of spectral energy distributions for B0–M9 stars (Pickles 1998) and interpolated the *Gaia* DR2 instrumental bandpasses and the extinction curve of Fitzpatrick (1999; with a nominal total to selective extinction value $R(V) = 3.1$) on the Pickles wavelength vector to determine an appropriate extinction correction.

The resulting extinction-corrected $G - G_{\text{RP}}$ color was then used to obtain a better photometric spectral type estimate, which we used in turn to correct the raw $G - G_{\text{RP}}$ color anew. This step was repeated until the photometric spectral type estimate of a star remained unchanged. A total of four iterations were needed for the de-reddening correction to converge for all MUTA stars. The resulting extinction vectors and corrected color-magnitude diagram of MUTA are shown in Figure 13.

In Tables 7 and 8, we provide reddening values $R(G)$ and $R(G_{\text{RP}})$ as a function of spectral types or uncorrected *Gaia* DR2 $G - G_{\text{RP}}$ colors, which can be used to de-redden the *Gaia* DR2 photometry of main-sequence or young stars with the following relations:

$$G_{\text{corr}} = G_{\text{uncorr}} - E(B - V) \cdot R(G), \quad (4)$$

$$G_{\text{RP,corr}} = G_{\text{RP,uncorr}} - E(B - V) \cdot R(G_{\text{RP}}). \quad (5)$$

Table 7. *Gaia* DR2 de-reddening relations as a function of spectral type that account for its large photometric bandpasses.

Spectral Type	$R(G)$ (mag)	$R(G_{\text{RP}})$ (mag)	$R(G_{\text{BP}})$ (mag)
B3	3.112 ± 0.001	1.938 ± 0.001	3.670 ± 0.001
B5	3.10 ± 0.02	1.936 ± 0.002	3.65 ± 0.02
B7	3.029 ± 0.001	1.926 ± 0.001	3.566 ± 0.001
B9	3.002 ± 0.006	1.925 ± 0.001	3.540 ± 0.006
A1	2.962 ± 0.003	1.919 ± 0.001	3.503 ± 0.002
A3	2.939 ± 0.006	1.916 ± 0.001	3.488 ± 0.004
A5	2.880 ± 0.001	1.904 ± 0.001	3.452 ± 0.001
A7	2.840 ± 0.001	1.901 ± 0.001	3.431 ± 0.001
A9	2.782 ± 0.001	1.893 ± 0.001	3.400 ± 0.001
F1	2.724 ± 0.001	1.885 ± 0.001	3.369 ± 0.001
F3	2.724 ± 0.001	1.885 ± 0.001	3.369 ± 0.001
F5	2.693 ± 0.005	1.883 ± 0.001	3.348 ± 0.002
F7	2.637 ± 0.001	1.874 ± 0.001	3.311 ± 0.001
F9	2.632 ± 0.003	1.873 ± 0.001	3.308 ± 0.002
G1	2.61 ± 0.01	1.869 ± 0.001	3.291 ± 0.009
G3	2.577 ± 0.004	1.865 ± 0.001	3.264 ± 0.004
G5	2.568 ± 0.001	1.864 ± 0.001	3.254 ± 0.001
G7	2.55 ± 0.01	1.864 ± 0.001	3.240 ± 0.008
G9	2.526 ± 0.004	1.863 ± 0.001	3.221 ± 0.003
K1	2.491 ± 0.008	1.858 ± 0.001	3.192 ± 0.008
K3	2.40 ± 0.01	1.843 ± 0.002	3.128 ± 0.007
K5	2.316 ± 0.008	1.829 ± 0.001	3.052 ± 0.008
K7	2.224 ± 0.001	1.803 ± 0.001	2.997 ± 0.001
K9	2.193 ± 0.004	1.786 ± 0.002	3.004 ± 0.001
M1	2.118 ± 0.006	1.755 ± 0.002	2.985 ± 0.003
M3	1.960 ± 0.006	1.699 ± 0.002	2.949 ± 0.001
M5	1.847 ± 0.003	1.654 ± 0.001	2.922 ± 0.001

NOTE—See section 5 for more details.

¹¹ Available at http://astro.umontreal.ca/~gagne/ultracool_dwarfs.php

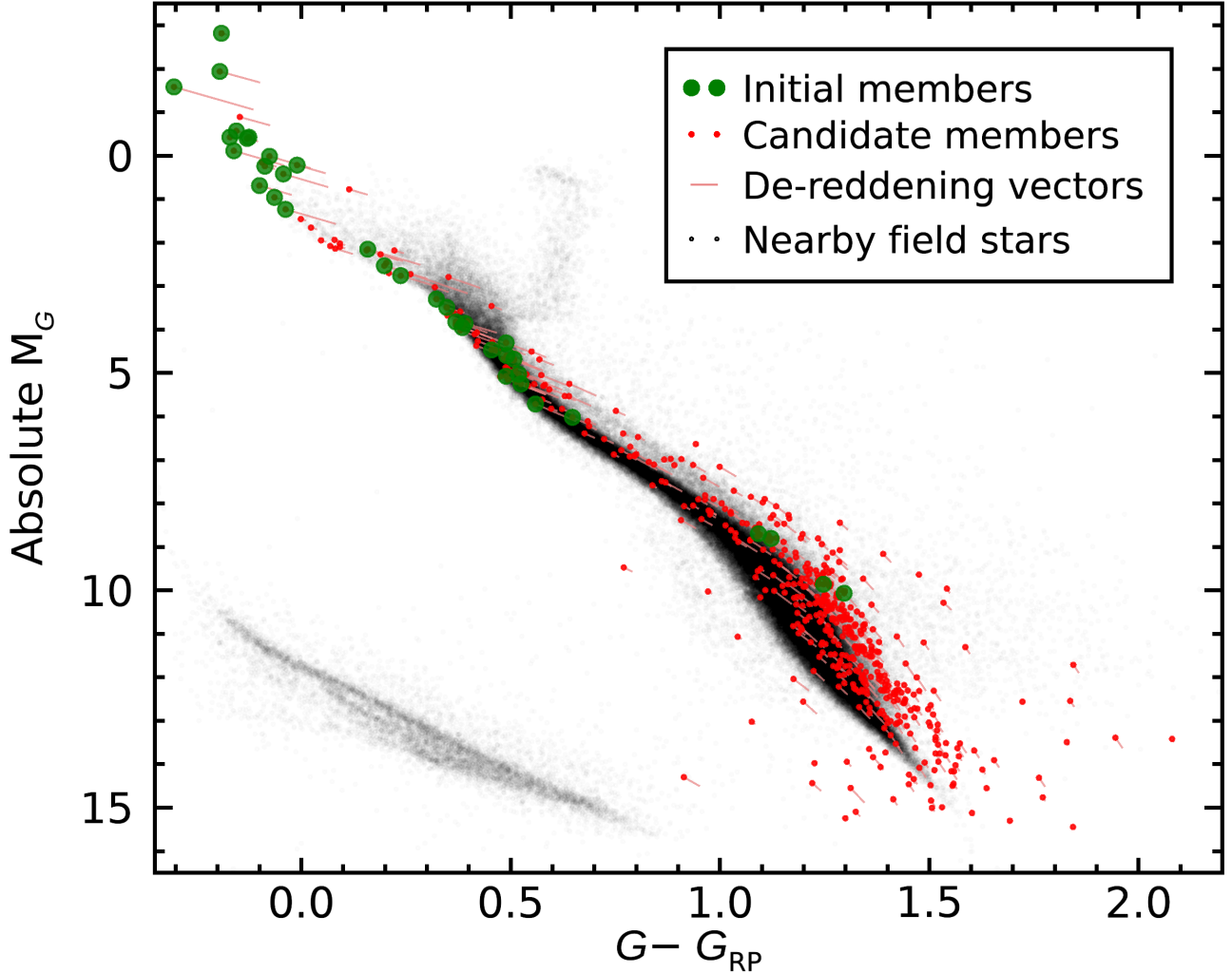


Figure 13. *Gaia* DR2 color-magnitude diagram of our initial list of MUTA members (green circles) and additional candidate members (red dots). De-reddening vectors are indicated with red lines (dots are located at the corrected position). A proper de-reddening correction that accounts for the wide *Gaia* DR2 bandpasses moves low-mass stars parallel to the sequence, and moves higher-mass stars mostly towards the left. See Section 5 for more details.

Table 8. *Gaia* DR2 de-reddening relations as a function of uncorrected $G - G_{\text{RP}}$.

Uncorrected $G - G_{\text{RP}}$	$R(G)$ (mag)	$R(G_{\text{RP}})$ (mag)	$R(G_{\text{BP}})$ (mag)
-0.18	1.938 ± 0.001	3.112 ± 0.001	3.670 ± 0.001
-0.08	1.930 ± 0.002	3.05 ± 0.02	3.59 ± 0.02
0.02	1.923 ± 0.002	2.99 ± 0.01	3.53 ± 0.01
0.12	1.919 ± 0.001	2.961 ± 0.009	3.504 ± 0.007
0.22	1.908 ± 0.003	2.90 ± 0.02	3.47 ± 0.01
0.32	1.90 ± 0.01	2.80 ± 0.08	3.40 ± 0.05
0.42	1.881 ± 0.003	2.68 ± 0.03	3.34 ± 0.02
0.52	1.865 ± 0.001	2.570 ± 0.005	3.257 ± 0.004
0.62	1.860 ± 0.001	2.507 ± 0.006	3.206 ± 0.006
0.72	1.842 ± 0.001	2.397 ± 0.009	3.124 ± 0.007
0.82	1.823 ± 0.005	2.30 ± 0.02	3.04 ± 0.01
0.92	1.796 ± 0.003	2.211 ± 0.005	3.000 ± 0.001
1.02	1.769 ± 0.003	2.157 ± 0.006	3.000 ± 0.001
1.12	1.735 ± 0.003	2.057 ± 0.008	2.965 ± 0.001
1.22	1.687 ± 0.002	1.930 ± 0.004	2.944 ± 0.001
1.32	1.656 ± 0.001	1.852 ± 0.003	2.924 ± 0.001
1.42	1.641 ± 0.001	1.818 ± 0.001	2.912 ± 0.001

NOTE—See section 5 for more details.

6. DISCUSSION

In this section, we discuss various properties of the MUTA members and of their population as a whole. Photometric spectral type estimates and additional substellar candidates are discussed in Sections 6.1 and 6.2. This is followed by an estimation of the isochronal age of MUTA (Section 6.3) and a discussion of the cooling ages of the two hot white dwarf candidate members of MUTA (Section 6.4). We discuss literature lithium absorption measurements for K- to G-type members of MUTA in Section 6.5, and discuss the present-day mass function of MUTA in Section 6.6. The stellar activity of its members is assessed in Section 6.7. MUTA is placed in context with the Galactic kinematic structure recently unveiled by Kounkel & Covey (2019) in Section 6.8.

6.1. Photometric Spectral Type Estimates

The extinction correction method described above directly provides photometric spectral type estimates for MUTA candidates and members with no spectral type information in the literature. We used a slightly different method to estimate the photometric spectral types of objects near the substellar regime with near-infrared 2MASS–WISE colors $J - W_2 > 1.5$, corresponding to a spectral types $\simeq M6$ and later (Gagné et al. 2015). For these redder objects, we used the spectral type to $J - W_2$

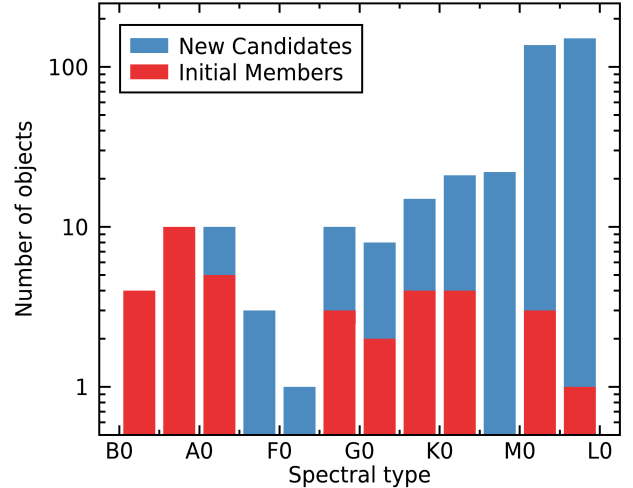


Figure 14. Distribution of observed and estimated photometric spectral types for initial MUTA members (red bars) and candidate members (blue bars). Data from *Gaia* DR2 allowed us to recover candidate members with photometric spectral types as late as M9. Two hot white dwarf candidates are excluded from this figure. See Section 6.1 for more details.

relation of Gagné et al. (2015) to determine a more accurate subtype given that the *Gaia* DR2 $G - G_{\text{RP}}$ colors are more spread and based on lower-quality detections in these cases (e.g., see Smart et al. 2019). All photometric spectral type estimates are shown in Figure 14.

6.2. Substellar Objects

In Figures 15 and 16, we show near-infrared color-magnitude sequences of MUTA candidates based on 2MASS and *WISE* photometry, compared with those of field-aged and young L-type or later low-mass stars and brown dwarfs. In both cases, the MUTA sequence forms a prolongation of the young substellar sequences at brighter absolute magnitudes, and there is a small overlap indicating that a few MUTA candidates discussed here may have spectral types as late as $\simeq L0$ (although at the age of MUTA the substellar boundary is near spectral type M7; Allard et al. 2012; Baraffe et al. 2015; Filippazzo et al. 2015). Kirkpatrick et al. (2011) devised a rejection criterion based on *WISE* photometry to distinguish extragalactic sources from brown dwarfs, but our only MUTA candidates with a sufficient W_3 -band detection were not red enough in $W_1 - W_2$ color to apply the rejection criterion.

6.3. Isochronal Age

The locus of MUTA candidates and members compiled in this work forms a sequence in color-magnitude space that sits between those of the Pleiades association (112 ± 5 Myr; Dahm 2015) and the Tucana-

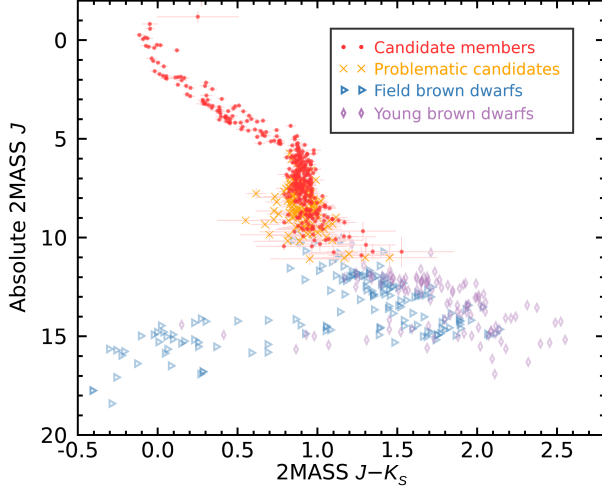


Figure 15. Absolute 2MASS J -band magnitudes versus $J - K_s$ colors for field (rightward blue triangles) and young (purple diamonds) brown dwarfs compared with all MUTA candidates and members (filled red circles). The MUTA candidates barely reach the sequence of young L-type brown dwarfs, and seem brighter or redder than the field brown dwarfs sequence, as expected for young objects. A fraction of the candidates with problematic *Gaia* DR2 colors (orange crosses) do not follow the MUTA sequence, which is expected if their photometry is contaminated by background objects. Only spectral types L0 and later are shown for all brown dwarf data. See Section 6.2 for more details.

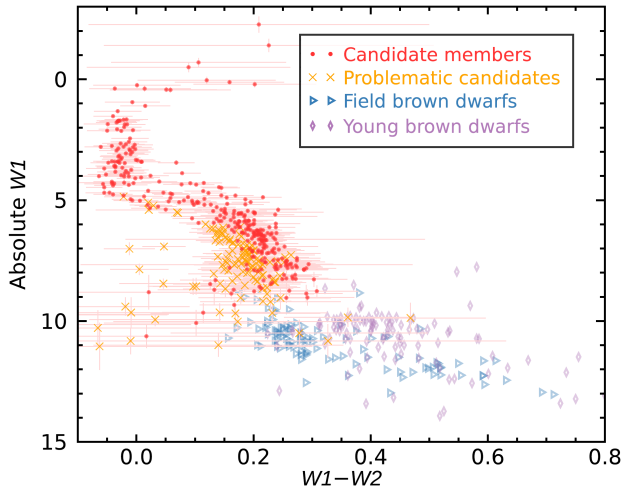


Figure 16. Absolute *WISE* $W1$ -band magnitudes versus $W1 - W2$ colors for field and young brown dwarfs compared with all MUTA candidates and members. Color coding is the same as for Figure 15. Only spectral types L0 and later are shown for brown dwarf data. See Section 6.2 for more details.

Horologium (see Zuckerman et al. 2001b; Torres et al. 2000), Columba and Carina associations ($\simeq 45$ Myr; Torres et al. 2008; Bell et al. 2015). We cross-matched all bona fide members of these four associations compiled by Gagné et al. (2018) with *Gaia* DR2 for this comparison, and built an empirical isochrone for each of them by fitting their sequence with a high-order polynomial. The cross matches with *Gaia* DR2 were all inspected for spurious matches by building finder charts similar to those discussed in Section 4.5. The color-magnitude positions of all members were corrected for extinction by interstellar dust with the method described in Section 5. This procedure only had a noticeable but small effect on the Pleiades members.

All known unresolved binaries were removed from these lists, and their color-magnitude diagrams were visually inspected to remove the obvious sequence of unresolved binaries and triples that were shifted up by 0.75 and 1.19 mag in *Gaia* DR2 G -band magnitude, respectively. The detailed lists of members used to build these isochrones will be presented in an upcoming publication, along with those of other nearby young associations.

Representing a young association’s color-magnitude sequence with a polynomial curve can be complicated by the fact that they contain many more low-mass stars (e.g., Bochanski et al. 2010), which would cause an overfitting of the data in the red part of the color-magnitude diagram. To avoid this, we first build a moving box average and standard deviation of the members’ absolute *Gaia* DR2 G -band magnitudes in bins of 0.05 mag in $G - G_{RP}$ colors, and we subsequently fit a 11-order (Tucana-Horologium, Columba and Carina) or 15-order (Pleiades) polynomial, which were found to be appropriate given the number of stars and the range of colors occupied by the members of these associations. Columba, Tucana-Horologium and Carina were combined as a single $\simeq 45$ Myr-old population as they all share the same age (Bell et al. 2015). This allowed us to build a more accurate empirical isochrone given the larger number of resulting members.

We used our initial list of MUTA members (Table 1) to determine an isochronal age for the association, by comparing each member’s absolute G -band magnitude with a hybrid isochrone built from a weighted sum of the $\simeq 45$ Myr and $\simeq 112$ Myr empirical isochrones described above. We assumed that the members are spread around the best-fitting hybrid isochrone along a Gaussian likelihood with a standard deviation of 0.35 mag, typical of other young associations. Members that are either known binaries or have a *Gaia* DR2 RUWE above 1.4 were not used for this isochronal age determination. These latter objects are identified in Figure 17, along

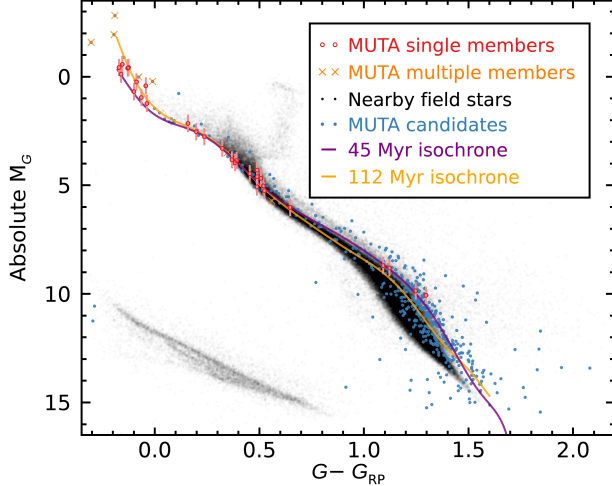


Figure 17. *Gaia* DR2 color-magnitude diagram of MUTA members used for isochrone fitting (red filled circles) and other candidates (blue filled circles) compared with field stars within 100 pc of the Sun (black dots) and empirical isochrones built from the Pleiades associations (orange line) and a combination of the Tucana-Horologium, Carina and Columba associations (purple line). MUTA objects flagged as potential unresolved or contaminated objects are identified with orange crosses. See Section 6.3 for more detail.

with the empirical isochrones built from the Pleiades and the Tucana-Horologium, Columba and Carina associations.

A one-dimensional grid search was performed to identify the linear combination of the $\simeq 45$ Myr and $\simeq 112$ Myr empirical isochrones that best matches the MUTA stars. A thousand values for a linear coefficient α_i were chosen with $\alpha \in [0, 1]$ to build a set of hybrid isochrones I_i built from the $\simeq 45$ Myr isochrone I_{45} and the $\simeq 112$ Myr isochrone I_{112} :

$$I_i = \alpha_i \cdot I_{45} + (1 - \alpha_i) \cdot I_{112}. \quad (6)$$

The goodness-of-fit of each hybrid isochrone for the 10^3 values of α_i were assessed by calculating the Gaussian likelihood that the *Gaia* DR2 absolute G -band magnitudes of MUTA members y_j and their associated standard deviations σ_j match the model I_{ij} in each color bin j :

$$\ln P_i = -0.5 \cdot \sum_j \left(\frac{y_j - I_{ij}}{\sigma_j + 0.35 \text{ mag}} \right)^2. \quad (7)$$

The best-fitting linear combination is displayed in Figure 18. The ages A_i corresponding to each hybrid isochrone I_i were taken as a linear combination of the individual empirical isochrones in logarithm space:

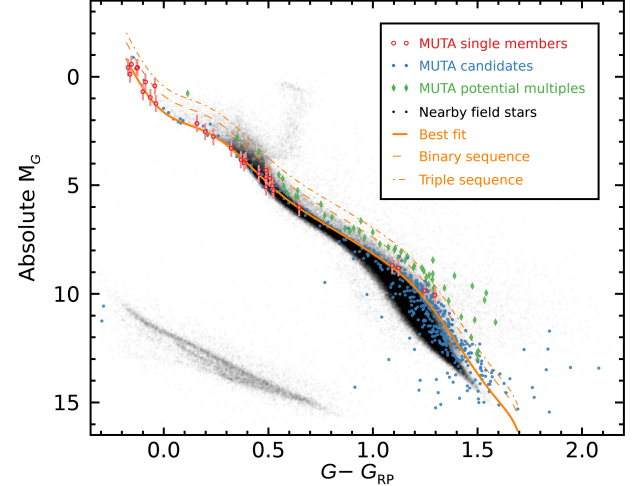


Figure 18. MUTA members used for isochrone fitting (red circles and error bars) fitted with a linear combination of empirical isochrones. The best fit, corresponding to an age of 62 ± 7 Myr, is represented with an orange line. Similar isochrones shifted by 0.75 mag and 1.19 mag are also shown as orange dashed and dash-dotted lines, respectively, to represent the locations of unresolved equal-luminosity binaries and triples. Other candidate members of MUTA are shown as blue circles, and those flagged as possible binaries are shown as green diamonds. See Section 6.3 for more detail.

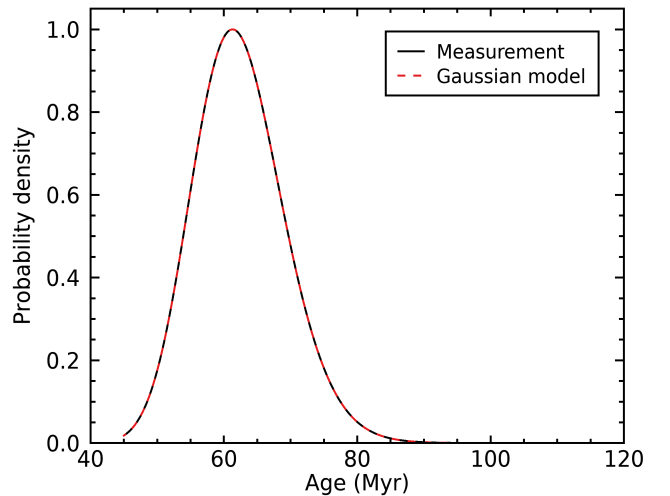


Figure 19. Relative probability density function for the isochronal age of MUTA determined from fitting a combination of empirical isochrones of nearby young associations (black line). A normal probability density function in logarithm age is also shown (red dashed line). The observed MUTA age is well represented by a Gaussian distribution at 62 ± 7 Myr. See Section 6.3 for more detail.

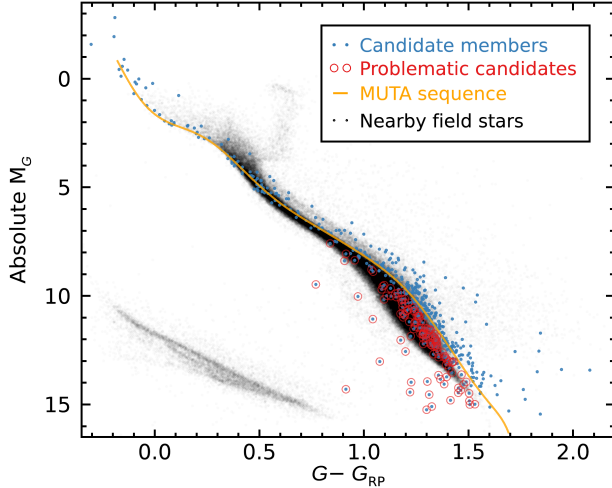


Figure 20. *Gaia* DR2 color-magnitude diagram of MUTA members and candidates (blue dots) compared with nearby *Gaia* DR2 entries (black dots) and the best-fitting hybrid isochrone for MUTA members. We identified all candidates with an absolute magnitude more than 0.35 mag fainter than this hybrid isochrone as problematic because they likely correspond to bad *Gaia* DR2 astrometric solutions, field-aged low-mass stars that have kinematics similar to MUTA by chance, or to sources contaminated by a background object. See Section 6.3 for more details.

$$\log A_i = \alpha_i \cdot \log (45 \text{ Myr}) + (1 - \alpha_i) \cdot \log (112 \text{ Myr}). \quad (8)$$

The resulting probability density function $P(A_i)$ is shown in Figure 19. It is well represented by a Gaussian in logarithm of age, with an average and characteristic width that correspond to $\log A(\text{yr}) = 7.79 \pm 0.05$, or an age of 62 ± 7 Myr.

We also calculated a probability density function for the relative age parameter α because the age estimates of both our reference populations could change in the future. For example, some recent lithium depletion boundary age estimates for the Pleiades are as old as 148 ± 19 Myr (Burke et al. 2004), and Kraus et al. (2014) estimated a slightly younger age for Tucana-Horologium based on the lithium depletion boundary: they found ages of 38 ± 2 Myr or 41 ± 2 Myr, depending on the evolutionary models that they used. The age of MUTA can thus be refined with the equation above (i.e., a simple interpolation in log age), replacing α_i with a Gaussian probability density function at 0.65 ± 0.12 for α . Using the two extreme ends of these age estimates for the Pleiades and Tucana-Horologium would correspond to MUTA ages of 55 ± 7 Myr, or 69 ± 10 Myr, placing two conservative boundaries for the possible age of MUTA.

All MUTA candidate members located more than 0.35 mag fainter than the best-fitting hybrid isochrone were marked as problematic candidates because they likely correspond to interloping field-aged M dwarfs or contaminated *Gaia* DR2 entries. This flagging procedure is displayed in Figure 20. This step has removed 135 objects from our list of good-quality candidates; we note that this number is comparable to the number of contaminants (192^{+25}_{-22}) we have estimated in Section 4.3 based on the number of old white dwarf interlopers.

6.4. White Dwarf Cooling Ages

In Section 4.3, we noted that our search for additional MUTA candidates yielded 12 white dwarfs seemingly co-moving with MUTA, 10 of which are clearly too cold, and therefore too old, to be credible members. The only two exceptions are WD 0340+103 (MUTA 125) and WD 0350+098 (MUTA 190), which seem to be aged about 200–800 Myr from a first comparison with total-age cooling tracks. However, both white dwarfs are so hot that a direct comparison of color-magnitude relations at visible wavelengths is imprecise, as this regime only samples the Rayleigh-Jeans end of their spectral energy distributions. Furthermore, the *Gaia* DR2 de-reddening procedure developed here cannot be applied to white dwarfs directly. For this reason, we investigated the properties of both white dwarfs in more details.

WD 0340+103 is an extremely hot white dwarf, which properties have been estimated at $\log g = 8.6$, $T_{\text{eff}} = 42,617$ K and a mass of $1.03 M_{\odot}$ by Gentile Fusillo et al. (2019). However, these properties were obtained by fitting models to the *Gaia* DR2 photometry of WD 0340+103, and the visible photometry of hot stars is relatively insensitive to their fundamental properties given that it only samples the Rayleigh-Jeans limit of their spectral energy distribution. For this reason, we obtained more reliable fundamental parameters by making use of spectroscopy instead of photometry.

We first determined the effective temperature and surface gravity of WD 0340+103 by fitting its SDSS optical spectrum (Ahn et al. 2012) with the grid of non-local thermodynamic equilibrium atmosphere models of A. Bédard (2020, in preparation). This yielded a very hot temperature of $83,000 \pm 2,000$ K, and $\log g = 8.83 \pm 0.08$. Because WD 0340+103 only exhibits hydrogen features given its DA spectral type, we assumed a pure-hydrogen atmospheric composition. We used the fitting procedure described in Bergeron et al. (1992) and Liebert et al. (2005): briefly, the normalized Balmer lines are adjusted with theoretical line profiles using the Levenberg-Marquardt least-squares method. The observed spectrum of WD 0340+103 was well reproduced by this

method, including the emission component at the core of the H α line, and as illustrated in Figure 21. The positions of the lower Balmer lines (H α , H β , and H γ) were used to measure a total redshift of $138 \pm 21 \text{ km s}^{-1}$, due in part to the gravitational redshift and radial velocity of WD 0340+103.

In a second step, we calculated the mass, radius, luminosity, and cooling age that correspond to the effective temperature and surface gravity of WD 0340+103 using the thick-hydrogen layer ($M_H/M = 10^{-4}$) cooling tracks of A. Bédard et al. (2020, in preparation), which are appropriate for the study of hot white dwarfs. Following Holberg & Bergeron (2006), we also computed the absolute SDSS g -band magnitude, which we combined with the observed (dereddened) SDSS g -band magnitude to evaluate its spectroscopic distance. The atmospheric and stellar parameters of WD 0340+103 are summarized in Table 9. Our analysis shows that WD 0340+103 is a highly unusual white dwarf: It is extremely hot, young, and massive. Furthermore, we note that the spectroscopic distance is slightly farther than its *Gaia* DR2 trigonometric distance, but the values are consistent within measurement errors.

We used the MESA Isochrones and Stellar Tracks (MIST; Choi et al. 2016) to estimate a progenitor mass of $6.7 \pm 0.4 M_\odot$ for WD 0340+103. This corresponds to a spectral type of about B2, just one subclass earlier than the earliest-type members of MUTA (29 Tau, 30 Tau, μ Tau and μ Eri are all B3 stars). This is consistent with the extremely young cooling age of only $270,000 \pm 30,000$ years which we derived for WD 0340+103. Such a progenitor star has a main-sequence lifetime of 59_{-6}^{+8} Myr, corresponding to a total age of 60_{-6}^{+8} Myr, consistent with our isochronal age of 62 ± 7 Myr. Combining both estimates in an error-weighted average allows us to refine our age estimate for MUTA at 61 ± 5 Myr. The core composition of this massive white dwarf likely does not consist of carbon and oxygen, but rather oxygen and neon (Lauffer et al. 2018; Camisassa et al. 2019). This is expected to have a significant effect on the calculated cooling age of about 20% (e.g., see Gagné et al. 2018b; Simon et al. 2015; Simon 2018), however, in the present scenario the age estimate of WD 0340+103 is completely dominated by its main-sequence lifetime, and its core composition will therefore not have any significant effect on our total age estimation.

The detailed properties of WD 0350+098 are harder to determine because of its lack of spectral lines, likely due to extreme Zeeman broadening caused by a strong magnetic field. Much like WD 0340+103, the age estimate based on *Gaia* DR2 photometry alone may be

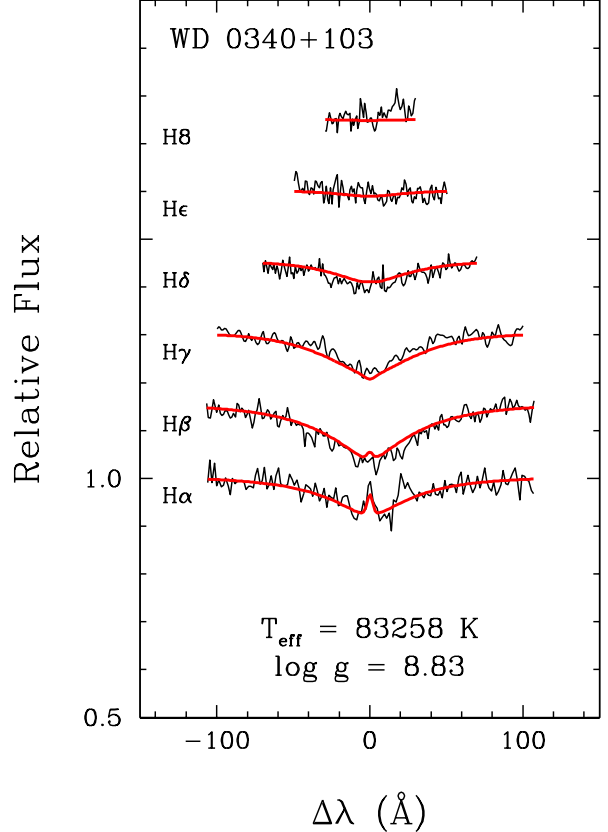


Figure 21. Model fit to the Balmers lines of WD 0340+103 (MUTA 125). See Section 6.4 for more details.

unreliable given its extremely blue colors and hot temperature. Adding UV photometry from *GALEX* (Martin et al. 2005) to better constrain its temperature yielded an estimate of $31,000 \pm 1,000$ K with a radius of $0.0073_{-0.0005}^{+0.0006} R_\odot$, however, these uncertainties are likely underestimated because the models we used do not include magnetic fields. These parameters would correspond to a mass of $1.09_{-0.05}^{+0.04} M_\odot$ and a surface gravity of $\log g = 8.75 \pm 0.09$. Using non-magnetic cooling tracks yields a cooling age estimate of 79_{-10}^{+20} Myr. The main-sequence lifetime that corresponds to the $6.1 \pm 0.5 M_\odot$ progenitor is 74_{-12}^{+15} Myr, making WD 0350+098 too old for MUTA membership if we take our analysis at face value. However, the lack of magnetic fields in our treatment could have introduced a significant bias in the determination of its cooling age and mass (and therefore its main-sequence lifetime), and for this reason we keep it as a candidate member of MUTA.

6.5. Lithium

The equivalent width of the Li I $\lambda 6708 \text{ Å}$ spectral line is a well-established age indicator. Because lithium burns at lower temperatures than hydrogen, it is rela-

Table 9. Properties of WD 0340+103 (MUTA 125)

Property	Value	Ref.
Position and Kinematics		
<i>Gaia</i> DR2 Source ID	36321786805002880	1
R.A. ep. 2015.5 ^a	03:43:14.370 ± 0.09	1
Decl. ep. 2015.5 ^a	+10:29:38.15 ± 0.06	1
$\mu_\alpha \cos \delta$ (mas yr ⁻¹)	31.51 ± 0.18	1
μ_δ (mas yr ⁻¹)	-22.55 ± 0.12	1
Parallax (mas)	6.8 ± 0.1	1
Trigonometric distance (pc)	145.7 ± 2.3	1
Spectroscopic distance (pc)	163.4 ⁺¹⁶ ₋₁₅	2
RV _{opt} ^b (km s ⁻¹)	14.3 ± 3.4	2
RV _{mes} (km s ⁻¹)	27 ± 21	2
Photometric Properties		
<i>G</i> _{BP} (<i>Gaia</i> DR2)	16.307 ± 0.009	1
<i>G</i> (<i>Gaia</i> DR2)	16.539 ± 0.001	1
<i>G</i> _{RP} (<i>Gaia</i> DR2)	16.766 ± 0.005	1
<i>u</i> _{AB} (SDSS DR12)	15.946 ± 0.005	3
<i>g</i> _{AB} (SDSS DR12)	16.298 ± 0.003	3
<i>r</i> _{AB} (SDSS DR12)	16.748 ± 0.004	3
<i>i</i> _{AB} (SDSS DR12)	17.090 ± 0.005	3
<i>z</i> _{AB} (SDSS DR12)	17.392 ± 0.016	3
Fundamental Properties		
Spectral type	DA	4
T _{eff} (K)	83,000 ± 2,000	2
log <i>g</i>	8.83 ± 0.08	2
Mass (M_\odot)	1.16 ± 0.04	2
Radius (R_\odot)	0.0069 ^{+0.0006} _{-0.0005}	2
log <i>L</i> / <i>L</i> _⊙	0.31 ± 0.08	2
Cooling age (Myr)	0.27 ± 0.03	2
Progenitor mass (M_\odot)	6.7 ± 0.4	2
Progenitor spectral type	B2	2
Total age (Myr)	60 ⁺⁸ ₋₆	2

^aJ2000 position at epoch 2015.5 from the *Gaia* DR2 catalog. Measurement errors are given in units of milliarcseconds.

^bOptimal radial velocity predicted by BANYAN Σ that assumes membership in MUTA.

References—(1) [Gaia Collaboration et al. 2018a](#), (2) This work, (3) [Alam et al. 2015](#), (4) [Kleinman et al. 2013](#).

tively fragile and will disappear over time if it is allowed to be transported in layers deep enough in a star to reach the threshold temperature for lithium burning. The temperature profile of a star, combined with the location of its convective layers, will determine whether lithium gets burned at all, and how fast it does so. Lower-mass stars (late-K or early-M spectral types) have deep convective layers that allow them to burn through all lithium within only $\simeq 30$ Myr ([Randich 2001](#)), whereas

higher-mass stars, with their shallower convective layers, burn lithium more gradually. It takes more than a billion years for stars with spectral types G0 and earlier to burn lithium in their photospheres such that the Li I $\lambda 6708$ Å absorption line disappears completely ([Jones et al. 1999](#)). As a result, the sequence in temperature versus Li I absorption line for K-type or earlier stars evolves slowly with time, and makes it possible to place weak constraints on the ages of such early-type stars (e.g., [Barrado y Navascués et al. 2001](#); [Soderblom et al. 1993](#)). Similarly, the K-type lithium depletion boundary, where stars below a given temperature stop displaying the lithium absorption line, can be used to place constraints on the age of a stellar population. The location of this boundary is, however, not very sensitive to age for populations $\simeq 10$ Myr and older ([Kraus et al. 2014](#)).

Brown dwarfs with masses below $\simeq 60 M_{\text{Jup}}$ do not burn lithium despite their fully convective structure, because they do not reach temperatures sufficient to do so even at their core (e.g., [Baraffe et al. 2015](#)). Low-mass stars and brown dwarfs with masses above $60 M_{\text{Jup}}$ burn their photosphere lithium slowly, causing the appearance of a second, age-dependent boundary where the lithium absorption line begins appearing again below a threshold in effective temperature. The effective temperatures, spectral types and bolometric luminosities at which this second, M-type lithium depletion boundary occurs, is a strong function of age over the first hundreds of millions of years that follow stellar formation. The lithium depletion boundary has therefore become a popular diagnostic tool to determine precise ages for stellar populations with known M-type stars (e.g., [Kraus et al. 2014](#); [Malo et al. 2014b](#); [Shkolnik et al. 2017](#)).

Measuring the equivalent width of the lithium absorption line accurately requires high-resolution spectroscopy, ideally with a resolving power $\lambda/\Delta\lambda > 10,000$ to avoid contamination from otherwise blended spectral lines such as Fe I ([Xing 2010](#)). Such measurements require long exposure times and they have thus typically only been obtained for known populations of nearby associations or open clusters. However, a literature search revealed that Li I equivalent width measurements have been obtained by [Magazzù et al. \(1997\)](#) for nine members or candidate members (and one low-likelihood candidate) of MUTA in a follow-up of *ROSAT* X-ray bright sources ([Neuhäuser et al. 1995](#)) in the vicinity of Taurus-Auriga. These measurements were obtained at a

relatively low resolving power ($\lambda/\Delta\lambda \simeq 8,400$),¹² meaning that the equivalent widths may be slightly overestimated because of line blending. We obtained effective temperatures for these ten stars from Xing (2010), Gaia Collaboration et al. (2018b) and Bai et al. (2019), where available, listed in Table 10 along with the lithium equivalent width measurements of Magazzù et al. (1997).

In Figure 22, we compare these available MUTA temperature versus lithium measurements with other literature data for stellar populations across a range of ages. The 20–25 Myr sequence was built from the β Pictoris moving group (β PMG, e.g., see Zuckerman et al. 2001a;

Zuckerman & Song 2004; Bell et al. 2015, measurements are from Mentuch et al. 2008; Malo et al. 2014b; Shkolnik et al. 2017). The 40–50 Myr sequence was built from the stellar populations of the Tucana-Horologium association discussed earlier (lithium equivalent width measurements are by Kraus et al. 2014) and the IC 2602 and IC 2391 open clusters (Randich 2001; Barrado y Navascués et al. 2004; Dobbie et al. 2010). The 110–125 Myr sequence was built from the Pleiades association (Soderblom et al. 1993; Jones et al. 1996; Bouvier et al. 2018), and the 150–175 Myr was built from the M35 open cluster (Barrado y Navascués et al. 2001; Bouy et al. 2015).

Table 10. Lithium equivalent width measurements for MUTA .

MUTA	Common	ROSAT	EW(Li)	T_{eff}	T_{eff}
ID	Name	Name	(mÅ)	(K)	Ref.
24	RX J0348.5+0832	RX J0348.5+0832	260	5409	2
27	RX J0338.3+1020	RX J0338.3+1020	250	5250	2
29	RX J0358.2+0932	RX J0358.1+0932	200	4855	1
94	V1267 Tau	RX J0331.1+1036	320	4967	1
159	TYC 71–542–1	RX J0347.9+0616	200	5794	2
195	2MASS J03545074+1232061	RX J0354.8+1232	0	4028	3
318 A	2MASS J04341953+0226260	RX J0434.3+0226	300	4714	1
350	TYC 91–702–1	RX J0442.9+0400	220	5247	2
362	V1831 Ori	RX J0450.0+0151	350	5247	1
376	TYC 665–150–1	RX J0357.3+1258	250	5943	2

NOTE—All lithium equivalent width measurements are from Magazzù et al. (1997). TYC 665–150–1 was excluded from Figure 22 because it is a low-likelihood candidate member of MUTA (its separation from the MUTA model in UVW space is 8.1 km s^{-1}). See section 6.5 for more details.

References—(1) Bai et al. 2019; (2) Xing 2010; (3) Gaia Collaboration et al. 2018b.

Although the available MUTA measurements do not span either of the lithium depletion boundaries, they seem consistent with an age in the range 20–125 Myr, with the caveat that our comparison sequences were built from higher-resolution spectra compared with MUTA measurements. This likely biases our range slightly towards young ages, but this result seems consistent with our previous age assessments based on empirical

isochrones and white dwarf cooling ages. Obtaining higher-resolution optical spectra for MUTA members, as well as extending the range of spectral types over which lithium equivalent widths are measured, will allow us to further constrain the age of MUTA.

6.6. Present-Day Mass Function

We used the empirically corrected MIST solar-metallicity model isochrones of Choi et al. (2016) as described by Gagné et al. (2018a)¹³ with a nominal stellar

¹² Magazzù et al. (1997) also obtained measurements at $\lambda/\Delta\lambda \simeq 4200$, but inspecting the Isaac Newton Group Archive at <http://casu.ast.cam.ac.uk/casuadc/ingarch/query> indicated that none of these lower-resolution observations have been obtained for MUTA objects.

¹³ We used the models based on the revised *Gaia* DR2 photometric zero points of Evans et al. (2018a) available at http://waps.cfa.harvard.edu/MIST/model_grids.html

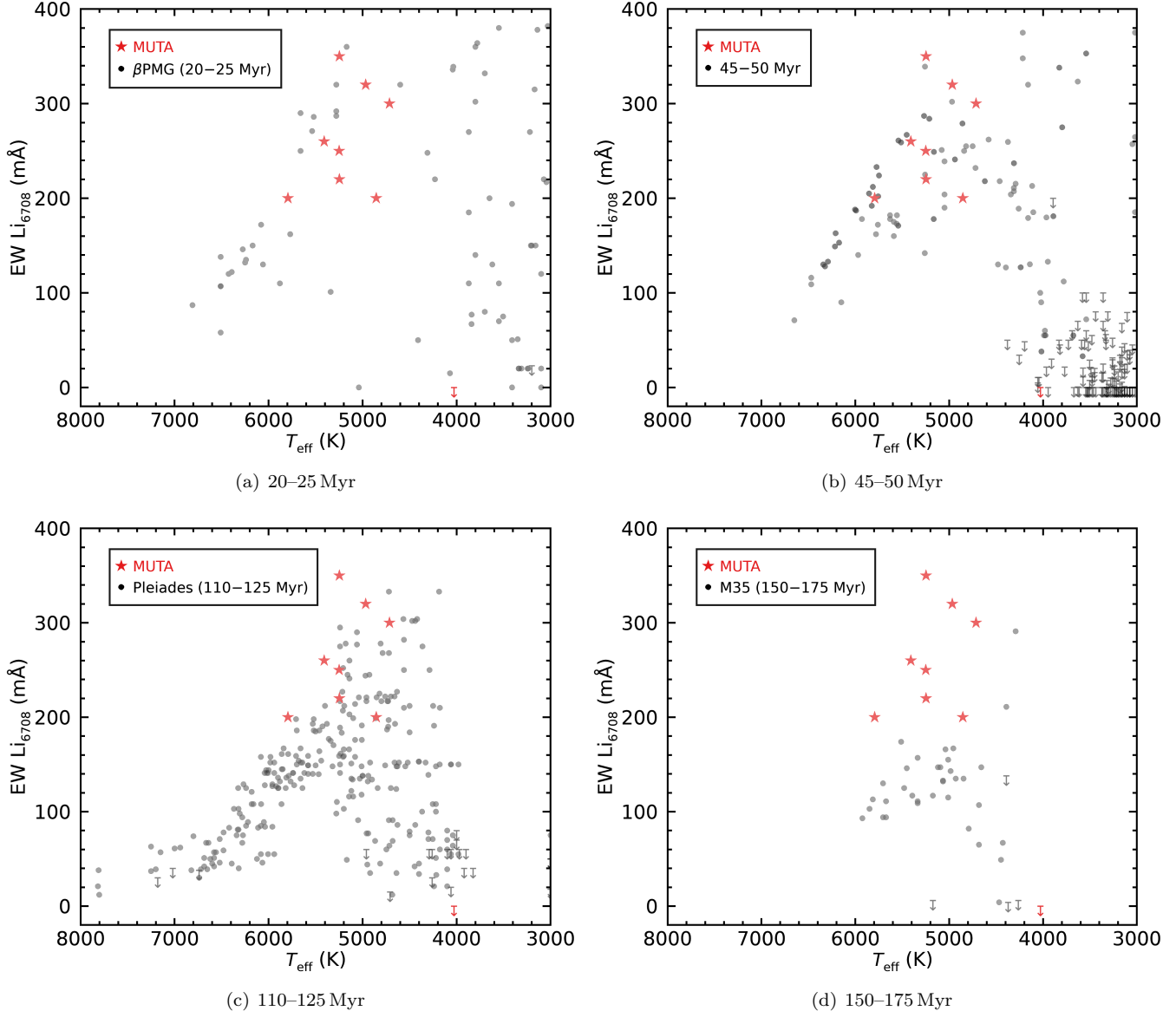


Figure 22. Effective temperature versus the equivalent width of the Li I $\lambda 6708 \text{ \AA}$ absorption line for MUTA members and candidates (red stars), compared with other known, coeval populations (grey circles). The 45–50 Myr sequence was built from members of the Tucana-Horologium association and IC 2602 and IC 2391 open clusters. Upper limits are indicated with downward arrows. Although all measurements for MUTA members are based on a lower resolving power ($\lambda/\Delta\lambda \approx 8,400$) compared with the reference sequences ($\lambda/\Delta\lambda > 10,000$), they indicate that MUTA seems roughly consistent with an age of 20–125 Myr. β PMG indicates the β Pictoris moving group. See Section 6.5 for more detail.

rotation of $v/v_{\text{crit}} = 0$ to estimate the masses of MUTA members and candidates based on their position in a *Gaia* DR2 absolute G versus $G - G_{\text{RP}}$ color-magnitude diagram. This method uses the differences between the empirical Pleiades sequence and the 112 Myr MIST isochrone to correct for systematic effects such as the increased stellar activity and strong magnetic fields of low-mass stars.

The masses for MUTA candidates with very red colors ($J - W2 > 1.5$) were estimated with the method of

Gagné et al. (2014), which is more reliable than extrapolating MIST isochrones or using lower quality *Gaia* DR2 photometry, but potentially suffers from different systematics. The method is based on a comparison of the absolute 2MASS J , H , K_S and *WISE* $W1$ and $W2$ photometry of MUTA candidates with BT-Settl models (Allard et al. 2012) in the same respective bandpasses, and combining the individual estimates in a likelihood analysis. These model-dependent mass estimates range from $\simeq 35 M_{\text{Jup}}$ to $0.2 M_{\odot}$, covering the substellar-to-

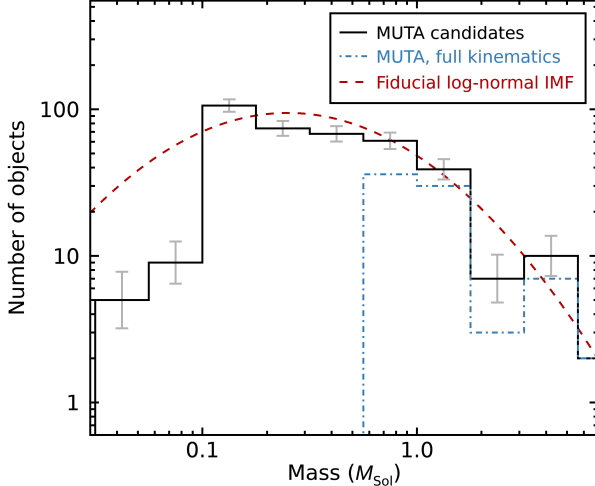


Figure 23. Present-day mass function of MUTA (thick black bars) compared with a fiducial log-normal initial mass function with a peak mass $0.25 M_{\odot}$ and a logarithm characteristic width of 0.5, anchored on the $> 0.2 M_{\odot}$ population of MUTA. Gray error bars represent uncertainties associated with Poisson statistics. The subset of members with full kinematics and therefore a more reliable membership are shown with a dash-dotted blue line. Our set of candidates is consistent with a complete population down to $\simeq 0.1 M_{\odot}$ if a log-normal mass function is realistic for MUTA, but the brown dwarfs population still seems mostly incomplete. We did not include the progenitor masses of the two white dwarf candidates in this figure. See Section 6.6 for more details.

stellar transition and overlapping slightly with the range of masses (0.1 – $6.0 M_{\odot}$) obtained with MIST isochrones for bluer targets.

The resulting present-day mass function of MUTA members and candidates is displayed in Figure 23 along with a fiducial log-normal mass function ($\sigma = 0.5$ dex, $m_c = 0.25 M_{\odot}$). We fitted its amplitude to our MUTA members with masses above $1 M_{\odot}$, but the width and central position were not fitted. This particular mass function was shown to be a good fit to other nearby young associations by Jeffries (2012). The log-normal mass function is a good match to our distribution of MUTA members and candidates down to $0.1 M_{\odot}$, indicating that its present-day mass function may be similar to other young associations of the Solar neighborhood. Assuming that the population of MUTA is complete above $0.2 M_{\odot}$ indicates that about 65 brown dwarf members would remain to be found, for a total stellar and substellar population of $\simeq 450$ members.

6.7. Stellar Rotation and Activity

Young stars lose angular momentum as they age, and their rotation periods consequently slow down with time. Because the rate of angular momentum loss depends on

the rotation period, members of stellar associations with a wide range of rotation periods will eventually converge to a tight sequence as a function of their mass (Barnes 2003; van Saders et al. 2016). The timescale for this convergence for Sun-like stars is < 650 Myr and decreases with increasing stellar mass (Delorme et al. 2011; Douglas et al. 2016; Curtis et al. 2019), but a partial sequence is apparent even at $\simeq 112$ Myr for higher-mass stars (Rebull et al. 2016).

Depending on the mass, this trend of longer rotation periods for older ages *reverses* for the youngest (pre-main-sequence) stars, as they spin up while contracting onto the main sequence. The youngest stars therefore also have longer rotation periods. The scatter at these younger ages is also larger because of a large spread in the initial rotation periods. Thus, the rotation period versus color sequence of MUTA can still be used as an additional test of our assigned age by comparing with similarly-aged groups.

As bounds for the expected age of MUTA, we used members the Pleiades ($\simeq 112$ Myr; Dahm 2015) and Praesepe clusters ($\simeq 800$ Myr; Brandt & Huang 2015), in addition to members of the Columba, Carina, and Tucana-Horologium associations discussed earlier ($\simeq 45$ Myr). We included the older Praesepe cluster as an example of a clearly older population in the color-rotation period diagram, because the differences between MUTA and the Pleiades are subtle. We collected the rotation period measurements of the Pleiades and Praesepe members from Rebull et al. (2016) and Douglas et al. (2017), respectively. We obtained light curves for each member of the younger three associations from the *TESS* or *K2* missions, where available. We restricted our sample to targets with *Gaia* DR2 $G - G_{\text{RP}} > 0.2$, as the variability period in bluer stars may be impacted by pulsations as much as rotation. For those observed by *K2* (16 stars), we used K2SFF processed light curves (Vanderburg & Johnson 2014). For *TESS* targets with short-cadence data, we used light curves from the Science Processing Operations Center (SPOC, Jenkins et al. 2016) and for others we extracted light curves from the full-frame images using Eleanor¹⁴ (Feinstein et al. 2019). We excluded targets with flux contamination ratios above 1, even when rotation consistent with youth was present in the curve.

¹⁴ <https://github.com/afeinstein20/eleanor>

Table 11. *TESS* and *K2* rotation periods.

Name	R.A. (hh:mm:ss.sss)	Decl. (dd:mm:ss.ss)	Period 1 (days)	Period 2 ^a (days)	Young Association ^b	Source
2MASS J03303685+1610599	03:30:36.887	+16:10:59.58	1.70	...	MUTA	2
2MASS J03350134+1418016	03:35:01.376	+14:18:01.14	4.38	...	MUTA	2
2MASS J03361762+2153391	03:36:17.665	+21:53:38.50	4.38	...	MUTA	2
2MASS J03371337+1307315	03:37:13.411	+13:07:30.93	0.66	...	MUTA	2
2MASS J03373508+1705162	03:37:35.111	+17:05:15.93	6.19	...	MUTA	2
RX J0338.3+1020	03:38:18.266	+10:20:16.32	3.24	...	MUTA	1
2MASS J03385230+1635406	03:38:52.328	+16:35:40.21	0.34	...	MUTA	2
TYC 1235–156–1	03:39:39.516	+15:29:54.47	4.43	...	MUTA	2
TYC 663–362–1	03:40:57.781	+13:09:03.06	2.59	...	MUTA	1
TYC 660–135–1	03:41:45.000	+10:54:27.46	5.12	...	MUTA	1
2MASS J03420359+1631392	03:42:03.617	+16:31:38.80	4.92	...	MUTA	2
HD 23376	03:44:58.957	+08:19:10.09	0.81	...	MUTA	1
BD+04 589	03:47:13.551	+05:26:23.49	4.75	...	MUTA	1
TYC 1252–301–1	03:47:23.901	+18:43:17.68	4.09	...	MUTA	2
BD+07 543	03:47:31.345	+07:57:26.39	3.57	...	MUTA	1
TYC 661–560–1	03:47:53.694	+11:48:57.98	1.55	...	MUTA	1
RX J0348.5+0832	03:48:31.461	+08:31:36.43	0.41	...	MUTA	1
EPIC 210811401	03:48:50.333	+20:02:27.56	5.10	...	MUTA	2
2MASS J03495031+1440552	03:49:50.345	+14:40:54.73	1.02	...	MUTA	2
PPM 119410	03:50:50.558	+11:00:05.12	1.80	...	MUTA	1
2MASS J03511041+1302467	03:51:10.454	+13:02:46.16	2.54	...	MUTA	1
EPIC 210361663	03:54:50.776	+12:32:05.61	3.26	...	MUTA	2
HD 286374	03:56:19.224	+11:25:10.84	1.57	...	MUTA	2
HD 286380	03:56:20.741	+10:47:47.24	2.51	...	MUTA	1
TYC 665–150–1	03:57:21.412	+12:58:16.37	0.86	...	MUTA	2
2MASS J03573875+1142322	03:57:38.786	+11:42:31.85	3.92	...	MUTA	2
RX J0358.2+0932	03:58:12.749	+09:32:21.97	1.44	...	MUTA	1
TYC 662–217–1	03:59:42.158	+12:10:08.14	4.80	...	MUTA	2
2MASS J04072953–0115000	04:07:29.559	−01:15:00.13	1.04	...	MUTA	1
TYC 74–1393–1	04:12:18.449	+00:01:31.28	2.94	...	MUTA	1
2MASS J04210781–0111328	04:21:07.848	−01:11:33.15	4.29	...	MUTA	1
TYC 668–737–1	04:21:24.386	+08:53:54.34	5.31	...	MUTA	1
BD–03 753	04:22:23.528	−02:40:04.13	0.90	...	MUTA	1
HD 27687	04:22:24.213	+06:31:45.14	0.53	0.39	MUTA	1
BD+05 638	04:22:33.022	+05:41:38.82	3.37	6.32	MUTA	1
HD 28356	04:28:32.733	+06:05:52.07	0.81	...	MUTA	1
BD–03 789	04:28:37.716	−03:15:44.58	1.72	...	MUTA	1
2MASS J04372578–0210117	04:37:25.800	−02:10:12.12	1.13	...	MUTA	1

Table 11 *continued*

Table 11 (*continued*)

Name	R.A. (hh:mm:ss.sss)	Decl. (dd:mm:ss.ss)	Period 1 (days)	Period 2 ^a (days)	Young Association ^b	Source
2MASS J04372971-0051241	04:37:29.730	-00:51:24.47	3.59	...	MUTA	1
2MASS J04391308-0045039	04:39:13.102	-00:45:04.39	0.42	...	MUTA	1
BD+06 731	04:39:15.500	+07:01:43.92	6.08	8.66	MUTA	1
TYC 4739-1225-1	04:39:20.251	-03:14:21.79	3.61	...	MUTA	1
BD-02 1047	04:52:07.364	-01:58:57.43	1.47	0.69	MUTA	1
TYC 4741-307-1	04:56:18.287	-01:53:33.04	2.44	...	MUTA	1
HD 37402	05:34:26.201	-60:06:14.58	1.93	...	CAR	1
HD 42270	05:53:29.503	-81:56:52.20	1.87	...	CAR	1
HD 43199	06:10:52.922	-61:29:58.79	0.52	...	CAR	1
AL 442	06:11:30.043	-72:13:37.79	0.85	...	CAR	1
AB Pic	06:19:12.941	-58:03:14.83	3.81	...	CAR	1
HIP 32235	06:43:46.270	-71:58:34.45	3.94	...	CAR	1
HIP 33737	07:00:30.501	-79:41:45.06	5.21	...	CAR	1
2MASS J07013884-6236059	07:01:38.844	-62:36:05.98	3.93	5.58	CAR	1
2MASS J07065772-5353463	07:06:57.714	-53:53:45.75	2.87	...	CAR	1
2MASS J08040534-6316396	08:04:05.300	-63:16:39.11	2.01	...	CAR	1
2MASS J08194309-7401232	08:19:43.099	-74:01:23.22	0.42	...	CAR	1
2MASS J09032434-6348330	09:03:24.265	-63:48:32.65	4.42	...	CAR	1
2MASS J09180165-5452332	09:18:01.547	-54:52:32.85	0.37	...	CAR	1
HIP 46063	09:23:34.921	-61:11:35.61	3.92	...	CAR	1
2MASS J09315840-6209258	09:31:58.328	-62:09:25.46	1.93	...	CAR	1
TWA 21	10:13:14.666	-52:30:53.85	4.43	...	CAR	1
HD 14691	02:22:01.693	-10:46:40.40	0.46	...	COL	1
2MASS J03083950-3844363	03:08:39.597	-38:44:36.32	0.69	...	COL	1
2MASS J03320347-5139550	03:32:03.559	-51:39:54.87	5.56	...	COL	1
HIP 17248	03:41:37.453	+55:13:05.02	4.70	...	COL	1
2MASS J04091413-4008019	04:09:14.199	-40:08:01.98	3.28	...	COL	1
HIP 19775	04:14:22.624	-38:19:01.54	1.74	...	COL	1
CD-36 1785	04:34:50.821	-35:47:21.13	2.31	...	COL	1
HD 29329	04:46:00.914	+76:36:37.66	0.92	...	COL	1
HIP 22226	04:46:49.568	-26:18:08.93	0.89	...	COL	1
HD 31242	04:51:53.585	-46:47:13.11	3.01	...	COL	1
HD 272836	04:53:05.246	-48:44:38.49	4.60	...	COL	1
HIP 23316	05:00:51.910	-41:01:06.56	2.29	...	COL	1
2MASS J05195695-1124440	05:19:56.985	-11:24:44.48	4.38	...	COL	1
2MASS J05241317-2104427	05:24:13.213	-21:04:43.14	4.17	...	COL	1
HIP 25709	05:29:24.132	-34:30:55.43	6.14	2.75	COL	1
AH Lep	05:34:09.189	-15:17:03.54	2.10	...	COL	1
HD 37484	05:37:39.655	-28:37:34.70	0.82	...	COL	1
2MASS J05395494-1307598	05:39:54.968	-13:08:00.11	1.89	...	COL	1

Table 11 *continued*

Table 11 (*continued*)

Name	R.A. (hh:mm:ss.sss)	Decl. (dd:mm:ss.ss)	Period 1 (days)	Period 2 ^a (days)	Young Association ^b	Source
AI Lep	05:40:20.753	-19:40:11.12	1.69	...	COL	1
HD 38397	05:43:35.843	-39:55:24.50	2.27	...	COL	1
HIP 28036	05:55:43.189	-38:06:16.10	0.95	...	COL	1
HD 41071	06:00:41.325	-44:53:49.75	5.46	...	COL	1
HIP 30030	06:19:08.069	-03:26:21.01	1.36	...	COL	1
CD-40 2458	06:26:06.918	-41:02:53.59	4.21	...	COL	1
HIP 490	00:05:52.680	-41:45:12.23	3.00	...	THA	1
2MASS J00125703-7952073	00:12:57.525	-79:52:08.03	0.99	...	THA	1
HIP 1113	00:13:53.335	-74:41:18.61	3.62	...	THA	1
2MASS J00144767-6003477	00:14:47.860	-60:03:48.67	0.49	...	THA	1
2MASS J00152752-6414545	00:15:27.705	-64:14:55.61	3.69	...	THA	1
GJ 3017	00:15:36.842	-29:46:01.77	0.84	...	THA	1
HIP 1481	00:18:26.332	-63:28:39.90	2.31	2.59	THA	1
2MASS J00235732-5531435	00:23:57.506	-55:31:44.58	2.44	2.99	THA	1
HIP 1993	00:25:14.853	-61:30:49.12	4.37	...	THA	1
UPM J0027-6157	00:27:33.500	-61:57:17.79	0.55	...	THA	1
2MASS J00284683-6751446	00:28:47.106	-67:51:45.46	0.33	...	THA	1
2MASS J00332438-5116433	00:33:24.551	-51:16:44.33	0.35	...	THA	1
HIP 2729	00:34:51.397	-61:54:58.95	0.38	...	THA	1
2MASS J00393579-3816584	00:39:35.930	-38:16:59.55	6.41	...	THA	1
2MASS J00394063-6224125	00:39:40.905	-62:24:13.39	0.38	...	THA	1
UPM J0042-5444	00:42:10.272	-54:44:44.09	1.78	...	THA	1
CD-78 24	00:42:20.705	-77:47:40.20	2.59	...	THA	1
2MASS J00425349-6117384	00:42:53.702	-61:17:39.23	1.04	...	THA	1
HIP 3556	00:45:28.320	-51:37:34.85	5.97	9.13	THA	1
2MASS J00485254-6526330	00:48:52.746	-65:26:33.71	1.01	...	THA	1
2MASS J00493566-6347416	00:49:35.887	-63:47:42.33	4.95	...	THA	1
UPM J0113-5939	01:13:40.523	-59:39:35.06	0.32	...	THA	1
2MASS J01180670-6258591	01:18:06.926	-62:58:59.85	0.35	...	THA	1
2MASS J01211297-6117281	01:21:13.152	-61:17:28.86	0.43	...	THA	1
CD-34 521	01:22:04.571	-33:37:04.47	9.61	...	THA	1
UPM J0122-6318	01:22:45.334	-63:18:45.24	0.46	...	THA	1
HIP 6485	01:23:21.433	-57:28:51.25	3.47	...	THA	1
2MASS J01233280-4113110	01:23:32.961	-41:13:11.76	0.74	...	THA	1
2MASS J01275875-6032243	01:27:58.956	-60:32:24.76	0.34	...	THA	1
HIP 6856	01:28:08.842	-52:38:19.81	6.36	...	THA	1
2MASS J01375879-5645447	01:37:58.967	-56:45:45.33	0.71	...	THA	1
HD 10863	01:46:01.170	-27:20:56.49	0.44	...	THA	1
2MASS J01504543-5716488	01:50:45.620	-57:16:49.23	0.71	...	THA	1
2MASS J01505688-5844032	01:50:57.087	-58:44:03.63	1.65	...	THA	1

Table 11 *continued*

Table 11 (*continued*)

Name	R.A. (hh:mm:ss.sss)	Decl. (dd:mm:ss.ss)	Period 1 (days)	Period 2 ^a (days)	Young Association ^b	Source
2MASS J01532494-6833226	01:53:25.212	-68:33:22.92	0.60	...	THA	1
HIP 9141	01:57:49.093	-21:54:06.12	3.04	...	THA	1
2MASS J02001992-6614017	02:00:20.178	-66:14:02.14	0.63	...	THA	1
HIP 9685	02:04:35.299	-54:52:54.45	0.44	...	THA	1
2MASS J02045317-5346162	02:04:53.332	-53:46:16.75	0.70	...	THA	1
UCAC3 92-4597	02:07:01.904	-44:06:38.51	0.39	3.00	THA	1
HIP 9892	02:07:18.209	-53:11:56.88	2.39	...	THA	1
HIP 9902	02:07:26.315	-59:40:46.23	1.71	...	THA	1
2MASS J02125819-5851182	02:12:58.366	-58:51:18.42	1.60	...	THA	1
2MASS J02205139-5823411	02:20:51.580	-58:23:41.37	1.28	...	THA	1
2MASS J02242453-7033211	02:24:24.829	-70:33:21.25	0.52	...	THA	1
2MASS J02294869-6906044	02:29:48.952	-69:06:04.36	0.46	...	THA	1
2MASS J02321934-5746117	02:32:19.520	-57:46:11.93	0.86	...	THA	1
UPM J0234-5128	02:34:18.835	-51:28:46.44	0.46	...	THA	1
2MASS J02383255-7528065	02:38:32.880	-75:28:06.41	0.63	...	THA	1
CD-53 544	02:41:47.002	-52:59:52.61	0.52	...	THA	1
2MASS J02420204-5359147	02:42:02.231	-53:59:14.88	0.57	2.47	THA	1
2MASS J02420404-5359000	02:42:04.237	-53:59:00.22	0.57	...	THA	1
CD-58 553	02:42:33.187	-57:39:36.95	7.40	...	THA	1
HD 17250	02:46:14.687	+05:35:32.64	1.21	...	THA	1
2MASS J02474639-5804272	02:47:46.569	-58:04:27.47	9.45	...	THA	1
2MASS J02502222-6545552	02:50:22.440	-65:45:55.27	1.29	...	THA	1
2MASS J02523550-7831183	02:52:35.919	-78:31:18.08	0.71	...	THA	1
2MASS J02553178-5702522	02:55:31.954	-57:02:52.41	0.49	...	THA	1
2MASS J03050556-5317182	03:05:05.712	-53:17:18.46	0.44	...	THA	1
2MASS J03104941-3616471	03:10:49.532	-36:16:47.39	0.66	...	THA	1
2MASS J03114544-4719501	03:11:45.581	-47:19:50.27	4.81	...	THA	1
HIP 15247	03:16:40.753	-03:31:49.69	1.03	...	THA	1
2MASS J03244056-3904227	03:24:40.680	-39:04:22.95	0.34	8.05	THA	1
2MASS J03291649-3702502	03:29:16.628	-37:02:50.37	0.54	...	THA	1
CD-46 1064	03:30:49.233	-45:55:57.44	3.92	...	THA	1
CD-44 1173	03:31:55.768	-43:59:13.61	2.93	...	THA	1
2MASS J03454058-7509121	03:45:40.854	-75:09:11.91	0.70	...	THA	1
HD 24636	03:48:11.720	-74:41:38.44	5.72	0.84	THA	1
2MASS J03512287-5154582	03:51:23.001	-51:54:58.01	0.43	...	THA	1
HD 25284	04:00:03.918	-29:02:16.64	0.31	2.27	THA	1
HD 25402	04:00:32.079	-41:44:54.40	3.56	...	THA	1
2MASS J04013874-3127472	04:01:38.846	-31:27:47.35	0.46	...	THA	1
BD-15 705	04:02:16.556	-15:21:30.22	3.85	...	THA	1
2MASS J04074372-6825111	04:07:43.905	-68:25:10.85	1.02	...	THA	1

Table 11 *continued*

Table 11 (*continued*)

Name	R.A. (hh:mm:ss.sss)	Decl. (dd:mm:ss.ss)	Period 1 (days)	Period 2 ^a (days)	Young Association ^b	Source
2MASS J04133609–4413325	04:13:36.194	−44:13:32.40	0.78	...	THA	1
WOH S 6	04:21:39.275	−72:33:55.53	4.55	...	THA	1
2MASS J04274963–3327010	04:27:49.718	−33:27:01.17	0.67	...	THA	1
HIP 21632	04:38:44.007	−27:02:01.97	2.40	...	THA	1
2MASS J04435860–3643188	04:43:58.683	−36:43:18.81	1.61	...	THA	1
2MASS J04440099–6624036	04:44:01.138	−66:24:03.15	7.94	...	THA	1
2MASS J04470041–5134405	04:47:00.509	−51:34:40.23	6.25	...	THA	1
TYC 8083–45–5	04:48:00.760	−50:41:25.40	8.13	...	THA	1
HIP 22295	04:48:05.485	−80:46:44.64	1.24	...	THA	1
CD–30 2310	05:18:29.092	−30:01:32.16	1.70	...	THA	1
TYC 8098–414–1	05:33:25.647	−51:17:12.77	5.21	...	THA	1
HIP 32435	06:46:13.720	−83:59:28.55	1.59	...	THA	1
HIP 84642	17:18:14.645	−60:27:27.57	4.17	...	THA	1
2MASS J19225071–6310581	19:22:50.700	−63:10:59.23	0.86	...	THA	1
2MASS J20291446–5456116	20:29:14.491	−54:56:13.29	0.88	...	THA	1
2MASS J21100614–5811483	21:10:06.195	−58:11:49.78	0.56	...	THA	1
2MASS J21163528–6005124	21:16:35.368	−60:05:14.13	0.99	...	THA	1
HIP 105388	21:20:50.012	−53:02:04.64	3.45	...	THA	1
UPM J2127–6841	21:27:50.634	−68:41:04.64	0.34	...	THA	1
2MASS J21370885–6036054	21:37:08.927	−60:36:07.04	2.00	...	THA	1
2MASS J21380269–5744583	21:38:02.765	−57:44:59.89	0.68	...	THA	1
HIP 107345	21:44:30.211	−60:58:40.34	4.53	...	THA	1
2MASS J21504048–5113380	21:50:40.563	−51:13:39.59	1.05	...	THA	1
HIP 107947	21:52:09.822	−62:03:09.92	0.96	...	THA	1
2MASS J22021626–4210329	22:02:16.331	−42:10:34.73	4.51	...	THA	1
2MASS J22025453–6440441	22:02:54.624	−64:40:45.70	0.43	...	THA	1
UPM J2222–6303	22:22:39.816	−63:03:27.22	1.11	...	THA	1
2MASS J22244102–7724036	22:24:41.287	−77:24:04.82	0.67	...	THA	1
2MASS J22444835–6650032	22:44:48.534	−66:50:04.47	0.73	...	THA	1
2MASS J22463471–7353504	22:46:34.912	−73:53:51.52	1.65	...	THA	1
2MASS J23131671–4933154	23:13:16.833	−49:33:16.85	1.23	...	THA	1
2MASS J23170011–7432095	23:17:00.401	−74:32:10.53	0.83	...	THA	1
TYC 9344–293–1	23:26:10.958	−73:23:50.88	0.57	...	THA	1
2MASS J23273447–8512364	23:27:35.285	−85:12:37.17	0.90	...	THA	1
CD–86 147	23:27:50.213	−86:13:19.36	0.70	...	THA	1
2MASS J23285763–6802338	23:28:57.841	−68:02:35.08	0.37	...	THA	1
2MASS J23291752–6749598	23:29:17.728	−67:50:01.14	1.02	...	THA	1
2MASS J23382851–6749025	23:38:28.714	−67:49:03.52	0.44	...	THA	1
HIP 116748	23:39:39.712	−69:11:45.75	2.86	...	THA	1
2MASS J23424333–6224564	23:42:43.528	−62:24:57.60	0.52	...	THA	1

Table 11 *continued*

Table 11 (*continued*)

Name	R.A. (hh:mm:ss.sss)	Decl. (dd:mm:ss.ss)	Period 1 (days)	Period 2 ^a (days)	Young Association ^b	Source
2MASS J23452225-7126505	23:45:22.521	-71:26:51.46	1.61	...	THA	1
2MASS J23474694-6517249	23:47:47.152	-65:17:25.79	4.84	...	THA	1
2MASS J23524562-5229593	23:52:45.779	-52:30:00.51	0.91	...	THA	1

^aSecond rotation period candidate.

^bThe full names of young associations are: Carina (CAR), Columba (COL), the Tucana-Horologium association (THA) and the μ Tau Association (MUTA).

NOTE—Rotation periods are accurate to approximately 2%. Only a portion of the table is shown here. The full table is available as online-only additional material. See Section 6.7 for more details.

References—(1) *TESS* (Jenkins et al. 2016; Ricker et al. 2015); (2) *K2* (Vanderburg & Johnson 2014; Howell et al. 2014; Borucki et al. 2010).

We estimated the rotation periods for each star using two methods: a modified version of the Lomb-Scargle periodogram as described in Horne & Baliunas (1986), and the autocorrelation function as described in McQuillan et al. (2013). In both cases, we searched for periodic signals down to twice the Nyquist-sampling limit, and as long as a third of the total data coverage. Below the lower limit, we found that both algorithms are biased by the data sampling, particularly for long-cadence (30 min) data. We set the lower limit for a significant detection at three full rotations. We then flagged the peak in the periodogram and the second peak in the autocorrelation function as the likely period (see Figure 24 for an example). We only considered periodic signals with false-alarm probabilities $< 1\%$ and for which autocorrelation and Lomb-Scargle periods agreed within 10%. For six stars, the autocorrelation and Lomb-Scargle disagreed by an integer factor (alias), which we retained, provided the true rotation period was clear. Across all clusters, 14 out of 201 stars showed evidence of a second period, which we excluded from our sample as they are likely binaries (Douglas et al. 2017). As a final check, we visually inspected all phased light curves.

We created synthetic data sets, with random subsamples of half the data and each point perturbed by a random number following the measurement errors, to investigate the accuracy of our period determinations. We found that, when the correct period is identified, our assigned periods are accurate within 2%, with a fail rate of $\simeq 5\%$ where the measured period is wrong by 20% or more (usually off by an integer multiple). This assumes that all detected periods are associated with stellar rotation and not other phenomena. Periodic signals caused by binary systems, pulsations or flares could cause further false positives, if they passed our visual inspection.

The resulting rotation periods are shown in Figure 25 and listed in Table 11. While there is significant scatter in the sequence, Praesepe and Pleiades members have the longest typical rotation period at $G - G_{RP} < 0.8$, while members of young moving groups have the shortest periods, and MUTA members are located in between. On the cool end ($G - G_{RP} \gtrsim 1.1$), Pleiades rotations are the fastest, as the $\simeq 45$ Myr stars are still contracting, although we have fewer period measurements in MUTA in this regime. The overall trend is consistent with our assigned 61 ± 5 Myr age of MUTA based on empirical isochrones and the total age of the white dwarf WD 0340+103, though additional rotation period measurements would be useful to better map out its sequence.

Stellar rotation serves as a driver of magnetic activity through the dynamo effect (Reiners et al. 2012), and causes young stars to display enhanced UV and X-ray emission among other effects associated with an enhanced stellar activity (Kastner et al. 2003; Rodriguez et al. 2013; Malo et al. 2014a). We used data from the *ROSAT* all-sky survey (Boller et al. 2016) and the *GALEX* catalog (Martin et al. 2005) to verify that our population of MUTA members and candidates display this expected enhanced activity in a way that is consistent with other young associations of similar ages ($\simeq 10$ –150 Myr) in the Solar neighborhood, including β PMG and the AB Doradus moving group (ABDMG, Zuckerman et al. 2004; see Gagné et al. 2018 for a discussion of these associations). The resulting distributions are shown in Figures 26 and 27, and provide more evidence that MUTA consists of a coeval and young association.

6.8. μ Tau in the Context of the Galactic Structure

An unprecedented view of the local spatial and kinematic structure of the Galaxy was enabled with the ad-

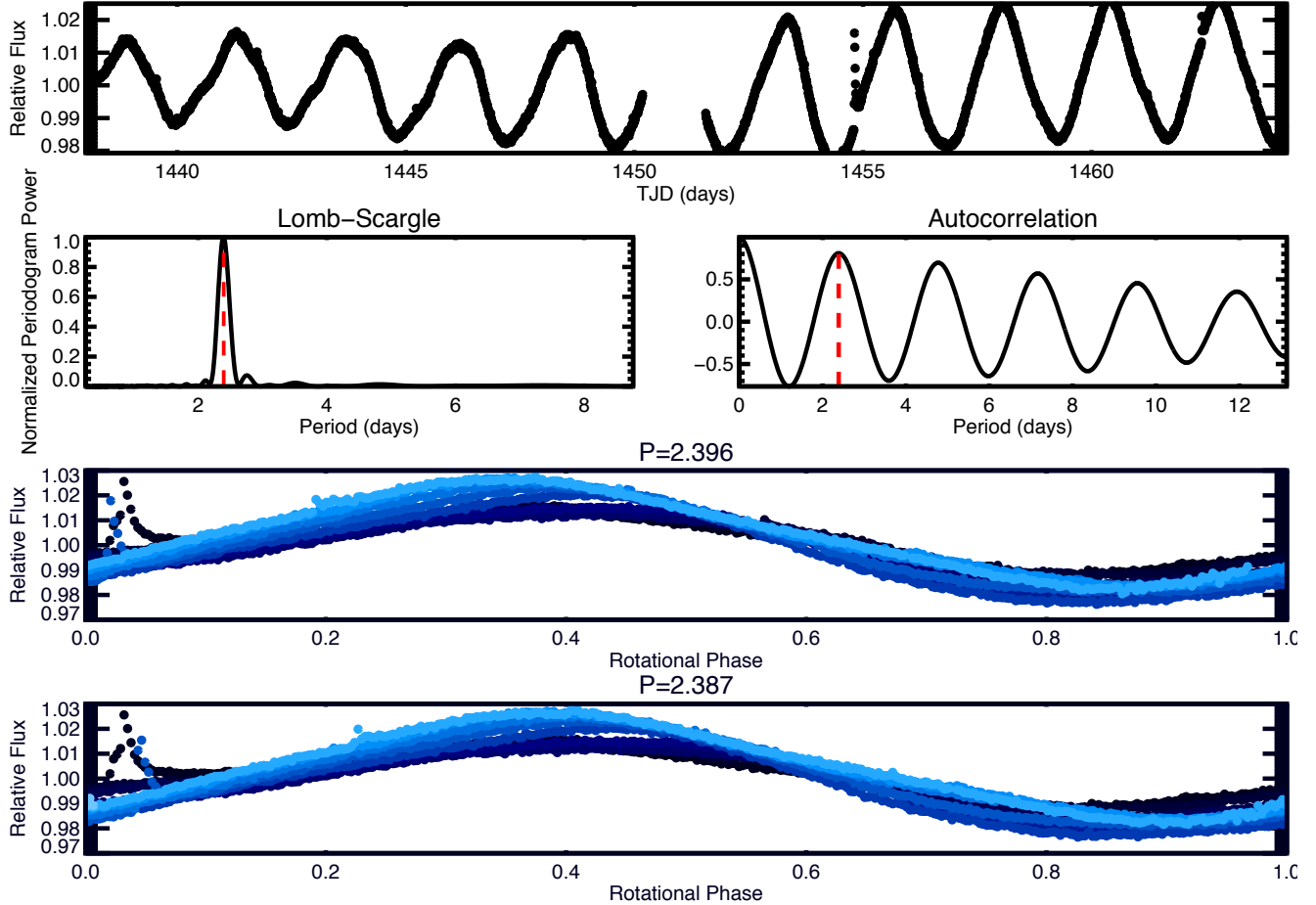


Figure 24. *TESS* light curve and rotation diagnostics of TIC178969585 (HD 29615), a G-type dwarf in the Tucana-Horologium association. The top panel shows the SPOC light curve, with the Lomb-Scargle power and autocorrelation function just below (the assigned period is marked with a red dashed line). The bottom two panels show the light curve phased to the period derived from the Lomb-Scargle (top) and autocorrelation function (bottom), color-coded by chronological order (lighter is later).

vent of *Gaia* DR2. Using these new data, Kounkel & Covey (2019) identified 1,901 groups of stars that appear co-moving and coeval, located within 30° of the Galactic plane and 1 kpc of the Sun. Their method used the HDBSCAN unsupervised clustering algorithm¹⁵ directly in the 5-dimensional parameter space of *Gaia* DR2 observables (sky position, proper motion and parallax) to identify over-densities; this did not allow them to efficiently recover the structure within about 70 pc of the Sun because the large spread of nearby associations on the sky introduces strong variation and correlations in the *Gaia* DR2 5-dimensional kinematic space of the members within a specific young association. Kounkel & Covey (2019) separated the over-densities among clusters and strings, the latter consisting of much larger structures with typical physical sizes of about 200 pc

and some of which also have extended kinematic distributions.

We cross-matched our sample of MUTA candidates and members with the full Kounkel & Covey (2019) catalog of clustered sources to determine whether MUTA had been recovered by their study. We found a total of 72 matches with our list, all with a single Kounkel & Covey (2019) string named Theia 160 that contains a total of 300 stars. Only 4 of these stars are matches to our initial list of MUTA members (HD 28715, HD 27687, HD 28356, and TYC 668–737–1; respectively, MUTA 11, 17, 18, and 30 A). One likely explanation for the partial overlap is the $|b| < 30^\circ$ cut-off in Galactic latitude that they imposed, as approximately half of MUTA falls at $b < -30^\circ$. We show a comparison of Theia 160, MUTA and Taurus in Figure 28. Theia 160 is spatially more extended, but also shows a much larger spread in space velocities compared with MUTA, although they are centered at similar average velocities; MUTA mem-

¹⁵ See <https://hdbscan.readthedocs.io>.

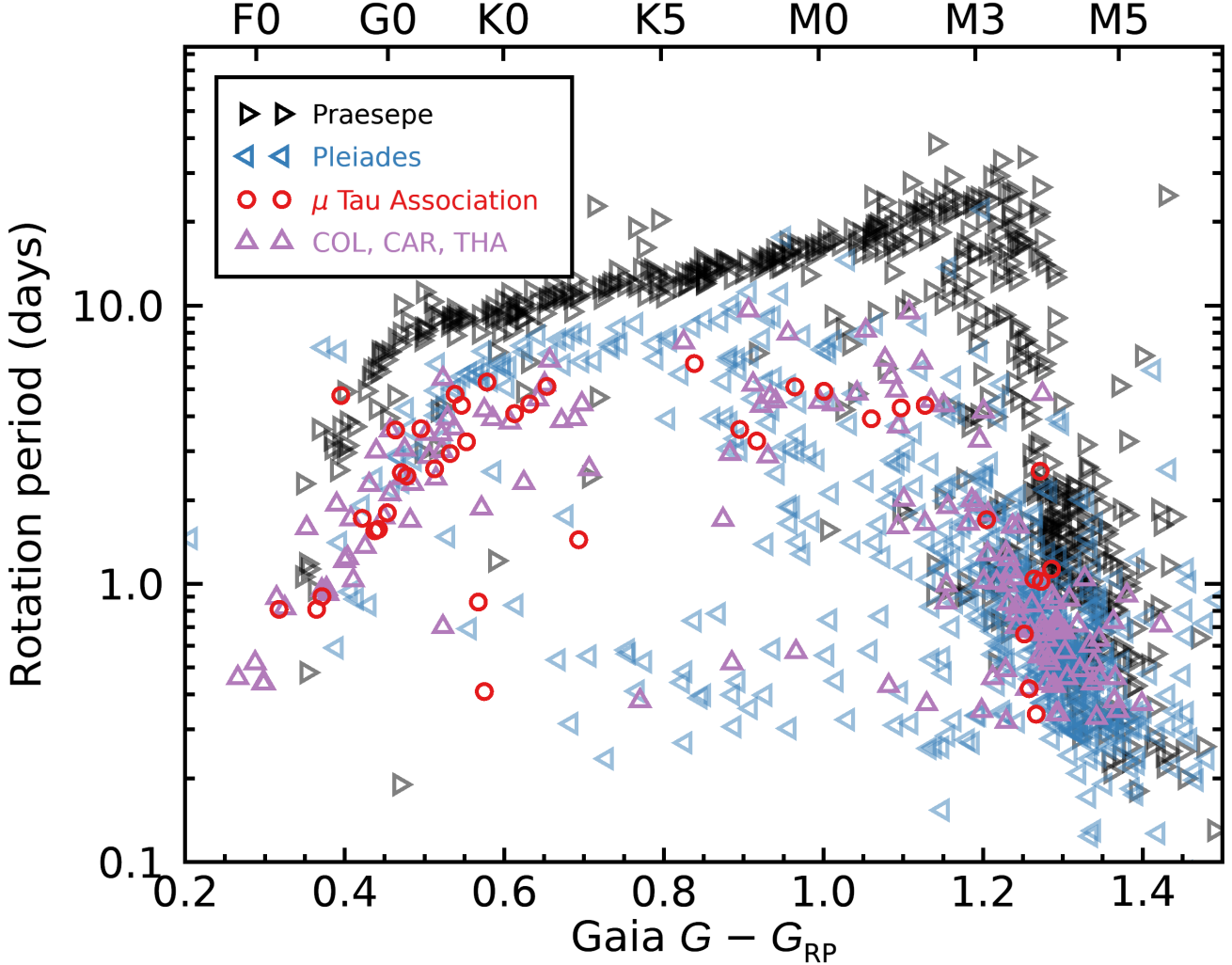


Figure 25. Rotation periods for stars in the Praesepe (black, $\simeq 800$ Myr) and Pleiades clusters (blue, $\simeq 112$ Myr), Columba (COL), Carina (CAR), or Tucana-Horologium (THA) associations (violet; $\simeq 45$ Myr), and MUTA (red; $\simeq 60$ Myr) as a function of Gaia $G - G_{RP}$ color.

bers have a spread of $(2.8, 2.1, 1.6)$ km s $^{-1}$ in UVW space, whereas the spread of Theia 160 members is $(21.1, 1.7, 8.9)$ km s $^{-1}$. This indicates that some interlopers may contaminate the sample of Theia 160 stars, and further investigation will be required to confirm this.

In addition to the similar kinematics between MUTA and Theia 160, Kounkel & Covey (2019) determined a model-dependent isochronal age of $\simeq 80$ Myr for Theia 160, which is close to our estimated age of 61 ± 5 Myr. It seems likely that MUTA and Theia 160 are related to each other; perhaps Theia 160 represents a stream or tidal tail around the more closely packed core of MUTA (analogous to the tidal tail around the Hyades cluster although the latter is much older; Röser et al. 2019), or it is simply a fragment of MUTA with some contaminating field stars that have more spread-

out space velocities. Investigating this further will require a spectroscopic follow-up of candidates in both MUTA and Theia 160 to complete the UVW measurements of all members in both groups—although the next data release of the *Gaia* DR2 mission will likely allow to complete the UVW velocities of most MUTA members—and determine spectroscopic signs of young ages. It is possible that our method did not recover the full spatial structure of MUTA, especially regions that would lack massive stars, because BANYAN Σ requires an initial kinematic model to work with, which we obtained from the initial collection of young or active stars described in Section 2. In addition to this, Kounkel & Covey (2019) uncovered a large kinematic structure (Theia 133) that encompasses the α Persei cluster, likely related to Cas-

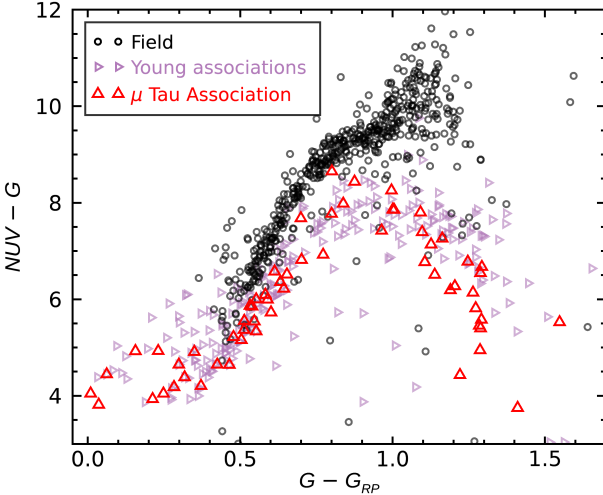


Figure 26. *GALEX* to *Gaia* DR2 $NUV - G$ color versus $G - G_{RP}$ for field stars (black circles), members of nearby young associations (rightward purple triangles) and MUTA candidates studied in this paper (upward red triangles). Our candidates are consistent with the young stellar population displaying a NUV excess compared with field stars of the same $G - G_{RP}$ color. See Section 6.7 for more details.

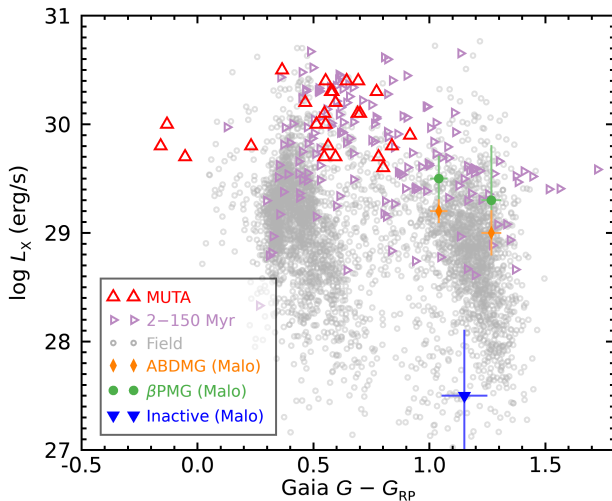


Figure 27. Absolute X-ray luminosity for field stars (grey circles), nearby young stars (rightward purple triangles) and our MUTA candidates (upward red triangles). The young M dwarf distributions of Malo et al. (2014a) are also shown for comparison. Young stars tend to emit more X-ray because they are more active. In the case of low-mass stars, this effect is compounded by the larger radius of younger M dwarfs. Field stars tend to be more active at both ends of the mass spectrum, consistent with their faster average rotation rates. β PMG indicates the β Pictoris moving group, and ABDMG indicates the AB Doradus moving group. See Section 6.7 for more details.

Tau and MUTA, as discussed in Section 2. This structure is also shown in Figure 28.

Liu et al. (2020) recently published the discovery of two new associations physically nearby (but unrelated to) the Taurus-Auriga star-forming region; e Tau and u Tau. The group that they identified as e Tau has significant overlap with our definition of MUTA; 104 of their 119 members are in also in our list (18 in our initial members, 79 in our candidate members, 6 in our low-likelihood candidate members, and 1 in our list of rejected members). The 15 remaining objects not in our catalogs that they list as e Tau members either have a Bayesian membership probability below 90% or a best-case scenario separation above 5 km s^{-1} with our kinematic model, which explains why we have not recovered them. We identified in this paper a total of 444 candidate members that Liu et al. (2020) did not discuss: 18 in our initial members, 277 candidate members and 149 in our low-likelihood candidate members. An additional 12 objects in our MUTA lists (4 initial members, 6 candidate members and 2 low-likelihood candidates) are listed as u Tau members by Liu et al. (2020). The isochrone age of $\simeq 50$ Myr determined by Liu et al. (2020) is similar to our 61 ± 5 Myr, but is based on model isochrones rather than empirical ones.

The fact that Kounkel & Covey (2019) and Liu et al. (2020) may have uncovered spatial extensions of MUTA, and the presence of a large structure of additional stars coeval with MUTA and α Persei hints that it would be valuable to parse the local Solar neighborhood with an overdensity detection algorithm that is not hindered by the lack of radial velocity measurements or the large spread and correlations of sky positions, proper motions and parallaxes of nearby cluster members. Such a study would have the potential to uncover extended structures and connections between the Kounkel & Covey (2019) groups and the known nearby young associations in the Solar neighborhood, as well as new nearby associations entirely.

7. CONCLUSIONS

We presented and characterized the μ Tau Association, a young stellar population consisting of hundreds of members at about 150 pc from the Sun. We built a BANYAN Σ spatial-kinematic model for this association to identify additional candidate members with *Gaia* DR2 and to allow other teams to search for new members. The *Gaia* DR2 photometry and parallaxes of MUTA members allowed us to make a comparison with empirical sequences of the Pleiades, Tucana-Horologium, Carina and Columba members to determine an isochronal age relative to these other young as-

sociations. This resulted in an age estimate of 62 ± 7 Myr for MUTA. We identified a white dwarf (WD 0340+103) that is the remnant of a B2 MUTA member that left its planetary nebula phase 270,000 years ago, and used its total age to further constrain the age of MUTA at 61 ± 5 Myr. We found literature measurements of the lithium equivalent width for K-type to G-type members of MUTA and showed that they are consistent with our age determination. The members of this new association have a *Gaia* DR2 colors versus *TESS* rotation periods sequence consistent with a young age, and display an enhanced level of stellar activity compared with the field population based on UV and X-ray, consistent with a young coeval population. We also showed that its present-day mass function is similar to other known young associations. MUTA is likely part of an extended network of stars coeval and co-moving with the α Persei cluster that are currently dissolving. A master table with all candidates and members of the MUTA association is also provided here (Table 12).

The MUTA association is a new laboratory to study stellar and exoplanet evolution at an age which was not well sampled by other associations within the Solar neighborhood. Its distance of $\simeq 150$ pc will make it harder to identify its substellar population, but upcoming wide area surveys such as Pan-STARRS 3 π (Magnier et al. 2010) and CatWISE (Eisenhardt et al. 2019) may be able to do so in the near future. The extended ROentgen Survey with an Imaging Telescope Array (eROSITA; Predehl et al. 2014) on the Spektrum-Roentgen-Gamma (SRG) space telescope will also likely allow us to better study the activity of the low-mass stars in MUTA.

ACKNOWLEDGMENTS

We thank the anonymous reviewer for thoughtful and constructive comments. We thank Patrick Dufour, Aaron Rizzuto and Benjamin Tofflemire for useful comments. We thank Za Gureto Muta for guidance in choosing an acronym for the μ Tau Association. This work was partially carried under a Banting grant from the Natural Sciences and Engineering Research Council of Canada (NSERC). This research made use of: the SIMBAD database and VizieR catalog access tool, operated at the Centre de Données astronomiques de Strasbourg, France (Ochsenbein et al. 2000); data products from the Two Micron All Sky Survey (*2MASS*; Skrutskie et al. 2006), which is a joint project of the University of Massachusetts and the Infrared Processing and Analysis Center (IPAC)/California Institute of Technology (Caltech), funded by the National Aeronautics and Space Administration (NASA) and the National Science Foundation (Skrutskie et al. 2006); data products from the *Wide-field Infrared Survey Explorer* (*WISE*; and Wright et al. 2010), which is a joint project of the University of California, Los Angeles, and the Jet Propulsion Laboratory (JPL)/Caltech, funded by NASA. The Digitized Sky Surveys (DSS) were produced at the Space Telescope Science Institute under U.S. Government grant NAG W-2166. The images of these surveys are based on photographic data obtained using the Oschin Schmidt Telescope on Palomar Mountain and the UK Schmidt Telescope. The plates were processed into the present compressed digital form with the permission of these institutions. The Second Palomar Observatory Sky Survey (POSS-II) was made by the California Institute of Technology with funds from the National Science Foundation, the National Geographic Society, the Sloan Foundation, the Samuel Oschin Foundation, and the Eastman Kodak Corporation. The Oschin Schmidt Telescope is operated by the California Institute of Technology and Palomar Observatory. This work presents results from the European Space Agency (ESA) space mission Gaia. Gaia data are being processed by the Gaia Data Processing and Analysis Consortium (DPAC). Funding for the DPAC is provided by national institutions, in particular the institutions participating in the Gaia Multi-Lateral Agreement (MLA). The Gaia mission website is <https://www.cosmos.esa.int/gaia>. The Gaia archive website is <https://archives.esac.esa.int/gaia>. The Digitized Sky Surveys were produced at the Space Telescope Science Institute under U.S. Government grant NAG W-2166. Part of this research was carried out at the Jet Propulsion Laboratory, California Institute of Technology, under a contract with the National Aeronautics and Space Administration (80NM0018D0004). TJD and EEM and gratefully acknowledge support from the Jet Propulsion Laboratory Exoplanetary Science Initiative and NASA award 17-K2GO6-0030. EEM acknowledges support from NASA grant NNX15AD53G.

Table 12. Main list of all systems of interest to MUTA identified in this work.

Name	Units	Type	Format	Description
muta_id	...	char	a6	μ Tau Association (MUTA) identification number.
main_name	...	char	a25	Main target name. SIMBAD-resolvable names are preferred; short names in the format J0236+2026 are given otherwise.
gaiadr2_id	...	char	a25	<i>Gaia</i> DR2 identification number.
tm_name	...	char	a25	2MASS designation.
aw_name	...	char	a25	AllWISE designation.
rosat_name	...	char	a25	<i>ROSAT</i> designation.
tyc_name	...	char	a25	Tycho catalog designation.
hip_name	...	char	a25	Hipparcos catalog designation.
simbad_id	...	char	a25	Principal SIMBAD identifier.
spt	...	char	a10	Literature spectral type. Spectral type estimates based on <i>Gaia</i> DR2 colors are given between parentheses. (WD) indicates likely white dwarfs.
spt_ref	...	char	a25	Reference for literature spectral type.
member_type	...	char	a2	Membership type. IM: Member from our initial list. CM: Candidate member. LM: Low-priority candidate member. R: Rejected candidate member.
source	...	char	a6	Source from which the target was obtained. INIT: Initial list described in Section 2. GAIA: Originates from our <i>Gaia</i> DR2-based search for additional candidate members described in Section 4. COM: Originates from our comover search described in Section 4.1. VIS: Originates from our visual identification of comover candidates described in Section 4.5. OH2017: Originates from a Oh et al. (2017) group with a partial match to our MUTA members and candidates.
mem_prob	%	R*4	f7.1	BANYAN Σ probability for membership in MUTA.
uvw_sep	km s $^{-1}$	R*4	f7.1	Smallest possible separation from the center of the BANYAN Σ model in <i>UVW</i> space.
xyz_sep	km s $^{-1}$	R*4	f7.1	Smallest possible separation from the center of the BANYAN Σ model in <i>XYZ</i> space.
ra	deg	R*8	f21.16	<i>Gaia</i> DR2 right ascension (J2000) at epoch 2015.5 in the ICRS reference frame.
dec	deg	R*8	f21.16	<i>Gaia</i> DR2 declination (J2000) at epoch 2015.5 in the ICRS reference frame.
pmra	mas yr $^{-1}$	R*4	f10.5	<i>Gaia</i> DR2 proper motion in right ascension, including the $\cos\delta$ jacobian term.
pmdec	mas yr $^{-1}$	R*4	f10.5	<i>Gaia</i> DR2 proper motion in declination.
epmra	mas yr $^{-1}$	R*4	f10.5	Measurement error for <i>Gaia</i> DR2 proper motion in right ascension.
epmdec	mas yr $^{-1}$	R*4	f10.5	Measurement error for <i>Gaia</i> DR2 proper motion in declination.
plx	pc	R*4	f10.5	<i>Gaia</i> DR2 parallax.
eplx	pc	R*4	f10.5	Measurement error for <i>Gaia</i> DR2 parallax.
ruwe	...	R*4	f7.1	Re-normalised unit weight error of the <i>Gaia</i> DR2 astrometric solution. See Section 4.4 for more details.
rv	km s $^{-1}$	R*4	f7.1	Radial velocity measurement from the literature.
erv	km s $^{-1}$	R*4	f7.1	Measurement error for radial velocity measurement.
rv_ref	...	char	a25	Reference for literature radial velocity measurement.

Table 12 *continued*

Table 12 (*continued*)

Name	Units	Type	Format	Description
pred_rv	km s^{-1}	R*4	f7.1	Predicted radial velocity that maximizes MUTA membership probability obtained from BANYAN Σ , only listed for targets without a radial velocity measurement.
epred_rv	km s^{-1}	R*4	f7.1	1σ confidence range on predicted radial velocity that maximizes MUTA membership probability.
gaia_g	mag	R*8	f12.5	<i>Gaia</i> DR2 <i>G</i> -band magnitude.
egaia_g	mag	R*8	f12.5	Measurement error for <i>Gaia</i> DR2 <i>G</i> -band magnitude.
gaia_grp	mag	R*4	f12.5	<i>Gaia</i> DR2 G_{RP} -band magnitude.
egaia_grp	mag	R*4	f12.5	Measurement error for <i>Gaia</i> DR2 G_{RP} -band magnitude.
gaia_brp	mag	R*4	f12.5	<i>Gaia</i> DR2 G_{BP} -band magnitude.
egaia_brp	mag	R*4	f12.5	Measurement error for <i>Gaia</i> DR2 G_{BP} -band magnitude.
tmass_j	mag	R*4	f10.3	2MASS <i>J</i> -band magnitude.
etmass_j	mag	R*4	f10.3	Measurement error for 2MASS <i>J</i> -band magnitude.
tmass_h	mag	R*4	f10.3	2MASS <i>H</i> -band magnitude.
etmass_h	mag	R*4	f10.3	Measurement error for 2MASS <i>H</i> -band magnitude.
tmass_k	mag	R*4	f10.3	2MASS K_S -band magnitude.
etmass_k	mag	R*4	f10.3	Measurement error for 2MASS K_S -band magnitude.
aw_w1	mag	R*4	f10.3	AllWISE <i>W1</i> -band magnitude, W1MPRO entry in the original catalog.
eaw_w1	mag	R*4	f10.3	Measurement error for AllWISE <i>W1</i> -band magnitude, W1SIGMPRO entry in the original catalog.
aw_w2	mag	R*4	f10.3	AllWISE <i>W2</i> -band magnitude, W2MPRO entry in the original catalog.
eaw_w2	mag	R*4	f10.3	Measurement error for AllWISE <i>W2</i> -band magnitude, W2SIGMPRO entry in the original catalog.
aw_w3	mag	R*4	f10.3	AllWISE <i>W3</i> -band magnitude, W3MPRO entry in the original catalog.
eaw_w3	mag	R*4	f10.3	Measurement error for AllWISE <i>W3</i> -band magnitude, W3SIGMPRO entry in the original catalog.
ebv	mag	R*4	f7.1	$E(B - V)$ reddening based on the STILISM reddening map combined with <i>Gaia</i> DR2 distance and sky position. See Section 5 for more details.
eebv	mag	R*4	f7.1	Measurement error for $E(B - V)$ reddening.
galex_nuv	mag	R*4	f7.1	<i>GALEX NUV</i> -band magnitude.
egalex_nuv	mag	R*4	f7.1	Measurement error for <i>GALEX NUV</i> -band magnitude.
galex_fuv	mag	R*4	f7.1	<i>GALEX FUV</i> -band magnitude.
egalex_fuv	mag	R*4	f7.1	Measurement error for <i>GALEX FUV</i> -band magnitude.
rosat_hr1	...	R*4	f10.3	<i>ROSAT</i> hardness ratio HR1.
rosat_hr2	...	R*4	f10.3	<i>ROSAT</i> hardness ratio HR2.
rosat_counts	ct/s	R*4	f10.3	<i>ROSAT</i> X-ray counts.
erosat_counts	ct/s	R*4	f10.3	Measurement error for <i>ROSAT</i> X-ray counts.
rosat_lx	...	R*4	f10.3	Absolute X-ray luminosity $\log L_X / L_{\odot}$ calculated from <i>ROSAT</i> X-ray data and <i>Gaia</i> DR2 trigonometric distance.
erosat_lx	...	R*4	f10.3	Measurement error for absolute X-ray luminosity.
li_ew	mÅ	R*4	f7.1	Lithium absorption line equivalent width.
spt_ref	...	char	a25	Reference for lithium absorption line equivalent width.

Table 12 *continued*

Table 12 (*continued*)

Name	Units	Type	Format	Description
teff	K	R*4	f7.1	Effective temperature.
teff_ref	...	char	a25	Reference for effective temperature.
is_primary	...	int	i3	1: Single stars or primary (brightest) star in a multiple system. 0: Companion star in a multiple system.
mult_letter	...	char	a3	Identifier letter for multiple system components.
sep_parent	asec	R*8	f12.5	Separation from parent star calculated from <i>Gaia</i> DR2 positions.
esep_parent	asec	R*8	f12.5	Measurement error for separation.
pa_parent	deg	R*8	f12.5	Position angle with respect to parent star calculated from <i>Gaia</i> DR2 positions.
epa_parent	deg	R*8	f12.5	Measurement error for position angle.
comover_gaiadr2_id	...	char	a40	<i>Gaia</i> DR2 identification number for comoving star (parent or companion). Multiple entries are separated by a semicolon.
oh2017_group_id	...	char	a4	Comoving group identification number from Oh et al. (2017).

NOTE—The full table data are available as online-only additional material.

JG wrote the codes, manuscript, generated figures and led the analysis; *TJD* compiled an initial list of new candidates and generated Figure 1; *EEM* first identified the over-density associated with MUTA, led the turnoff age analysis, the investigation of HD 27860 and provided the initial members list; *AWM* led the rotation periods analysis, wrote part o f Section 6.7 and built Figures 24 and 25, *JKF* provided help with parsing the *Gaia* DR2 data and general comments, and *AB* provided the atmosphere analysis of WD 0340+103 and Figure 21.

Software: BANYAN Σ ([Gagné et al. 2018](#)), Eleanor ([Feinstein et al. 2019](#)).

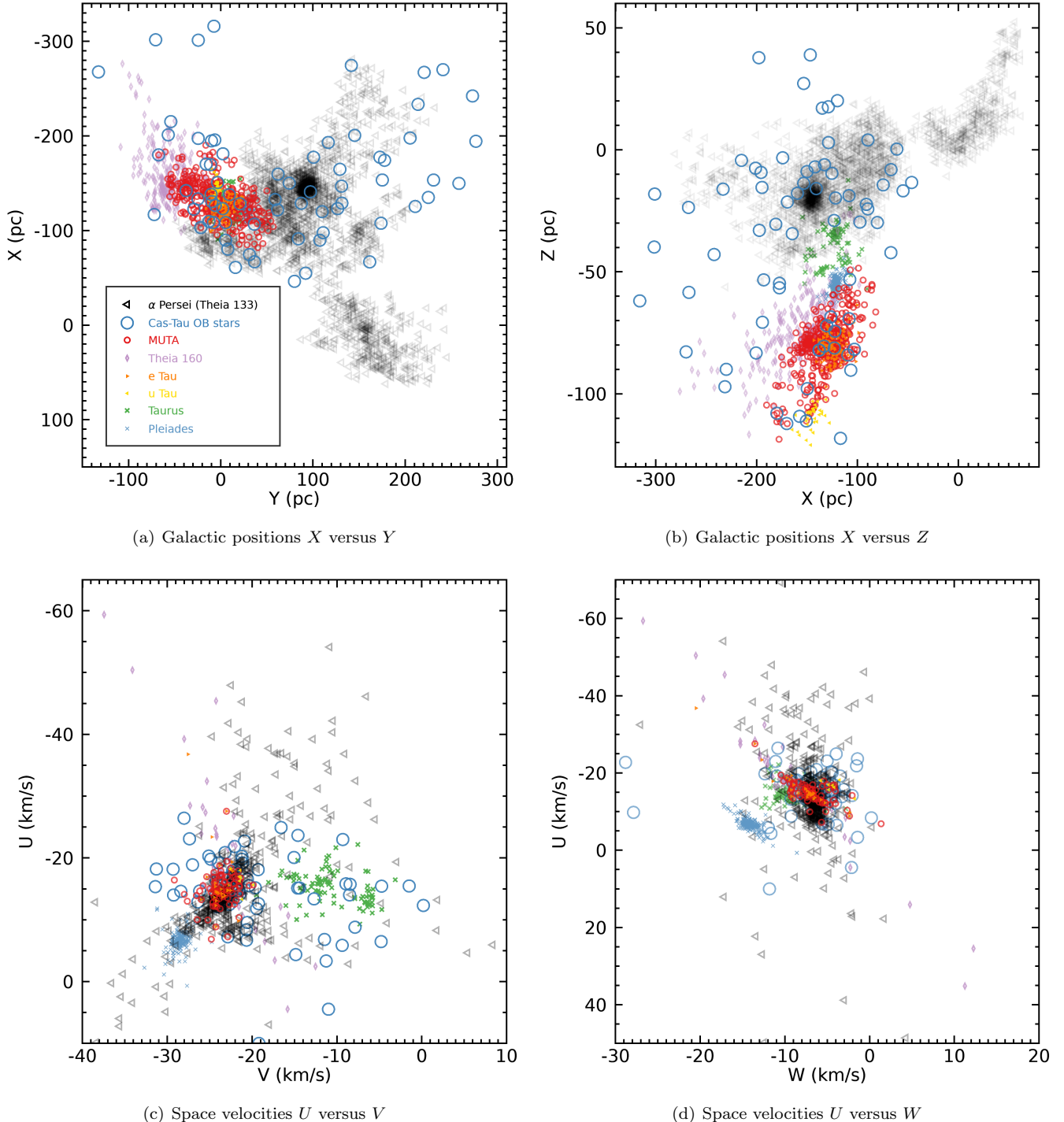


Figure 28. Spatial and kinematic distribution of MUTA candidates and members discussed in this work (red circles), compared with the neighbor Taurus association (rightward green triangles) and the Theia 160 kinematic string (blue diamonds). The similar kinematics and isochronal ages of Theia 160 and MUTA indicate that these two Galactic structures may be related to one another. See Section 6.8 for more detail.

REFERENCES

- Abt, H. A. 2008, *The Astrophysical Journal Supplement Series*, 176, 216
- Ahn, C. P., Alexandroff, R., Allende Prieto, C., et al. 2012, *The Astrophysical Journal Supplement*, 203, 21
- Alam, S., Albareti, F. D., Allende Prieto, C., et al. 2015, *The Astrophysical Journal Supplement Series*, 219, 12
- Allard, F., Homeier, D., & Freytag, B. 2012, *Philosophical Transactions of the Royal Society A: Mathematical*, 370, 2765
- Avvakumova, E. A., Malkov, O. Y., & Kniazev, A. Y. 2013, *Astronomische Nachrichten*, 334, 860
- Babusiaux, C., van Leeuwen, F., Barstow, M., et al. 2018, *Astronomy & Astrophysics*, 616, A10
- Bai, Y., Liu, J., Bai, Z., Wang, S., & Fan, D. 2019, *AJ*, 158, 93
- Baraffe, I., Homeier, D., Allard, F., & Chabrier, G. 2015, *Astronomy & Astrophysics*, 577, A42
- Barnes, S. A. 2003, *ApJ*, 586, 464
- Barrado y Navascués, D., García López, R. J., Severino, G., & Gomez, M. T. 2001, *A&A*, 371, 652
- Barrado y Navascués, D., Stauffer, J. R., & Jayawardhana, R. 2004, *The Astrophysical Journal*, 614, 386
- Beavers, W. I., & Cook, D. B. 1980, *Astrophysical Journal Supplement Series*, 44, 489
- Bell, C. P. M., Mamajek, E. E., & Naylor, T. 2015, *Monthly Notices of the Royal Astronomical Society*, 454, 593
- Bergeron, P., Saffer, R. A., & Liebert, J. 1992, *The Astrophysical Journal*, 394, 228
- Bergeron, P., Wesemael, F., Dufour, P., et al. 2011, *The Astrophysical Journal*, 737, 28
- Bertelli, G., Nasi, E., Girardi, L., & Marigo, P. 2009, *Astronomy and Astrophysics*, 508, 355
- Bidelman, W. P., Ratcliff, S. J., & Svolopoulos, S. 1988, *Astronomical Society of the Pacific*, 100, 828
- Blaauw, A. 1956, *The Astrophysical Journal*, 123, 408
- Bochanski, J. J., Hawley, S. L., Covey, K. R., et al. 2010, *The Astronomical Journal*, 139, 2679
- Boller, T., Freyberg, M. J., Trümper, J., et al. 2016, *Astronomy & Astrophysics*, 588, A103
- Borucki, W. J., Koch, D., Basri, G., et al. 2010, *Science*, 327, 977
- Bouvier, J., Barrado, D., Moraux, E., et al. 2018, *A&A*, 613, A63
- Bouy, H., Bertin, E., Barrado, D., et al. 2015, *A&A*, 575, A120
- Brandt, T. D., & Huang, C. X. 2015, *The Astrophysical Journal*, 807, 24
- Burke, C. J., Pinsonneault, M. H., & Sills, A. 2004, *The Astrophysical Journal*, 604, 272
- Camisassa, M. E., Althaus, L. G., Córscico, A. H., et al. 2019, *A&A*, 625, A87
- Cannon, A. J., & Pickering, E. C. 1993, *VizieR On-line Data Catalog*, 3135
- Capitanio, L., Lallement, R., Vergely, J. L., Elyajouri, M., & Monreal-Ibero, A. 2017, *Astronomy and Astrophysics*, 606, A65
- Chambers, K. C., Magnier, E. A., Metcalfe, N., et al. 2016, *arXiv.org*, arXiv:1612.05560
- Choi, J., Dotter, A., Conroy, C., et al. 2016, *The Astrophysical Journal*, 823, 102
- Cowley, A. 1972, *Astronomical Journal*, 77, 750
- Cowley, A., Cowley, C., Jaschek, M., & Jaschek, C. 1969, *Astronomical Journal*, 74, 375
- Cowley, A. P. 1968, *Publications of the Astronomical Society of the Pacific*, 80, 453
- Cropper, M., Katz, D., Sartoretti, P., & et al. 2018, *Astronomy & Astrophysics*, 616, A5
- Curtis, J. L., Agüeros, M. A., Mamajek, E. E., Wright, J. T., & Cummings, J. D. 2019, *The Astronomical Journal*, 158, 77
- Dahm, S. E. 2015, *The Astrophysical Journal*, 813, 108
- de Zeeuw, P. T., Hoogerwerf, R., de Bruijne, J. H. J., Brown, A. G. A., & Blaauw, A. 1999, *The Astronomical Journal*, 117, 354
- Delorme, P., Collier Cameron, A., Hebb, L., et al. 2011, *MNRAS*, 413, 2218
- Dobbie, P. D., Lodieu, N., & Sharp, R. G. 2010, *Monthly Notices of the Royal Astronomical Society*, 409, 1002
- Douglas, S. T., Agüeros, M. A., Covey, K. R., et al. 2016, *The Astrophysical Journal*, 822, 47
- Douglas, S. T., Agüeros, M. A., Covey, K. R., & Kraus, A. 2017, *The Astrophysical Journal*, 842, 83
- Douglas, S. T., Agüeros, M. A., Covey, K. R., & Kraus, A. 2017, *ApJ*, 842, 83
- Dupuy, T. J., & Liu, M. C. 2012, *The Astrophysical Journal Supplement*, 201, 19
- Eisenhardt, P. R. M., Marocco, F., Fowler, J. W., et al. 2019, *arXiv.org*, arXiv:1908.08902
- ESA. 1997, *The Hipparcos and Tycho catalogues. Astrometric and photometric star catalogues derived from the ESA Hipparcos Space Astrometry Mission*, 1200
- Evans, D. S. 1967, *Determination of Radial Velocities and their Applications*, 30, 57
- Evans, D. W., Riello, M., De Angeli, F., et al. 2018a, *arXiv.org*, arXiv:1804.09368
- . 2018b, *Astronomy & Astrophysics*, 616, A4
- Faherty, J. K., Bochanski, J. J., Gagné, J., et al. 2018, *The Astrophysical Journal*, 863, 91

- Faherty, J. K., Riedel, A. R., Cruz, K. K., et al. 2016, *The Astrophysical Journal Supplement Series*, 225, 10
- Feinstein, A. D., Montet, B. T., Foreman-Mackey, D., et al. 2019, *PASP*, 131, 094502
- Filippazzo, J. C., Rice, E. L., Faherty, J., et al. 2015, *The Astrophysical Journal*, 810, 158
- Fitzpatrick, E. L. 1999, *The Publications of the Astronomical Society of the Pacific*, 111, 63
- Flower, P. J. 1996, *Astrophysical Journal* v.469, 469, 355
- Fontaine, G., Brassard, P., & Bergeron, P. 2001, *The Publications of the Astronomical Society of the Pacific*, 113, 409
- Gagné, J., & Faherty, J. K. 2018, *The Astrophysical Journal*, 862, 138
- Gagné, J., Faherty, J. K., & Mamajek, E. E. 2018a, *The Astrophysical Journal*, 865, 136
- Gagné, J., Fontaine, G., Simon, A., & Faherty, J. K. 2018b, *The Astrophysical Journal Letters*, 861, L13
- Gagné, J., Lafrenière, D., Doyon, R., Malo, L., & Artigau, É. 2014, *The Astrophysical Journal*, 783, 121
- Gagné, J., Roy-Loubier, O., Faherty, J. K., Doyon, R., & Malo, L. 2018c, *The Astrophysical Journal*, 860, 43
- Gagné, J., Schneider, A., & Cushing, M. 2018, *Finder Charts Python Package v1.0*, Zenodo, doi:10.5281/zenodo.1237017
- Gagné, J., Faherty, J. K., Cruz, K. L., et al. 2015, *The Astrophysical Journal Supplement Series*, 219, 33
- Gagné, J., Mamajek, E. E., Malo, L., et al. 2018, *The Astrophysical Journal*, 856, 23
- Gaia Collaboration, Brown, A. G. A., Vallenari, A., et al. 2018a, *Astronomy & Astrophysics*, 616, A1
- Gaia Collaboration, Brown, A. G. A., Vallenari, A., et al. 2018b, *A&A*, 616, A1
- Gentile Fusillo, N. P., Tremblay, P.-E., Gänsicke, B. T., et al. 2019, *Monthly Notices of the Royal Astronomical Society*, 482, 4570
- Gontcharov, G. A. 2006, *Astronomy Letters*, 32, 759
- Gray, R. O., Corbally, C. J., Garrison, R. F., et al. 2006, *The Astronomical Journal*, 132, 161
- Gray, R. O., Corbally, C. J., Garrison, R. F., McFadden, M. T., & Robinson, P. E. 2003, *The Astronomical Journal*, 126, 2048
- Grenier, S., Baylac, M. O., Rolland, L., et al. 1999, *Astronomy and Astrophysics Supplement*, 137, 451
- Gullikson, K., Kraus, A. L., & Dodson-Robinson, S. 2016, *The Astronomical Journal*, 152, 40
- Hambly, N. C., Cropper, M., Boudreault, S., et al. 2018, *Astronomy & Astrophysics*, 616, A15
- Heckmann, O., & Lübeck, K. 1958, *Zeitschrift für Astrophysik*, 45, 243
- Hohle, M. M., Neuhauser, R., & Schutz, B. F. 2010, *Astronomische Nachrichten*, 331, 349
- Holberg, J. B., & Bergeron, P. 2006, *The Astronomical Journal*, 132, 1221
- Hollands, M. A., Tremblay, P. E., Gänsicke, B. T., Gentile-Fusillo, N. P., & Toonen, S. 2018, *Monthly Notices of the Royal Astronomical Society*, 480, 3942
- Horne, J. H., & Baliunas, S. L. 1986, *ApJ*, 302, 757
- Howell, S. B., Sobeck, C., Haas, M., et al. 2014, *Publications of the Astronomical Society of the Pacific*, 126, 398
- Jaschek, M., & Jaschek, C. 1980, *Astronomy & Astrophysics Supplement Series*, 42, 115
- Jeffries, R. D. 2012, *Low-Mass Stars and the Transition Stars/Brown Dwarfs - EES2011*, 57, 45
- Jenkins, J. M., Twicken, J. D., McCauliff, S., et al. 2016, *Society of Photo-Optical Instrumentation Engineers (SPIE) Conference Series*, Vol. 9913, *The TESS science processing operations center*, 99133E
- Jones, B. F., Fischer, D., & Soderblom, D. R. 1999, *AJ*, 117, 330
- Jones, B. F., Shetrone, M., Fischer, D., & Soderblom, D. R. 1996, *AJ*, 112, 186
- Kastner, J. H., Crigger, L., Rich, M., & Weintraub, D. A. 2003, *The Astrophysical Journal*, 585, 878
- Kenyon, S. J., Gómez, M., & Whitney, B. A. 2008, *Handbook of Star Forming Regions*, I, 405
- Kharchenko, N. V., Scholz, R. D., Piskunov, A. E., Röser, S., & Schilbach, E. 2007, *Astronomische Nachrichten*, 328, 889
- Kirkpatrick, D. J., Cushing, M. C., Cruz, K. K., et al. 2011, *The Astrophysical Journal Supplement*, 197, 19
- Kirkpatrick, D. J., Gelino, C. R., Cushing, M. C., et al. 2012, *The Astrophysical Journal*, 753, 156
- Kleinman, S. J., Kepler, S. O., Koester, D., et al. 2013, *The Astrophysical Journal Supplement*, 204, 5
- Kounkel, M., & Covey, K. 2019, arXiv.org, 122
- Kowalski, P. M., & Saumon, D. 2006, *The Astrophysical Journal*, 651, L137
- Kraus, A. L., Shkolnik, E. L., Allers, K. N., & Liu, M. C. 2014, *The Astronomical Journal*, 147, 146
- Lallemand, R., Vergely, J. L., Valette, B., et al. 2014, *Astronomy and Astrophysics*, 561, A91
- Lallemand, R., Capitanio, L., Ruiz-Dern, L., et al. 2018, *Astronomy and Astrophysics*, 616, A132
- Lauffer, G. R., Romero, A. D., & Kepler, S. O. 2018, *MNRAS*, 480, 1547
- Lawrence, A., Warren, S. J., Almaini, O., et al. 2007, *Monthly Notices of the Royal Astronomical Society*, 379, 1599

- Lesh, J. R. 1968, *Astrophysical Journal Supplement*, 17, 371
- Liebert, J., Bergeron, P., & Holberg, J. B. 2005, *The Astrophysical Journal Supplement Series*, 156, 47
- Lindgren, L., Hernández, J., Bombrun, A., et al. 2018, *Astronomy & Astrophysics*, 616, A2
- Liu, J., Fang, M., & Liu, C. 2020, *The Astronomical Journal*, 159, 105
- Liu, M. C., Dupuy, T. J., & Allers, K. N. 2016, *The Astrophysical Journal*, 833, 96
- Lodie, N., Pérez-Garrido, A., Smart, R. L., & Silvotti, R. 2019, *Astronomy and Astrophysics*, 628, A66
- Luhman, K. L. 2018, *The Astronomical Journal*, 156, 271
- Luri, X., A Brown, A. G., Sarro, L., et al. 2018, *Astronomy & Astrophysics*, 616, A9
- Mace, G. N. 2014, *ProQuest Dissertations And Theses; Thesis (Ph.D.)–University of California*, 56
- Magazzù, A., Martín, E. L., Sterzik, M. F., et al. 1997, *A & A Supplement series*, 124, 449
- Magnier, E. A., Liu, M., Goldman, B., et al. 2010, *Highlights of Astronomy*, 15, 818
- Makarov, V. V., & Urban, S. 2000, *Monthly Notices of the Royal Astronomical Society*, 317, 289
- Malo, L., Artigau, É., Doyon, R., et al. 2014a, *The Astrophysical Journal*, 788, 81
- Malo, L., Doyon, R., Feiden, G. A., et al. 2014b, *The Astrophysical Journal*, 792, 37
- Malo, L., Doyon, R., Lafrenière, D., et al. 2013, *The Astrophysical Journal*, 762, 88
- Mamajek, E. E. 2005, *The Astrophysical Journal*, 634, 1385
- Martin, D. C., Fanson, J., Schiminovich, D., et al. 2005, *The Astrophysical Journal*, 619, L1
- Mason, B. D., Wycoff, G. L., Hartkopf, W. I., Douglass, G. G., & Worley, C. E. 2001, *The Astronomical Journal*, 122, 3466
- McMahon, R. G., Banerji, M., Gonzalez, E., et al. 2013, *The Messenger*, 154, 35
- McQuillan, A., Aigrain, S., & Mazeh, T. 2013, *MNRAS*, 432, 1203
- Meingast, S., Alves, J., & Fürnkranz, V. 2019, *Astronomy and Astrophysics*, 622, L13
- Mentuch, E., Brandeker, A., van Kerkwijk, M. H., Jayawardhana, R., & Hauschildt, P. H. 2008, *ApJ*, 689, 1127
- Mignard, F., Klioner, S., Lindgren, L., et al. 2018, *Astronomy & Astrophysics*, 616, A14
- Molnar, M. R. 1972, *The Astrophysical Journal*, 175, 453
- Nesterov, V. V., Kuzmin, A. V., Ashimbaeva, N. T., et al. 1995, *Astronomy and Astrophysics*, 110, 367
- Neuhaeuser, R., Sterzik, M. F., Schmitt, J. H. M. M., Wichmann, R., & Krautter, J. 1995, *A&A*, 295, L5
- Ochsenbein, F., Bauer, P., & Marcout, J. 2000, *Astronomy and Astrophysics Supplement*, 143, 23
- Oh, S., Price-Whelan, A. M., Hogg, D. W., Morton, T. D., & Spergel, D. N. 2017, *The Astronomical Journal*, 153, 257
- Pecaut, M. J., & Mamajek, E. E. 2013, *The Astrophysical Journal Supplement*, 208, 9
- Perryman, M. A. C., Lindegren, L., Kovalevsky, J., et al. 1997, *Astronomy and Astrophysics* 323, 323, L49
- Perryman, M. A. C., Brown, A. G. A., Lebreton, Y., et al. 1998, *Astronomy & Astrophysics*, 331, 81
- Pickles, A. J. 1998, *The Publications of the Astronomical Society of the Pacific*, 110, 863
- Predehl, P., Andritschke, R., Becker, W., et al. 2014, in *Society of Photo-Optical Instrumentation Engineers (SPIE) Conference Series*, Vol. 9144, Proc. SPIE, 91441T
- Randich, S. 2001, *A&A*, 377, 512
- Rasmuson, N. H. 1921, *Meddelanden från Lunds Astronomiska Observatorium Series II*, 26, 3
- Rebull, L. M., Stauffer, J. R., Bouvier, J., et al. 2016, *AJ*, 152, 113
- Reiners, A., Joshi, N., & Goldman, B. 2012, *The Astronomical Journal*, 143, 93
- Reino, S., de Bruijne, J., Zari, E., d'Antona, F., & Ventura, P. 2018, *Monthly Notices of the Royal Astronomical Society*, 477, 3197
- Ricker, G. R., Winn, J. N., Vanderspek, R., et al. 2015, *Journal of Astronomical Telescopes*, 1, 014003
- Riedel, A. R., Blunt, S. C., Lambrides, E. L., et al. 2017, *The Astronomical Journal*, 153, 95
- Riello, M., De Angeli, F., Evans, D. W., et al. 2018, *Astronomy & Astrophysics*, 616, A3
- Rodriguez, D. R., Zuckerman, B., Kastner, J. H., et al. 2013, *The Astrophysical Journal*, 774, 101
- Röser, S., & Schilbach, E. 2019, *Astronomy and Astrophysics*, 627, A4
- Röser, S., Schilbach, E., & Goldman, B. 2019, *Astronomy and Astrophysics*, 621, L2
- Sartoretti, P., Katz, D., Cropper, M., et al. 2018, *Astronomy & Astrophysics*, 616, A6
- Shkolnik, E. L., Allers, K. N., Kraus, A. L., Liu, M. C., & Flagg, L. 2017, *The Astronomical Journal*, 154, 69
- Simon, A. 2018, PhD thesis
- Simon, A., Fontaine, G., & Brassard, P. 2015, 19th European Workshop on White Dwarfs, 493, 137
- Skrutskie, M. F., Cutri, R. M., Stiening, R., et al. 2006, *The Astronomical Journal*, 131, 1163
- Smart, R. L., Marocco, F., Sarro, L. M., et al. 2019, *Monthly Notices of the Royal Astronomical Society*, 485, 4423

- Soderblom, D. R., Jones, B. F., Balachandran, S., et al. 1993, *Astronomical Journal* (ISSN 0004-6256), 106, 1059
- Soubiran, C., Jasniewicz, G., Chemin, L., et al. 2018, *Astronomy & Astrophysics*, 616, A7
- Tang, S.-Y., Pang, X., Yuan, Z., et al. 2019, *The Astrophysical Journal*, 877, 12
- Torres, C. A. O., da Silva, L., Quast, G. R., de la Reza, R., & Jilinski, E. 2000, *The Astronomical Journal*, 120, 1410
- Torres, C. A. O., Quast, G. R., da Silva, L., et al. 2006, *Astronomy and Astrophysics*, 460, 695
- Torres, C. A. O., Quast, G. R., Melo, C. H. F., & Sterzik, M. F. 2008, *Young Nearby Loose Associations*, ed. B. Reipurth, Vol. I (The Southern Sky ASP Monograph Publications)
- Tremblay, P. E., Bergeron, P., & Gianninas, A. 2011, *The Astrophysical Journal*, 730, 128
- van Leeuwen, F. 2007, *Astronomy & Astrophysics*, 474, 653
- van Saders, J. L., Ceillier, T., Metcalfe, T. S., et al. 2016, *Nature*, 529, 181
- Vanderburg, A., & Johnson, J. A. 2014, *PASP*, 126, 948
- White, R. J., Gabor, J. M., & Hillenbrand, L. A. 2007, *The Astronomical Journal*, 133, 2524
- Wichmann, R., Torres, G., Melo, C. H. F., et al. 2000, *Astronomy and Astrophysics*, 359, 181
- Wilson, R. E. 1953, *Washington, 0*
- Woolley, R., Penston, M. J., Harding, G. A., et al. 1981, *Royal Observatory Annals*, 14
- Wright, C. O., Egan, M. P., Kraemer, K. E., & Price, S. D. 2003, *The Astronomical Journal*, 125, 359
- Wright, E. L., Eisenhardt, P. R. M., Mainzer, A. K., et al. 2010, *The Astronomical Journal*, 140, 1868
- Xing, L. F. 2010, *ApJ*, 723, 1542
- Zuckerman, B. 2019, *The Astrophysical Journal*, 870, 27
- Zuckerman, B., & Song, I. 2004, *Annual Review of Astronomy & Astrophysics*, 42, 685
- Zuckerman, B., Song, I., & Bessell, M. S. 2004, *The Astrophysical Journal*, 613, L65
- Zuckerman, B., Song, I., Bessell, M. S., & Webb, R. A. 2001a, *The Astrophysical Journal*, 562, L87
- Zuckerman, B., Song, I., & Webb, R. A. 2001b, *The Astrophysical Journal*, 559, 388